COMPACT MICROWAVE DEVICES BASED ON NONLINEAR TRANSMISSION LINE AND SUBSTRATE INTEGRATED WAVEGUIDE

By

WENJIA TANG

A dissertation submitted to the Graduate Faculty in

Engineering in partial fulfillment

of the requirements for the degree of Doctor of Philosophy,

The City University of New York

2012

This manuscript has been read and accepted for the
Graduate Faculty in Electrical Engineering in satisfaction of the
Dissertation requirement for the degree of Doctor of Philosophy

Dr. Jizhong Xiao

Date

Chair of Examining Committee

Dr. Mumtaz K. Kassir

Date

Executive Officer

Dr. Ping-Pei Ho

Dr. Tarek Saadawi

Dr. Yi Sun

Dr. Thao Nguyen

Supervisory Committee

THE CITY UNIVERSITY OF NEW YORK

Abstract

COMPACT MICROWAVE DEVICES BASED ON NONLINEAR TRANSMISSION LINE AND SUBSTRATE INTEGRATED WAVEDUIDE

by

Wenjia Tang

Advisor: Professor Jizhong Xiao

Nonlinear transmission line (NLTL) and substrate integrated waveguide (SIW) are the most popular integration techniques in microwave area, which have a wild application in the military, civilian and robot wireless communication systems. The motivation to apply these technologies to microwave devices is to reduce the physical size, improve integration and achieve superior electrical performance. My research areas cover phase shifter, delay line, frequency translator, power divider and antenna design.

I am the first one to introduce the theory of perfectly linear phase shifter by using a specially doped diode in left-handed (LH) NLTL. Through creating an equivalent Advanced Design System (ADS) model, we prove this theory by the simulation results, which agree with the theoretical analysis well. This novel LH NLTL technology is also used in the delay line for the first time to make a fabricated circuit with compact size and decent electrical performance. Another innovative application of LH NLTL in our study is to incorporate it in frequency translators by taking advantage of its linear phase variation to get broad bandwidth, low spurs and low cost. Compared with LH NLTL, right-handed (RH) NLTL is also widely used and featured with low insertion loss. By replacing $\lambda/4$ section lines in a conventional Wilkinson power divider with RH NLTL, a compact and

frequency tunable Wilkinson power divider is presented for the first time. The proposed circuit has excellent performance with less than 3% of the physical volume of the original Wilkinson power divider structure.

For the later part of our research work, a Substrate Integrated Waveguide (SIW) cylinder conformal multi-beam antenna fed by a conformal Butler matrix is originally proposed and realized. The slots antennas and Butler matrix are fabricated on a single substrate to reduce the size, weight and cost, and enhance the manufacture reliability concurrently. Furthermore, the far-field pattern algorithm for cylinder conformal antenna is proposed and its calculation result agrees with experimental data.

PREFACE

After three years of working experience in the microwave research field, I joined the Ph.D. program at the electrical engineering department of the City College of New York (CCNY), City University of New York (CUNY City College) in 2007. During this period of Ph.D. study, I found an interesting phenomenon regarding electrical appliances. Half a century ago, people bought a radio mainly for getting information but the motivation has totally changed now. My friend Mike has five tablet personal computers not just for information but more importantly, for fun. Electrical products are more like a fashion instead of necessities and people spend a large amount of money to upgrade them. I believe this is the fundamental drive for the electrical industry. Meanwhile I found the designing trend of the electrical appliances: smaller physical size and lower cost. Following this clue, I started my research with the goal of applying this motivation in microwave field to design compact microwave devices with superior performance. Inspired by this finding, I focused my research on designing compact microwave devices with superior performance. This dissertation covers several areas, including transmission line, power divider, frequency translator, phase shifter and antenna. Most of the research is carried out at CUNY City College under the supervision of my former mentor, Dr. Hoogjoon Kim, and my current Ph.D. advisor, Dr. Jizhong Xiao. In the past several years, every effort was made to present the solutions to the challenging problems in a

clear and lucid manner. Therefore, most of our ideas have been tested through experiments and have potential improvements for current microwave devices in the market.

Wenjia Tang

January 2012

ACKNOWLEDGEMENTS

The writing of a dissertation can be a lonely and isolating experience, yet it is obviously not possible without the personal and practical support of numerous people. Thus, my sincere gratitude goes to my family, my friends, and my companions and superiors for their love, support, and patience over the last few years.

First and foremost, I would like to express my sincere gratitude to my former mentor, Dr. Hoogjoon Kim for his inspiration, support and guidance during my early years in the electrical engineering Ph. D. program. I am grateful to my current Ph. D. advisor, Dr. Jizhong Xiao for his trust, guidance and the efforts to ensure the quality of my research and dissertation. Without their assistance and advice, this research would not be possible.

I would like to thank all committee members: Dr. Ping-Pei Ho, Dr. Yi Sun, Dr. Tarek Saadawi and Dr. Thao Nguyen. Their insightful comments and suggestions enhance the technical soundness of this dissertation.

Finally, I am grateful to my parents, Yueqin Jiang and Jianchao Tang for their trust and encouragement. Their support is so important that has been through tremendous perseverance and involved untold sacrifices. Also my wife, Tingting, her love plays a big role. I also would like to thank my friends for their generosity and kindness. Special thanks go to Jiho Ryu, Shi Wu, Qihua Yang and Yonghui Shu. The discussions with them substantially contribute to my work and broaden my knowledge.

TABLE OF CONTENTS

LIST OF TABLES

LIST OF FIGURES

1.0 INTRODUCTION

In this chapter, we focus on the motivations and contributions of each project. Meanwhile the fundamental knowledge of left-handed nonlinear transmission line (LH NLTL) and substrate integrated waveguide (SIW) is introduced.

1.1 MOTIVATION

Currently there are two main research directions in transmission line field attracting people's attentions. One is nonlinear transmission line (NLTL), which has replaced the position of microstrip line in many applications because of its smaller physical size. The other one is substrate integrated waveguide (SIW), which is widely recognized as upgraded version for rectangular waveguide also for its small size advantage.

In the past century, human being has made tremendous efforts to reduce the physical size of electrical equipment. The most phenomenal example is the evolution of the computer. It was as big as a room when it was first invented while the tablet today has only the size of a book with more functions and higher processing speed. I believe this minimization trend continues to be the fundamental drive in electronic products in the

future. Therefore, the following research topics are chosen to meet the demands of the fast developing industry.

The first part of this dissertation (chapters 2~5) focuses on the application of NLTL in a variety of microwave devices. After thorough reading of the literature reports of right-handed (RH) NLTL and left-handed (LH) NLTL in the past five years, we realize that the primary advantages of the NLTL are extremely small size, linear phase, broad bandwidth and voltage tunability. Therefore, we want to incorporate these superior features in current microwave devices. With the approach of simulations and experiments, we successfully demonstrate the advantages of NLTL in novel applications of microwave devices.

The latter part of this dissertation (chapter 6) describes a conformal SIW multi-beam antenna mounted on a cylinder fed by a Butler matrix. The SIW multi-beam antenna is fabricated on printed circuit board (PCB) instead of conventional metal waveguides. By combining the benefits of SIW and typical rectangular waveguide design methods, we make the conformal multi-beam antenna with good electrical performance, compact size and low cost.

My research covers the following microwave devices including phase shifter, delay line, frequency translator, power divider and antenna.

1.1.1 Linear phase shifter for broadband frequency

The primary application of linear phase shifter is in beam-steering antenna array to control the beam direction. One of the state-of-the-art techniques is the ferrite phase shifter [1], which offers great flexibility but has the disadvantages of bulkiness,

expensiveness and requirement of accurate calibration. Besides the ferrite phase shifters, monolithic microwave integrated circuit (MMIC) technology based phase shifters are also widely used in phase array. They have advantages such as small size, light weight, high reliability, high reproducibility and low cost [2].

In terms of different control technologies, the phase shifters are divided into two types [3]. One is digital phase shifter, whose phase dynamic range can be changed by only a few of discrete values. The other type is analog phase shifter, whose phase shift can be varied in a continuous way by corresponding control signal. Since this phase shifter has a wider application due to higher tuning resolution and more phase shift values, we have decided to use this analog phase shifter in our design in chapter 2. Among the second type analog phase shifters, most of the studies reported in literatures use right-handed (RH) NLTL structures [4]. Because the RH NLTL propagation constant is not linearly proportional to its bias voltage, none of these phase shifters can achieve a perfect linear phase variation. Contrast to those works, our design of phase shifter takes advantage of the left-handed (LH) NLTL's special feature and the varactor with novel capacitance variation according to bias voltage. Our simulation study demonstrates that the proposed phase shifter based on this specially designed varactor with fixed doping parameter can achieve perfectly linear phase shift.

1.1.2 Compact tunable group delay line

Group delay is defined as the rate of change of transmission phase angle with respect to the frequency. Normally group delay is a useful measure of time distortion, and is calculated by differentiating the phase response versus frequency of the device under test

(DUT) with respect to the frequency. The group delay can also be expressed as the slope of the phase response at any given frequency. The variations in the group delay cause signal distortion, which deviates from linear phase.

The main application of the group delay line is in circuit modules and board level interconnections to achieve the necessary clock skew [5]. As the clock rate of electronic devices and modern computers increases, timing errors become the critical bottleneck in high-speed circuit design. Clock skew, which is used in circuit components at specific time, needs to be strictly controlled within small tolerance level [6]. To meet the tight clock skew requirement, the propagation delay variation through the delay line should be controlled within a small range such as several picoseconds.

There are numerous transmission delay lines reported in the last two decades. The most traditional way is to increase the signal traveling time by extending the length of the conducing trace [7]. However, the most popular meander and spiral routing line has its own drawbacks [8, 9].This type of delay lines consist of segments of transmission lines closely packed together. The coupling phenomenon among segments of the meander line causes additional capacitance, which degrades the total signal delay. Another drawback is that these meander lines have fixed length, thus the group delay cannot be changed.

In this work, we demonstrate a new method of making a compact, tunable delay line based on LH NLTL. Compared with the conventional meander lines, our proposed circuit has following features such as compact size and large tunable delay, low power consumption and infinite tuning resolution.

1.1.3 Low spurious broadband frequency translator

A frequency translator is a two ports network, which changes the input frequency to a desired value at the output. Given an input signal of a certain frequency, an ideal frequency translator generates an output signal whose frequency is shifted by some desired amount from that of the input. A maximum of power is produced at the desired frequency, and no power is produced at other frequencies. Frequency translator is also named as frequency shifter [10], frequency converter [11], and synchrodyne [12]. The main application of the frequency translator covers microwave relay station [13], microwave reflectometer system for network analyzers [14] and velocity deception electronic counter measures (ECM) system [15].

An ideal frequency translator requires a phase shifter with perfectly linear phase shift versus applied DC bias because a saw tooth modulation is used to translate the original frequency [15]. In addition, phase variation should be exactly 360 degrees to suppress spurious signals at the output. However, most phase shifters reported in the literature cannot satisfy all the properties mentioned above and are not suitable to be used as a good frequency translator [16, 17].

NLTL is an attractive technology for the phase shifter in the frequency translator. In paper [14], the authors demonstrated a frequency translator with NLTL whose structure consists of varactor diodes placed periodically on a transmission line as shunt elements. The frequency translator made with a RH NLTL works for a wide frequency band, but it has many spurious signals. One of the main reasons is that the phase variation is not linear. To minimize spurious signals, the authors had to adjust the modulation signal using a high-resolution digital analog converter (DAC) card. In another paper [17] ,

authors developed a 360 degree analog coplanar waveguide (CPW) MMIC phase shifter for the frequency translator but the output spurs are quite high due to the nonlinear phase shifter.

In our design, we use a linear phase shifter based on LH NLTL. Due to its linear phase variation versus bias voltage, spurious frequencies are greatly reduced and the cost is quite low compared to RH NLTL in [14].

1.1.4 Compact, tunable Wilkinson power divider

Wilkinson power divider was invented around 1960 by Ernest Wilkinson. Its major function is to split an input signal into two equal phase output signals, or combine two equal-phase signals into one in the opposite direction. The key component is the quarter-wave transformer, which matches the split ports to the common port. Because a lossless reciprocal three-port network cannot have all ports simultaneously matched, Wilkinson added one resistor, which does a lot more than allowing all three ports to be matched. It also fully isolates port 2 from port 3 at the center frequency. The resistor adds no resistive loss to the power split, so an ideal Wilkinson splitter is highly efficient.

However, Wilkinson power divider has some drawbacks such as a large size and a limited bandwidth. Thus, numerous articles have been published in this field to study the solutions to these problems [18-22]. In [18], the authors, J. Kim, G. M. Rebeiz use synthetic lumped element transmission lines to replace $\lambda/4$ sections in a conventional Wilkinson power divider to minimize the size. In this case, although the size is very small, the divider suffers from large insertion loss and narrowband performance. To increase bandwidth, multiple $\lambda/4$ sections should be used at the expense of large physical

size [19]. Recently, several dual-band and broadband power dividers are reported [20, 21, 23], but they still require microstrip transmission lines that make the size of the power divider large.

Because the NLTL can be used as a broadband and compact phase shifter [24, 25], our main approach is to replace the λ/4 sections of the conventional Wilkinson power divider with the lumped element NLTLs to minimize size and incorporate frequency tunability. The experiment result shows excellent small size and good electrical performance.

1.1.5 Conformal SIW multi-beam Antenna

Conformal array antennas are widely used in military and civilian applications due to their benefits of aerodynamic superiority, wide-angle coverage and volume reduced. A typical application of the conformal antenna is the aircraft radar, which needs low profile, light weight and excellent performance for navigation and communication. Another important utilization of this conformal array antenna is in mobile robots. In [3, 4] a directional antenna is mounted on the robot for localization of unknown radio sources. However, this directional antenna has limitation in beam coverage since the radiation direction is fixed. In [5] Graefenstein J. et al rotated the directional antenna to achieve high accuracy of localization. Nevertheless, the rotated antenna is driven by a motor, which is slow and energy inefficient. Therefore, the multi-beam antenna provides a new option for above robots to overcome this problem.

There are lots of conformal antennas in today's market. Most of them use a number of discrete antennas arrayed along the circumference of the cylinder [26]. Among all kinds

of these antennas, slots antenna is the most popular one in all fields. It adds advantages of fabrication simplicity, high efficiency and low cross-polarization level [27] to previous models. Currently most of the slots antenna is made on rectangular waveguides. However, the rectangular waveguide components are bulky and costly because high precision mechanical tuning is required in manufacture [27].

Our work applies SIW technology to overcome above drawbacks. Furthermore, because of the tolerance control advantage, SIW technique is appropriate for mass production to significantly reduce the manufacture cost.

1.2 FUNDAMENTALS AND LITERATURE REVIEWS OF ELECTROMAGNETIC METAMATERIALS

Electromagnetic metamaterials (MTMs) are broadly defined as artificial homogeneous electromagnetic structures with unusual properties, which are not readily available in nature. An effectively homogeneous structure is a structure whose structural average cell size p is much smaller than the guided wavelength λ_g. Therefore, this average cell size should be at least smaller than a quarter of wavelength, $p < \lambda_g/4$. We refer to the condition $p = \lambda_g/4$ as the effective homogeneity limit or effective-homogeneity condition, to ensure that refractive phenomena dominates over scattering/diffraction phenomena when a wave propagates inside the MTM medium. If the condition of effective-homogeneity is satisfied, the structure behaves as a real material. The structure is thus electromagnetically uniform along the direction of propagation. The constitutive

parameters are the permittivity ε and the permeability μ, which are related to the refractive index n by

$$n = \pm\sqrt{\varepsilon_r \mu_r}\ , \tag{1.1}$$

where ε_r and μ_r are the relative permittivity and permeability related to the free space permittivity and permeability by ε_o=8.854 $\cdot 10^{-12}$ and $\mu_o = 4\pi \cdot 10^{-12}$, respectively. In (1.1), sign $\pm$ for the double-valued square root function has been admitted.

The four possible sign combinations in the pair (ε, μ) are (+, +), (+, -), (-, +), (-, -), as illustrated in the diagram of Figure 1.1. Whereas the first three combinations are well known in conventional materials, the last one [(-, -)], with simultaneously negative permittivity and permeability, corresponds to the new class of left-handed (LH) materials. Because of their double negative parameters, LH materials are characterized by antiparallel phase and group velocities, or negative refractive index (NRI).

LH structures are clearly MTMs, according to the definition given above, since they are artificial (fabricated by human hands), effectively homogeneous ($p < \lambda_g/4$), and exhibit highly unusual properties ($\varepsilon_r, \mu_r < 0$). It should be noted that, although the term MTM has been used most in reference to LH structures in the literature, MTMs might encompass a much broader range of structures. However, LH structures have been by far the most popular of the MTMs, due to their exceptional property of negative refractive index [28] .

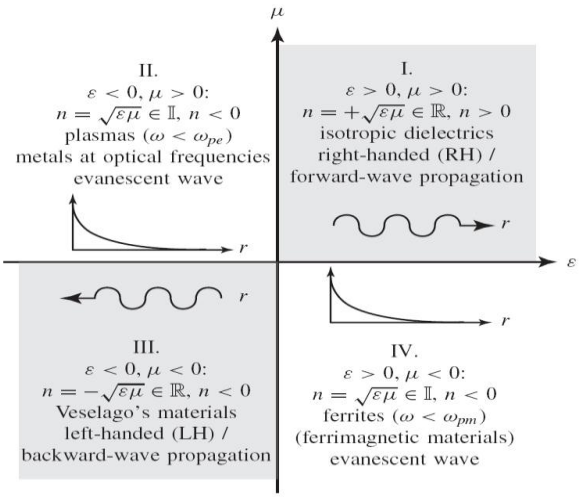

Figure 1.1 Permittivity-permeability (ε-μ) and refractive index (n) diagram [28]

Back in 1968, Veselago first investigated theoretically materials with simultaneously negative permittivity and permeability, or left-handed materials, and pointed out some of their electrodynamic properties, such as reversal of Snell's law, Doppler effect, and Cerenkov radiation [29]. In his paper, Veselago called these 'substances' LH to express the fact that they would allow the propagation of electromagnetic waves with the electric field, the magnetic field, and the phase constant vectors building a left-handed triad, compared with conventional materials where this triad is known to be right-handed.

Recently, these materials have attracted a tremendous renewal of interest, because of the demonstration of their practical realizability [30-32]. LH effects have also been demonstrated in some band structure of photonic crystals [33], where the lattice constant is usually of the order of λ/2. LH materials generally have diffraction sites with interdistance much smaller than wavelength so that they can be considered as homogeneous media.

The special features of LH metamaterials, verified by full-wave analysis in [34, 35], are promising for a diversity of optical/microwave applications, such as beam steerers, modulators, band-pass filters, super lenses [36], microwave components [37-39], and antennas [40]. However, the originally presented LH structures presented originally were impractical for microwave applications because they are lossy and feature with narrow bandwidth. A structure made of resonating elements generally does not constitute a good transmission medium for a modulated signal because the quality factor is intrinsically associated with each resonator [41]. In a resonator, the loaded quality factor Q_l is related to the unloaded quality factor Q_u and the external quality factor Q_e by the relation

$$\frac{1}{Q_l} = \frac{1}{Q_u} + \frac{1}{Q_e}, \tag{1.2}$$

which expresses the fact that the total transmission loss ($\propto 1/Q_l$) through a resonator is equal to the sum of the dielectric/ohmic losses in the resonator ($\propto 1/Q_u$) and the coupling losses in the transitions with the external (source/load) circuits ($\propto 1/Q_e$). The loaded quality factor, which is the quantity actually measured and eventually relevant in terms of transmission, is also obtained from the magnitude of the transmission parameter (S_{21}) as

$$Q_l = \frac{f_r}{B} \tag{1.3}$$

where f_r is the resonance frequency and B is the 3 dB bandwidth, while the unloaded quality factor is defined as

$$Q_u = \omega \frac{\text{average energy stored in resonator}}{\text{power dissipated in resonator}}. \tag{1.4}$$

These formulas show that, for given dielectric (dielectric loss $\propto \tan\delta$) and metal (ohmic loss $\propto 1/\sigma$, σ: conductivity) materials, there is an unavoidable trade-off between bandwidth and transmission level. Minimum transmission loss, or equivalently maximum $Q_{l,}$ is achieved at the resonance frequency f_r by minimizing the bandwidth B, according to (1.3), because in this case very little power is dissipated in the cavity since its bandwidth is extremely narrow so that Q_u is maximized, according to (1.4). Therefore, in this case, good transmission characteristics can be obtained. Nevertheless, bandwidth is so restricted that a modulated signal, even with a modest bandwidth, cannot be transmitted without distortion through the resonating structure. Bandwidth can naturally be increased, but this immediately results in a decrease of Q_l according to (1.3) and therefore an increase of transmission loss. In conclusion, a modulated signal cannot be transmitted efficiently through a resonating propagation medium.

Due to the weakness of resonant-type LH structures, there was a need for alternative architectures. Therefore, recognizing the analogy between LH waves and conventional backward waves, three groups introduced a nonlinear transmission line approach of metamaterials: Eleftheriades etal [40, 42], Oliner [43] and Caloz [44, 45]. In fact, hypothetical “backward-wave” uniform transmission lines, without any suggestion for a

practical implementation, have been briefly described in a few textbooks, such as [46]. The incremental circuit model for such a transmission line is shown in Figure 1.2.

The fundamental characteristics of the transmission line in Figure 1.2 are straightforwardly derived by theory. Let us consider here the lossless case for simplicity. The complex propagation constant γ, the propagation constant β, the characteristic impedance Z_c, the phase velocity v_p, and the group velocity v_g of the transmission line are given by

$$\gamma = j\beta = \sqrt{Z'Y'} = -j\frac{1}{\omega\sqrt{L'_L C'_L}} \tag{1.5}$$

$$\beta = -\frac{1}{\omega\sqrt{L'_L C'_L}} < 0 \tag{1.6}$$

$$Z_c = \sqrt{\frac{L'_L}{C'_L}} > 0 \tag{1.7}$$

$$v_p = \frac{\omega}{\beta} = -\omega^2\sqrt{L'_L C'_L} < 0 \tag{1.8}$$

$$v_g = \omega^2\sqrt{L'_L C'_L} > 0 \tag{1.9}$$

The last two equations immediately show that phase and group velocities in such a transmission line would be antiparallel. The phase velocity v_g, associated with the direction of phase propagation or wave vector β, is negative, whereas the group velocity v_g, associated with the direction of power flow or Poynting vector S, is positive. Thus, the transmission line in Figure 1.2 is left-handed, according to the definition. Because of their nonresonant nature, transmission line (TL) MTMs can be designed to exhibit

simultaneously low insertion loss and broad bandwidth. The lossless feature is achieved by a balanced design of the structure and good matching to the excitation ports, whereas broad-bandwidth is a direct consequence of the transmission line nature of the structure and can be controlled by its inductance and capacity parameters, which determine the cutoff frequency of the resulting high-pass structure. Another advantage of TL MTMs is that they could be fabricated in planar configuration, compatible with modern microwave integrated circuits (MICs). Finally, TL MTMs structures can benefit from the efficient and well-established transmission line theory for the competent design of microwave applications.

T. Itoh, et al presented a transmission line approach of left-handed materials based on nonresonant components [44], describing a procedure to realize an artificial left-handed transmission line (LH TL) with low loss and broad bandwidth and demonstrating a microstrip implementation of this line using interdigital capacitors and stub inductors. The microstrip implementation of the left-handed line has been shown, with moderate insertion loss and broad bandwidth to the order of 100%. However this kind of transmission line is not perfect since it has disadvantages such as large physical size and fixed operation frequency.

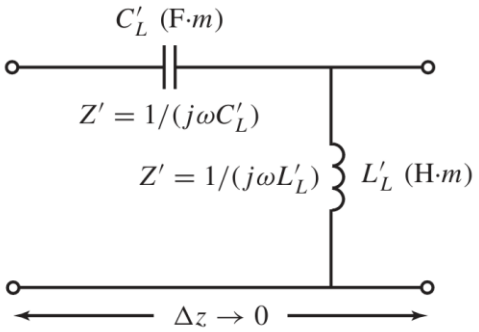

Figure 1.2 Incremental circuit model for a hypothetical uniform LH TL

In our work, a nonlinear transmission line (NLTL) is comprised of a transmission line periodically loaded with lumped inductors and varactors, where the capacitance nonlinearity arises from the variable depletion layer width, which depends on both the DC bias voltage and on the AC voltage of the propagating wave. The structures are shown in Figure 1.3. Although the structures are very simple, the principle is complicated [47]-[48].

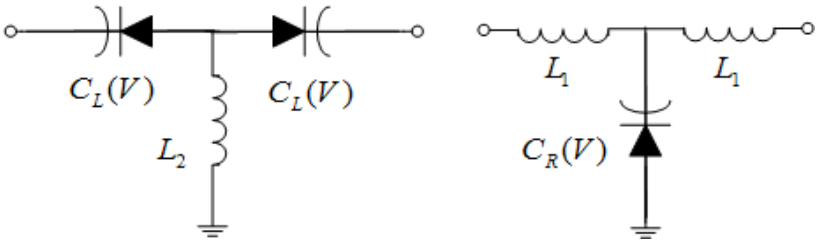

Figure 1.3 The circuit topology of a unit cell of LH and RH NLTLs.

Because the capacitance of the varactors can be controlled by voltage, this component can be tunable and this feature has been widely applied. Several microwave circuits with this NLTL structure have been reported. These examples are 'Bandpass Filter with Tunable Passband and 0 ° Phase Shift Near Center Frequency' [49], 'Linear Tunable

Phase Shifter Using a Left-Handed Transmission Line' [50], and 'A hybrid nonlinear delay line-based broadband phased antenna array' [51].

1.3 FUNDAMENTALS AND LITERATURE REVIEWS OF SUBSTRATE INTEGRATED WAVEGUIDE

Wireless components and systems have received increasing attention in recent years. The deployment of millimeter-wave (mm-wave) technology is critical for the evolution of wireless systems. The business success of these systems mainly relies on the cost-effective technology, which should be suitable for the mass-production of components and systems.

The core of these systems relates to the active parts, which includes devices such as amplifiers, mixers and local oscillators. Nowadays, these devices can be integrated into chip-sets at a lower cost. However, other components in mm-wave systems are too large to be integrated in the chip-sets, such as antennas, filters and so on. These additional components usually are packaged with chip-sets [5]. At low frequencies, microstrip or coplanar waveguides are normally used. At frequencies higher than 30GHz, transmission losses and radiation are quite high for microstrip and coplanar waveguides. Recently a promising candidate for developing this platform is substrate integrated waveguide (SIW) technology [6, 7]. SIW is integrated waveguide-like structures fabricated by using two rows of conducting cylinders or slots embedded in a dielectric substrate that electrically connect two parallel metal plates (Figure 1.4). Thus SIW could take the place of rectangular waveguide and be integrated in the standard printed circuit board (PCB) or

low-temperature co-fired ceramic (LTCC). Compared with the conventional rectangular waveguides, SIW shows similar propagation characteristics, field pattern and the dispersion characteristics. Furthermore, SIW preserves high quality-factor and high power-handing capability. Among all of these advantages, the most important one is the possibility to integrate several chip-sets on one substrate, which is called system-on-substrate (SOS) [8]. Due to the low cost, small tolerance and high quality, SOS could be an ideal platform for mm-wave systems.

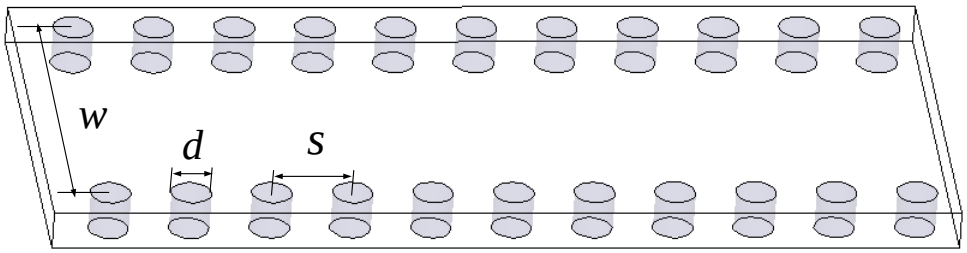

Figure 1.4 SIW schematic diagram

SIW technology has been widely used in microwave components such as filter [9], couplers [52], oscillators [53], power amplifiers [12], slots antennas [54] and circulators [13]. However, most of SIW components operate in the frequency range up to 30 GHz due to increased technological difficulties encountered in designing and manufacturing SIW structures over the mm-wave range.

SIW shows similar propagation characteristics to those of rectangular waveguides, if the metallic vias are closely spaced and radiation leakage can be neglected. Furthermore, SIW modes practically coincide with a subset of the guided modes of the rectangular waveguide, namely with the TE_{n0} modes, with n =1, 2…. The fundamental mode is

similar to the TE_{10} mode of a rectangular waveguide, with vertical electric current density on the sidewalls. Owing to this similarity between SIW and rectangular waveguide, empirical formulas have been obtained between the geometrical dimensions of the SIW and the effective width w_{eff} of the rectangular waveguide with the same propagation characteristics. These formulas allow for a preliminary dimensioning and design of SIW components, without any full-wave analysis tools. One of the most popular relations is derived in [55] as (1.10).

$$w_{eff} = w - \frac{d^2}{0.95s} \tag{1.10}$$

where d is the diameter of the metal vias, w represents their transverse spacing and s is their longitudinal spacing. Another way to get the propagation characteristics of SIW structures is to use full-wave analysis tools, such as Ansoft high-frequency simulation and CST Microwave Studio. In our work, the CST Microwave Studio is chosen for optimization.

A primary issue in the design of SIW structure is the loss minimization, which is critical when operating at mm-wave frequencies. There are three kinds of losses needed to be considered: conductor loss (caused by the finite conductivity of metal walls), dielectric loss (caused by the lossy dielectric material) and possibly radiation loss (caused by the energy leakage through the gaps) [56]. The conductor and dielectric losses are similar to the corresponding losses in rectangular waveguides filled with a dielectric medium. The conductor loss can be significantly reduced by increasing the substrate thickness since the attenuation constant is almost proportional to the inverse of substrate

thickness. The other geometrical dimensions of the SIW exhibit a negligible effect on conductor losses. Conversely, the dielectric loss caused by dielectric material can be reduced only by using a better dielectric substrate. The last radiation loss can be kept reasonably small if $s/d<2.5$. Therefore, the contribution of dielectric loss is predominant at mm-wave frequencies. Compared with traditional planar transmission lines such as microstrip line and coplanar waveguides, SIW structures can get comparable or lower losses [57].

Another important issue need to be addressed for the SIW is the performance in terms of dimensions and bandwidth. SIW is similar to rectangular waveguide and has limitation on bandwidth. The physical width of the SIW dominates the cutoff frequency of the fundamental mode. Recently, numerous waveguide topologies have been proposed to improve the compactness of SIW, such as substrate-integrated folded waveguide (SIFW) [58], half-mode substrate-integrated waveguide (HMSIW) [59], the folded half-mode substrate-integrated waveguide (FHMSIW) [60]. Meanwhile, in order to improve the SIW bandwidth, some novel configurations have been developed such as the substrate-integrated slab waveguide (SISW) [61] and the ridge waveguide in SIW technology [62, 63].

The last topic for SIW is the electromagnetic modeling. The development of SIW technology requires very accurate electromagnetic modeling for SIW components. Nowadays, full-wave numerical techniques are the most popular tools including commercial electromagnetic software and specially made numerical techniques. Electromagnetic algorithms such as integral-equation, finite-element or finite-difference methods have been presented [56, 64, 65]. Normally these algorithms not only deal with

metallic posts, but also inhomogeneous substrates. A particularly efficient numerical technique for the modeling of arbitrarily shaped SIW components is based on the BI-RME method [56], which is used to determine the wideband expression of the frequency response of SIW components in one shot. Therefore, time consumption can be reduced by avoiding repeated frequency-by-frequency electromagnetic analyses. In fact, once an equivalent circuit model is available, the direct synthesis of a component can be performed in a short time by using circuit computer-aided design tools without electromagnetic full-wave analysis.

1.4 CONTRIBUTIONS AND OUTLINE OF THE DISSERTATION

The contributions of this dissertation include perfectly linear phase shifter for broadband frequency, compact tunable large group delay line, low spurious broadband frequency translator, compact tunable Wilkinson power divider using tunable synthetic transmission line and conformal SIW multi-beam antenna. We present novel applications of nonlinear transmission line (NLTL) in the chapter 2-5 of this dissertation and conformal multi-beam antenna system using SIW technology in the chapter 6. All of these projects are presented for the first time. The brief summary of contributions are listed in Table 1.

Table 1 Contributions of the dissertation

Project Name	Contributions
perfectly linear phase shifter for broadband frequency	smaller size, lower power consumption, higher resolution, higher frequency achievable, perfectly linear phase shift
compact tunable large group delay line	smaller size, wider range electrical tunability, lower power consumption, higher resolution
low spurious broadband frequency translator	lower spurs, lower cost, broader bandwidth
compact tunable Wilkinson power divider using tunable synthetic transmission line	smaller size, broader bandwidth, wider range electrical tunability
conformal SIW multi-beam antenna	smaller size, lower cost, simpler fabrication, wider coverage, easier to mounted on cylinder

This dissertation consists of seven chapters, which systematically describes novel applications of LH NLTL and SIW technologies in microwave devices. Chapter 1 reviews the fundamentals of left-handed transmission line and substrate integrated waveguide theory in a general manner. Despite its review nature, motivations are described since they influence the presentation of topics in later chapters. Chapter 2 presents the research project of perfectly linear phase shifter for broadband frequency. In this part of work, we introduce a novel design method for achieving perfectly linear phase shifting and the math calculation results agree with the simulation results. Chapter 3 discusses the characteristics of compact tunable large group delay line. The theory of this novel group delay is illustrated. Meanwhile, the experiments results are provided to prove the novel circuit's superiority over conventional delay lines. Chapter 4 introduces the concept of a low spurious, broadband frequency translator using left-handed nonlinear transmission line. A more effective method to build a frequency translator without complicated DAC system is described. Chapter 5 is about the application of synthetic transmission line in Wilkinson power divider. Fundamental theory, design of experiments

and discussion of results are provided in individual sections of the chapter. Chapter 6 explores a special topic of conformal SIW multi-beam antenna. Conformal slots antenna concept and design method are presented. In the successive sections, the calculation approaches of Butler matrix and the main factors that degrade the bandwidth are analyzed. Besides, the conformal far field pattern calculation method is extensively discussed in section 6.8. In the following section, a preliminary discussion on measured results and calculated results are provided. Chapter 7 summarizes the contributions and discusses in detail how the challenges of narrow antenna bandwidth can be efficiently overcome and the new application field for LH NLTL.

2.0 PERFECTLY LINEAR PHASE SHIFTER FOR BROADBAND FREQUENCY USING A METAMATERIAL

In this chapter, we present an idea to design a novel phase shifter based on a metamaterial constructed with specially doped, cascaded varactors and shunt inductors. By utilizing the peculiar phase propagation properties inside this metamaterial we can achieve perfectly linear phase variation in response to bias voltage. The simulation results agree well with theoretical analysis and show perfectly linear phase variation for broadband frequency. The phase shifter can be made in a very compact form since its size is mainly determined by the cascaded varactors. Due to its compactness and high linearity, we believe it can enhance the current phased array radar and smart antenna systems.

2.1 INTRODUCTION OF PHASE SHIFTER

The phase shifter is a very important component for many applications in microwave and millimeter-wave systems. Due to the increasing demand for high-performance phased array radar and smart antenna systems, electronically tunable phase shifters are of great interest in the world of Radio Frequency (RF) and Microwave. The requirements are that such phase shifters must be ultra-compact, linear in phase variation, and broadband in nature [66], [67]. Most phase shifters reported in the literature however have various

shortcomings such as; large size [68], imprecise phase variation [69], complex circuitry [66], high power consumption [70], limited bandwidth [71], and nonlinear phase variation characteristics [25].

Recently much attention has been paid to metamaterials (MTMs) [29], [72], known as left-handed (LH) materials. The term left-handed is associated with these materials because the direction of phase propagation is opposite to that of power flow. Periodic loading of shunt inductors and series capacitors is one of the simplest means of constructing such a material. The result is an artificial transmission line called a 'left handed transmission line (LHTL)'. By replacing the capacitors with the varactors in a LHTL, a left-handed nonlinear transmission line (LH NLTL) can be constructed [73]. Due to the nonlinearity of the varactors, it has been shown that the LH NLTL could be used as a frequency multiplier or a phase shifter [74].

In this work, we demonstrate a novel method of making a perfectly linear phase shifter for broadband frequency by constructing a LH NLTL with a specially doped varactor. In addition to its excellent linearity in phase variation, this novel phase shifter has several advantages such as small size, no power consumption, infinite resolution and wide bandwidth.

2.2 DESCRIPTION OF THEORY

Varactor diodes are widely used in microwave circuits as tuning elements. The capacitance of the device can be changed according to the applied reverse-bias voltage across the diode. Generally, one side of the p-n junction (usually the p-side) diode is more

heavily doped (usually p-side). The concentration on the lightly doped side ($N_B(x)$) is described by (2.1)

$$N_B(x) = bx^m \qquad x > 0 \tag{2.1}$$

where b and m are constants for a certain doping profile [75] and x is a distance from p-n junction point. In order to create a large variation range of the capacitance, the condition $m < 0$ is chosen. In this case, the diode has an exponential doping profile making it a hyper-abrupt varactor. The relationship between the junction voltage and the junction capacitance for the above doping profile can be expressed by (2.2) [75],

$$C_d(V) = \frac{C_{J0}}{(1 + \frac{V}{V_{bi}})^{\frac{1}{m+2}}} \tag{2.2}$$

where V is the diode biasing voltage, C_{J0} is the zero-bias diode capacitance, V_{bi} is the built in diode voltage, C_d (V) is voltage variable diode capacitance. If m = -1.5 in (2.1) and (2.2), we have a specially doped hyper-abrupt diode with which a perfectly linear voltage dependent phase shifter for broadband frequency can be made. The doping profile described can be realized with a Molecular Beam Epitaxy (MBE) machine. Figure 2.1 shows a unit cell of a single LH NLTL. L_1, L_2 are used to feed reverse DC-bias to modulate the diode capacitance. A shunt inductor (L) is placed between two cascaded diodes.

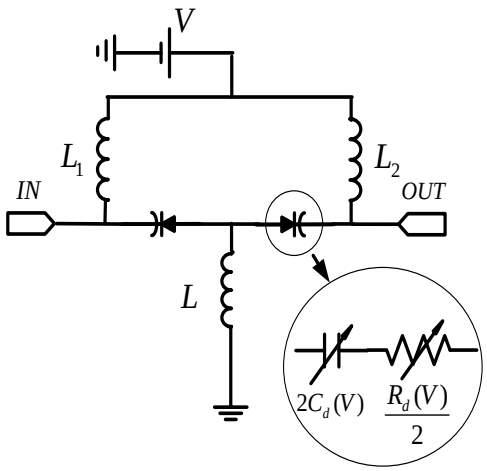

Figure 2.1 The circuit topology of a unit cell of LH NLTL and its equivalent circuit model

In the following equations, L is defined as the equivalent value of three shunted inductances. Since the inductance of L_1 and L_2, should be very large, the total inductance in a unit cell approximates L. The value of L can be calculated by (2.3) for the minimum return loss.

$$L \approx Z_0^2 \cdot C_d(V_{median}) \tag{2.3}$$

where Z_0 is the characteristic impedance of LH NL transmission line and equals 50 Ohm, $C_d(V_{median})$ is the median value of $C_d(V_{\max})$ and $C_d(V_{\min})$. The phase constant β analyzed in [75] presents the phase variation per unit cell:

$$\sin(\beta/2) = -\frac{1}{2\omega\sqrt{L \cdot C_d(V)}} \tag{2.4}$$

When the frequency is much higher than the cut-off frequency, defined as the Bragg cut-off frequency expressed by (2.5) [74], β can be approximated as (2.6).

$$\omega_B = \frac{1}{2\sqrt{L \cdot C_d(V)}} \tag{2.5}$$

$$\beta \approx -\frac{1}{\omega\sqrt{L \cdot C_d(V)}} \tag{2.6}$$

In the case when m = -1.5, the phase constant is approximated as (2.7).

$$\beta \approx -\frac{1}{\omega\sqrt{L \cdot C_{J0}}} - \frac{V}{\omega \cdot V_{bj}\sqrt{L \cdot C_{J0}}} \tag{2.7}$$

Here C_{J0}, L, and V_{bi} are constants. From (2.7), we see that the phase constant is perfectly linear to the bias voltage for any frequency higher than Bragg cut-off frequency.

2.3 RESULTS AND DISCUSSIONS

To prove the suggested idea, we run a simulation using Agilent ADS software. In the simulation, we set C_{J0} = 1 pf and V_{bi} = 0.7 V in equation (2.6) (the value of these parameters are depend on diode geometry, size and materials). Figure 2.2 shows capacitance variation according to bias voltage of the varactor.

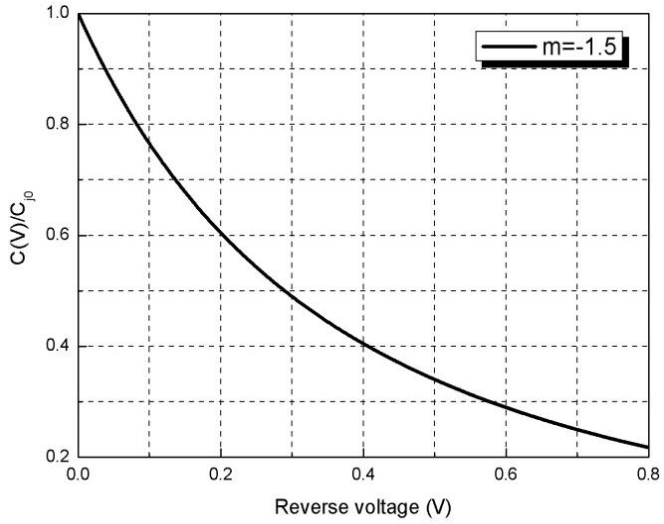

Figure 2.2 *C-V* curve of a varactor when m=-1.5, C_{J0} = 1 *pf* and V_{bi} = 0.7 *V*.

Using (2.4), the phase variation range ($\Delta\beta$) in the LH NLTL per unit cell can be expressed as (2.8):

$$\Delta\beta = 2\left\{\sin^{-1}\left(\frac{1}{2\omega\sqrt{L\cdot C_d(V_{\max})}}\right) - \sin^{-1}\left(\frac{1}{2\omega\sqrt{L\cdot C_d(V_{\min})}}\right)\right\} \qquad (2.8)$$

where $V_{\max}$ and $V_{\min}$ are the maximum and minimum reverse biasing voltages. The total phase variation ($\Delta\phi$) is defined by (2.9):

$$\Delta\phi = \Delta\beta \cdot n \qquad (2.9)$$

where n is the number of identical unit cells in the LH NLTL. In the simulation, we use ten of unit cells (n = 10) and set L = 1.01 nH to minimize reflection. Figure 2.3 shows the schematic of LH NLTL phase shifter.

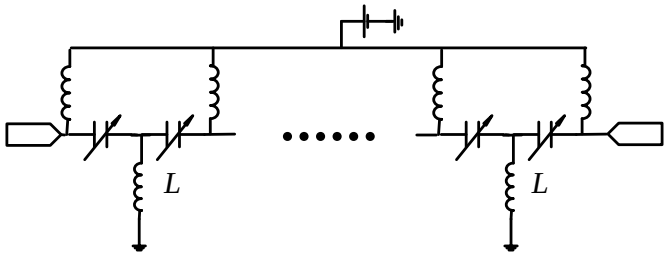

Figure 2.3 Schematic of the 10 sections LH NLTL phase shifter.

The simulation results are shown in Figure 2.4, Figure 2.5 and Figure 2.6. Figure 2.4 shows insertion loss variation for several bias voltages. The LH NLTL is a high pass filter, and the frequency of operation should be higher than the highest Bragg frequency that is 5.5 GHz. Also, since equation (2.8) is obtained with the assumption that the frequency of operation is much greater than the Bragg frequency, this condition must be adhered in order to ensure perfectly linear phase variation. We found that this phase shifter shows excellent performance for frequencies between 15 GHz-21 GHz. As can be seen in Figure 2.5, the phase variation is almost perfectly linear to the control voltage. Theoretical phase variation using equation (2.9) is also presented on the same graph. In the simulation, the maximum phase deviation from perfectly linear line is just $\pm 2.0^{o}$ for any frequencies between 15 GHz and 21 GHz. The fact that the simulation agrees well with theory, confirms that our suggested idea is feasible and accurate. Figure 2.6 (a) shows insertion loss and return loss variation for the operating frequency range. Since we did not account for the loss factors (resistances in the varactor and inductor) in the

simulation, the insertion loss is less than 0.5 dB for any bias voltage between 15 GHz and 21 GHz. The realistic insertion loss is expected to be somewhat higher if these factors are taken into account. The return loss (Figure 2.6 (b)) is less than -10 dB for any voltage bias, which means that the matching method is adequate. Other than its excellent linearity and low loss, the suggested phase shifter has the following advantages.

1.Compactness. The length of LH NLTL phase shifter is just several cascaded varactors only;

2. Infinite resolution. The LH NLTL phase shifter is analog phase shifter;

3. No power consumption. Because this phase shifter uses reverse bias of the varactor, no power is consumed;

4. Wideband and high frequency achievable. Theoretically, frequency of operation is from Bragg frequency to infinite frequency.

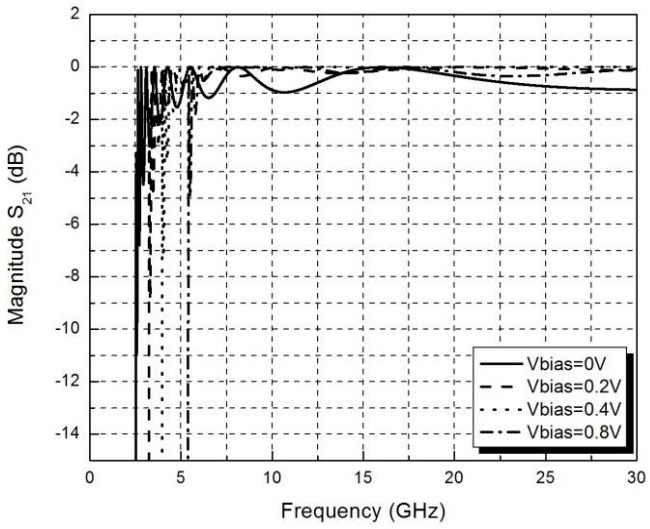

Figure 2.4 Insertion loss variation for several bias voltages, operating frequency for the phase shifter should be much higher than Bragg frequency to have a linear phase variation.

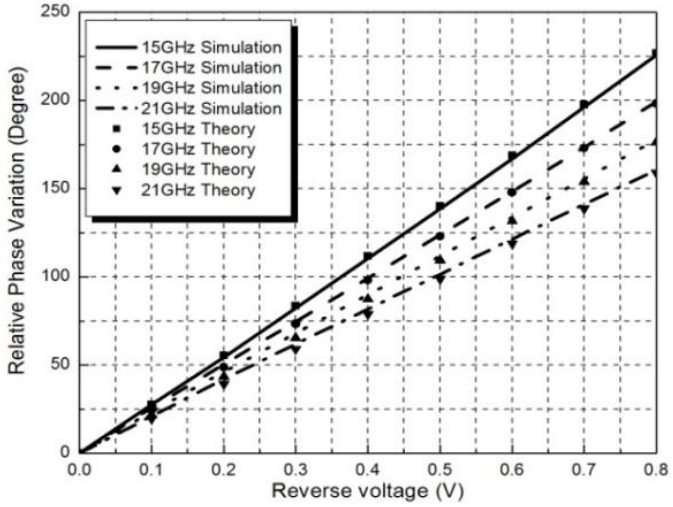

Figure 2.5 15-21 GHz phase variation, the maximum phase deviation is 2.5 º.

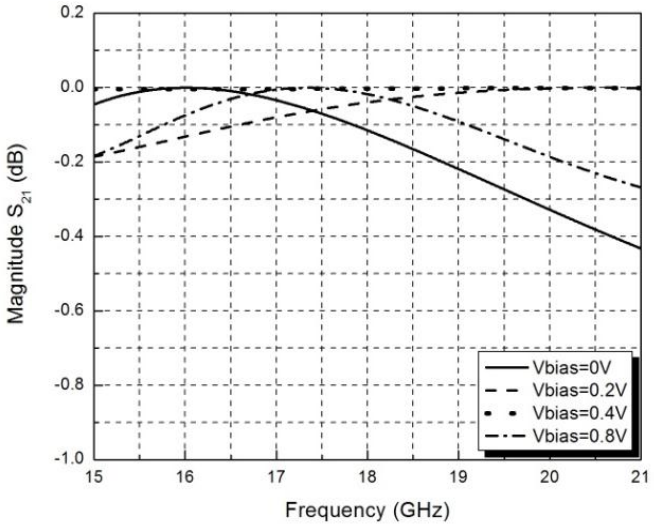

(a)

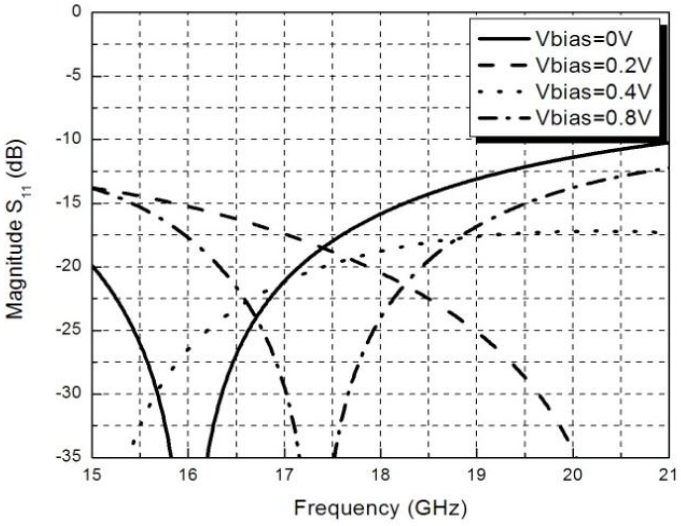

(b)

Figure 2.6 Insertion loss and return loss variation for the frequency between 15 GHz and 21 GHz. (a) Insertion loss variation. (b) Return loss variation.

2.4 SUMMARY

In this chapter, we presented a method to make a perfectly linear phase shifter for broadband frequency and proved the theory by simulation. With a specially doped hyper-abrupt varactor in the LH NLTL, a novel phase shifter can be made. This phase shifter has several additional advantages such as compactness, high resolution, no power consumption and wide bandwidth. Due to its excellent performance, it is an ideal candidate for modern phased array RADAR and smart antenna systems, which require accurate phase modulation and compactness.

3.0 COMPACT, TUNABLE LARGE GROUP DELAY LINE

In this chapter, we present a compact, tunable delay line based on left-handed nonlinear transmission line (LH NLTL). The widely tunable range of the large group delay is achieved by controlling a reverse bias voltage of series varactors in the LH NLTL. The proposed tunable delay line can be made in a very compact form since its size is dominated by the cascaded varactors. Our experiment shows that the fabricated prototype exhibits tunable group delay between 1.2 ns and 2.2 ns at a frequency of 1.42 GHz and good return loss. The circuit size is merely 1.6 cm in length.

3.1 INTRODUCTION OF GROUP DELAY LINE

Within the last decade, great progress in delay line system has been made and several applications in microwave systems were demonstrated [76-79]. These developments were based on traditional transmission line [76], surface acoustic wave (SAW) [77], magneto-static wave (MSW) device [78] or nonlinear transmission line [79]. All group delay variations are achieved by two methods: one is using the discontinuity in a two-port system where the transmission coefficient can have a nonlinear phase characteristic that enables group delay variation. The other is using the reflections that occur from impedance mismatches in the transmission system. The second method is dependent on

the reflection coefficients, the length of transmission lines and the line losses [80].

Due to the increasing requirement for high performance microwave devices and subsystems, ultra-compact, broadband, low loss electronically tunable delay lines are of great demand. Conventional printed circuit delay lines cannot meet the requirement of large delay time with small form factor. Also, surface acoustic wave (SAW) and magneto-static wave (MSW) device suffered from narrow bandwidth and bulky size [77, 78].

Recently, in [81], the authors have demonstrated a composite right/left-handed (CRLH) delay line, which works in a wide frequency band with good matching performance. It is well suitable for planar circuit fabrication technology. However, this circuit requires a large area and cannot be used in a compact circuit or system.

In this work, we demonstrate a new method of making a compact, tunable delay line based on left-handed nonlinear transmission line (LH NLTL) [82]. Tunable large group delay is achieved by varying the applied control voltage to the series varactors. In addition to its compact size and large tunable delay, this new delay line has several other advantages such as no power consumption and infinite tuning resolution.

3.2 DESCRIPTION OF THE COMPACT TUNABLE DELAY LINE

Left-handed transmission line (LHTL) is an artificial transmission line in which series capacitors and shunt inductors are periodically loaded [82]. By replacing the capacitors with the varactors in the conventional LHTL, left-handed nonlinear transmission line (LH NLTL) can be constructed [74]. By making use of the nonlinearity of the varactors, the LH NLTL could function as a tunable delay line. Figure 3.1 shows a unit cell of LH

NLTL.

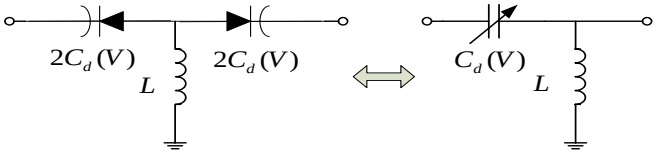

Figure 3.1 The circuit topology of a unit cell of LH NLTL and its equivalent circuit model

The phase propagation constant of LH NLTL [74] is given as (3.1)

$$\beta = -2\arcsin\frac{1}{2\omega\sqrt{L\cdot C_d(V)}} \tag{3.1}$$

where L is the inductance of the shunted inductor, $C_d(V)$ is the half value of diode capacitance. For the minimum return loss, the values of L should satisfy (3.2)

$$L \approx Z_0^2 \cdot C_d(V_{median}) \tag{3.2}$$

where Z_0 is the characteristic impedance of LH NLTL and is selected as 50 Ohm in this paper, $C_d(V_{median})$ is the median value of $C_d(V_{\max})$ and $C_d(V_{\min})$. The resulting group delay in LH NLTL is given as (3.3)

$$\tau_d = N\cdot\frac{d\beta}{d\omega} = \frac{2N}{\omega\sqrt{4\omega^2 L\cdot C_d(V)-1}} \tag{3.3}$$

where N is the section number. We found that the group delay equation expressed in (3.3) can be several nanoseconds when several unit cells are cascaded around Bragg cut-off frequency which is expressed by (3.4). Also, note that delay time can be adjusted with varactor capacitance which is a function of an applied bias voltage. At the Bragg cut-off frequency the line is mismatched and a very large group delay could be achieved.

$$\omega_B = \frac{1}{2\sqrt{L \cdot C_d(V)}} \tag{3.4}$$

In order to maximize delay time and good transmission performance, a frequency of interest should be a little bit higher than the Bragg cut-off frequency.

3.3 FABRICATION AND MEASUREMENT

To prove the theory we presented, a delay line cascaded five LH NLTL units was implemented on a FR-4 board (ε_r = 4.34) with substrate thickness of 1.53 mm. MACOM hyper-abrupt junction GaAs varactor diodes (MA46580) were attached using conductive silver epoxy. The diode capacitance variation range is from 1.3 to 0.8 *pf* for the voltage range of 0 – 2 V. The range is different from the spice model given by the manufacturer's datasheet because of parasitic effects caused by silver epoxy. According to equation (3.2), inductor value should be 2.6 *nH*. However, we found characteristic impedance equation was no longer valid around Bragg cut-off frequency. To have a good reflection performance around Bragg cut-off frequency, 4.7 *nH* inductors manufactured by Taiyo

Yuden were used. This was done with extensive simulation using Agilent ADS software.

Figure 3.2 shows the fabricated dime size delay line. For comparison, we also show that the regular 50 Ω microstrip transmission line that is used to achieve equivalent minimum and maximum group delay exhibited by the LH NLTL we fabricated. Because LH NLTL fabrication requires only several cascaded varactors and shunt inductors, the delay line is very compact. With five unit cells of a LH NLTL shown in Figure 3.2, a large tunable group delay that ranges from 1.2 ns to 2.2 ns was achieved at 1.42 GHz. The two equivalent transmission lines were fabricated with Rogers RO3010 (ε_r =10.2) substrate with a thickness of 1.28 mm. The length of equivalent transmission lines are 11.27 cm and 20.76 cm respectively.

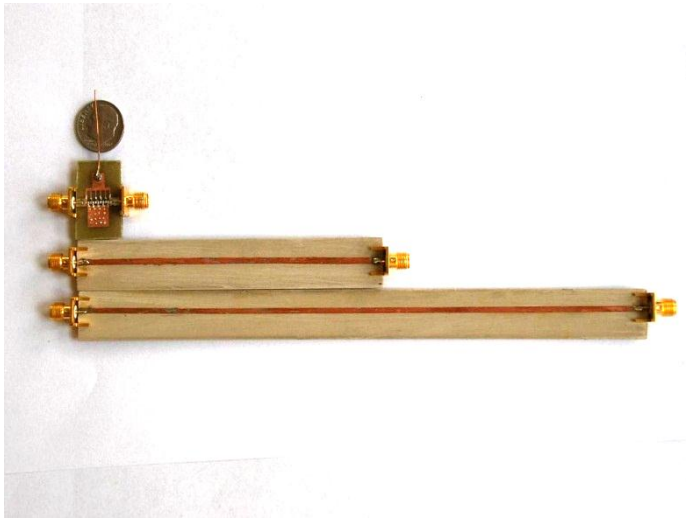

Figure 3.2 Fabricated 5-section LH NLTL delay line and equivalent maximum and minimum group delay line made with Rogers 3010 substrate (ε_r =10.2).

Figure 3.3 shows the measured S parameters according to the applied bias voltage (0 V to 2 V). To maximize the group delay time and achieve low insertion loss, we chose 1.42 GHz which is near Bragg cut-off frequency. Figure 3.4 shows the S parameters and

group delay when the applied voltage changes from 0 V to 2 V. There are two types of losses need to be considered in our LH NLTL delay line. The first loss comes from the choice of operating frequency, which should be chosen near the cut off frequency so that mismatch is generated to achieve large group delay (as can be seen in Figure 3.4, insertion loss is large around Bragg cut-off frequency). The second loss is from the resistance inside varactor diodes. Maximum resistance measured for a varactor is 6.3 Ohm when the reverse voltage changes from 0 V to 2 V. When we simulated the LH NLTL circuit using Agilent Advanced Design System, the result showed loss variation of 1.9 dB to 2.4 dB at 1.42 GHz. However, the measured insertion loss variation was from 3 dB to 5 dB. We concurred that the difference is from parasitic of the silver epoxy we used along with the dielectric loss from the PCB board. The return loss was maintained lower than -10 dB while changing delay time.

As Figure 3.4 shows, a maximum 2.2 ns group delay is achieved with 1 ns tunable range. The calculated group delay using equation (3.3) was also graphed for comparison. Although there is little difference between our calculations and measurements, the result confirmed with the theory. This proves the theory we developed for the LH NLTL is indeed justified.

In addition to the large group delay with small form factor, LH NLTL delay line provides tunable function with infinite resolution, because this delay line can be controlled by an analog voltage. Thus, delay time resolution is exclusively dependent on the Digital to Analog Converter (DAC) resolution. In addition, since this delay line uses reverse bias of the varactor, the power consumption is negligible.

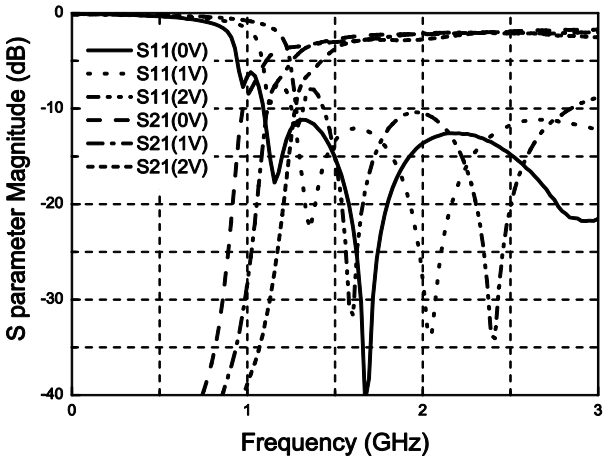

Figure 3.3 Measured insertion and return loss for several reverse bias voltages

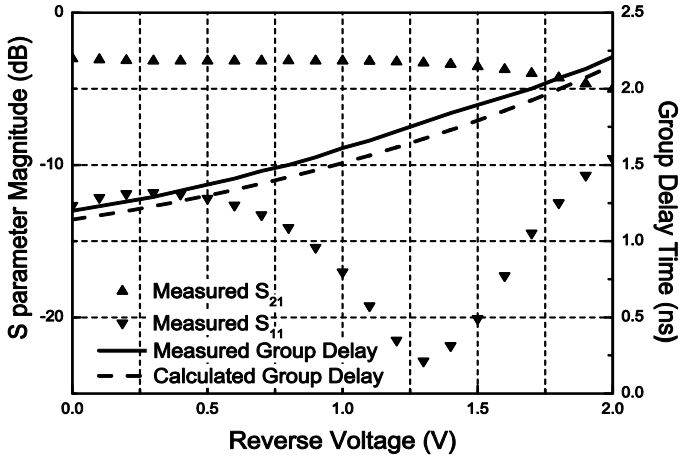

Figure 3.4 Measured S parameters and group delay time according to reverse bias voltage at 1.42 GHz. Maximum 2.2 nS delay with 1 nS delay adjustment was achieved while maintaining return loss less than -10 dB.

3.4 SUMMARY

In this chapter, we presented a novel method to make a compact, large delay line based on LH NLTL. Through experiments, we verified that this delay line offers a tunable large

group delay ranges from 1.2 nS to 2 nS at 1.42 GHz which is near the Bragg cut-off frequency. The delay time is a function of frequency and a number of LH NLTL sections. Its size is very compact compared to other delay circuits reported in literature. Because this circuit can achieve large group delay and delay adjustment with very small length, it is an ideal candidate for modern microwave systems, which require large group delay with small form factor such as a feed-forward amplifier.

4.0 LOW SPURIOUS, BROADBAND FREQUENCY TRANSLATOR USING LEFT-HANDED NONLINEAR TRANSMISSION LINE

In this chapter, we present a frequency translator based on a left-handed nonlinear transmission line (LH NLTL). The proposed LH NLTL can achieve a very linear phase variation as a function of applied DC bias for a broadband frequency that facilitates a low spurious, broadband frequency translation. Our experiment demonstrates that the LH NLTL enables frequency shift with 30 dB maximum spurious suppression. For any frequency between 3 GHz and 3.8 GHz, it was possible to achieve 100 KHz – 1 MHz frequency shift while the range of spurious suppression is between 21 dB and 30 dB. Because of its compactness and possibility of low-cost monolithic fabrication, this circuit is very useful for microwave instrumentation, or a coherent communication system where single sideband modulation is required.

4.1 INTRODUCTION OF FREQUENCY TRANSLATOR

Frequency translation is used in many microwave systems. One of the most important applications is to generate a false target signal in a velocity deception electronic counter measures (ECM) system [15], in which the target translates the frequency of the incoming signal to give false Doppler shift information. Other examples are a microwave

reflectometer system for network analyzers [14], microwave communication systems [83] and frequency scanned antennas [84].

An ideal frequency translator requires a phase shifter with perfectly linear phase shift versus applied DC bias because, in general, a saw tooth modulation is used to translate the original frequency [15]. In addition, phase variation should be exactly 360 degrees to suppress spurious signals at the output. However, most phase shifters reported in literature cannot satisfy all the properties mentioned above and are not suitable to be used as a good frequency translator [16, 17].

In [14], the authors demonstrated a frequency translator with nonlinear transmission line (NLTL) whose structure consists of varactor diodes placed periodically on a transmission line as shunt elements. The frequency translator made with a NLTL works for a wide frequency band, but it has many spurious signals whose magnitudes are quite large at the output. One of the main reasons is that the phase variation versus control voltage is not linear. To minimize spurious signals, the authors had to adjust the modulation signal using a high resolution DAC card [14]. In other words, they used a complex waveform as a phase shifter modulation signal instead of a general sawtooth modulation waveform to minimize the spurs.

In [74], the authors demonstrated a very linear phase shifter for broadband frequency in a compact form. It is based on a device called the left-handed nonlinear transmission line (LH NLTL) [48]. In this thesis, we demonstrate a novel method to make a compact, broadband and low spurious frequency translator based on the LH NLTL. Due to its linear phase variation versus bias voltage, spurious frequencies are greatly reduced.

4.2 FREQUENCY TRANSLATOR BASED ON LH NLTL

A frequency translator can shift up or down the frequency of a RF signal by a desired amount. A signal whose original frequency (f_0) can be increased or decreased by some amount (f_m) using phase modulation. If it is possible to change the phase of a signal by $\theta = 2\pi f_m t$, then it is possible to change the original frequency to a new (translated) frequency through the following equation.

$$V_o = \sin(2\pi f_o t + 2\pi f_m t) = \sin 2\pi(f_o + f_m)t. \tag{4.1}$$

where V_o is the output of a frequency translator. This function can be realized by applying a sawtooth modulation to a phase shifter, which changes the signal phase from 0 ºto 360 º, then goes back to 0 ºinstantaneously [85]. The amount of frequency shift is dependent on the frequency of sawtooth modulation. Thus, having a phase shifter whose phase varies at least 360 ºvery linearly according to the applied voltage at a certain frequency is essential to minimize the spurs at the output. To have a broadband frequency translator, a phase shifter should show such properties over a broad frequency range.

The key reason for the use of LH NLTL phase shifter as a frequency translator is due to its linear phase variation versus voltage and compactness. Figure 4.1 shows the unit cell of a LH NLTL phase shifter, which has two series varactors and a shunted inductor. In [74], the authors simply analyzed the dimensionless propagation constant, the Bragg cutoff frequency and the inductance of the shunt inductor. They demonstrated phase

variation in LH NLTL structure is very linear with the applied DC bias for broadband frequency. This applies to most abrupt and hyper-abrupt varactors.

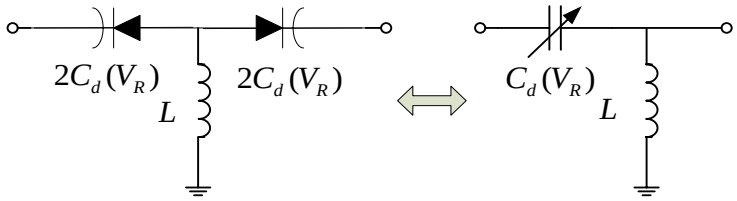

Figure 4.1 A unit cell of LH NLTL and its equivalent circuit model

Figure 4.2 shows a schematic diagram of our experiment to extract the modulated frequency. The phase shifter is serrodyne modulated at f_M. The input carrier frequency (f_0) changes to f_0+f_M at the output of the phase shifter. By combining this signal with an unmodulated original signal through a mixer, a pure modulated frequency (f_M) sinusoidal signal can be acquired at the output. Due to the insertion loss of the phase shifter, an attenuator is used in the other arm to maintain balance before mixing two signals.

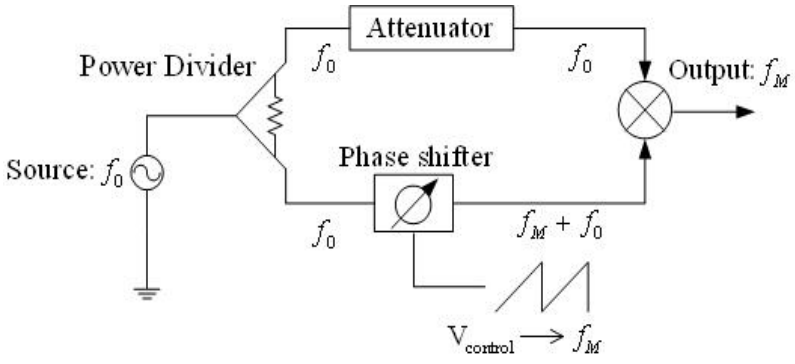

Figure 4.2 Schematic diagram of frequency translator to get a modulated frequency (f_M)

4.3 REALIZATION AND MEASUREMENTS

Our phase shifter shown in Figure 4.3 is realized on an FR4 board. MACOM hyper-abrupt junction GaAs flip-chip varactor diodes (MA46H120) are attached using conductive silver epoxy. The diode capacitance variation range is from 1.9 pF to 0.67 pF when DC bias voltage changes from 0 V to 5 V. The capacitance range is different from the spice model given by the manufacturer's datasheet because of parasitic effects caused by the silver epoxy. According to [7], the inductor value should be 1.6 nH. Inductors were implemented by connecting 0.11 mm diameter copper wire to the backside ground plane. The fabricated phase shifter shown in Figure 4.3 has seven sections of the LH NLTL unit cell. The circuit size is 9mm by 13 mm, neglecting the connector size.

The fabricated phase shifter has very linear phase variation between 3-3.8 GHz. Figure 4.4 shows the measured results for two frequencies (3.2 GHz and 3.5 GHz) versus reverse DC bias voltage. Compared with other phase shifters, the phase linearity of this LH NLTL is excellent. As mentioned before, this is a huge advantage when it is used as a frequency translator.

In this frequency translator experiment, Mini-Circuits 500-5000 MHz power splitter，300-4300 MHz mixer and Pasternack 10 dB attenuator are used.

The maximum resistance of the varactor is 4.5 Ω for the reverse bias voltage between 0 V to 5 V. In our prototype, seven sections of LH NLTL are cascaded to achieve more than 360 ºphase shift for frequencies between 3.0-3.8 GHz. When the circuit is simulated in Agilent ADS software, the maximum insertion loss is 6.1 dB. However, the maximum insertion loss measured is 10.3 dB, which is higher than the simulated result.

Figure 4.3 Fabricated 7-section LH NLTL phase shifter using FR4 substrate

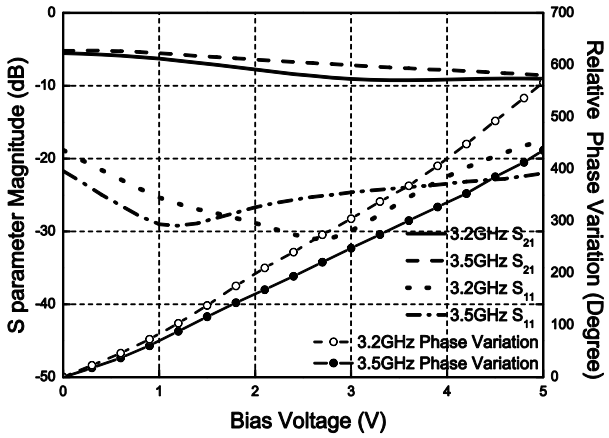

Figure 4.4 Measured results of the fabricated phase shifter at 3.2GHz and 3.5 GHz

The spurs are both from the variation of the magnitude and phase nonlinearity as we change DC bias. Because we have used fixed attenuator in the experiment, the variation of insertion loss in the phase shifter is one of the main reasons that cause the spurs. The other reason is the non-linearity of phase change versus bias. Compared with an ideal straight line, the maximum deviation is around 15 degrees for the whole frequency range. The deviation range is unique for different frequencies. Thus, to minimize spurs, a phase

shifter should show flat insertion loss variation and perfectly linear phase variation for the applied DC bias.

For the frequencies between 3-3.8 GHz, we have driven the frequency translator circuit shown in Figure 4.3 with 0 dBm input. The frequency translator worked fine for any modulation frequency between 100 KHz and 1 MHz. For those frequencies, the level of suppression between the translated frequency and the maximum spurious signal ranges from 21 dB to 30 dB. Figures 4.5 and 4.6 show the frequency spectrum of output signals for 3.2 GHz and 3.5 GHz respectively. The best performance is obtained at 3.5GHz as shown in Figure 4.6. We used modulation frequency of 100 kHz. The magnitude of the translated signal is around -25 dBm. The maximum unwanted sideband is 30 dB below the desired translated output. These results are much better than the results in [17]. In [17], the difference between the translated and maximum spurious frequency was 13dB. In [14], the authors delicately adjusted the modulation signal after the phase shifter calibration process and improved the performance of frequency translator. They achieved a 45 dB difference but it requires a significant effort and a very accurate DAC card. Table 2 compares the performance of the frequency translator with those reported in other papers.

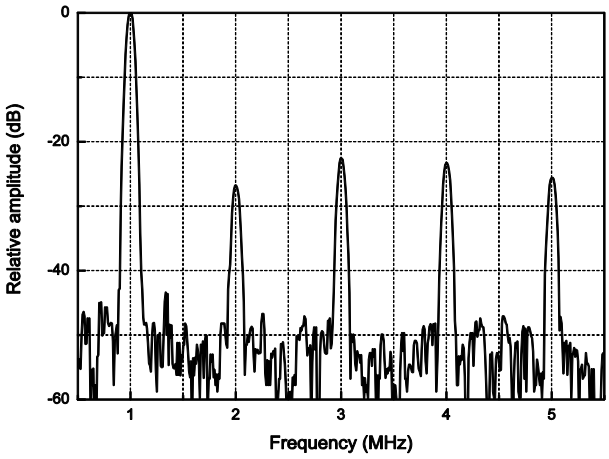

Figure 4.5 Spectrum of output signal at 3.2GHz, modulation frequency is 1 MHz

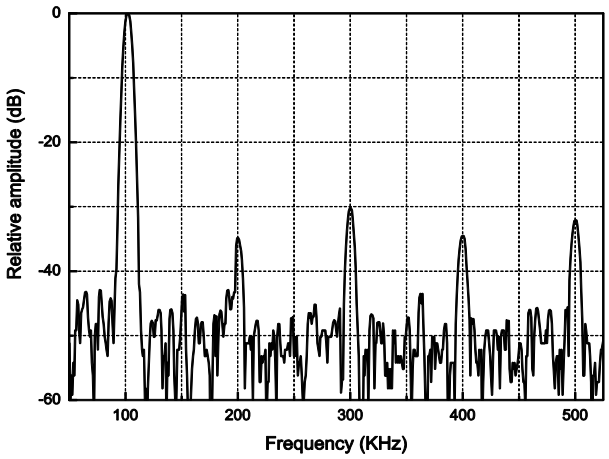

Figure 4.6 Spectrum of output signal at 3.5GHz, modulation frequency is100 KHz

Table 2. Performance Comparison of Frequency Translator

Reference	Conversion loss	Bandwidth	Spurs Rejection	Other Features
[17]	0 dB	200 MHz	13 dB	low cost
[14]	20 dB	2 GHz	45 dB	complex
Our work	25 dB	800 MHz	30 dB	simple

4.4 SUMMARY

In this chapter, we presented a frequency translator based on the LH NLTL for the first time and demonstrated our idea by experiment results. Due to its excellent linearity of the phase shifter versus DC bias voltage, the frequency-modulated signal has 30 dB carrier and spurious signal suppression without the adjustment of modulation signal. In addition, the LH NLTL phase shifter is an ideal component for a frequency translator, because this circuit can be made in a compact form and achieves more than 360 ºby cascading several unit cells. It can be easily made in a monolithic form, as it requires only varactors and inductors. Due to its excellent performance as a frequency translator as mentioned before, it is an ideal candidate for microwave instruments and velocity deception ECM systems where a compact, low-spurious frequency translator is needed.

5.0 COMPACT, TUNABLE WILKINSON POWER DIVIDER USING TUNABLE SYNTHETIC TRANSMISSION LINE

In this chapter, we present a very compact and frequency tunable Wilkinson power divider, which is presented for the first time. By replacing λ/4 section lines in a conventional Wilkinson power divider with varactor tunable, lumped-element synthetic transmission lines, dramatically size reduction and frequency tunability can be achieved. This proposed circuit has excellent performance. For tunable frequencies within 1 GHz, the insertion loss is less than 3.8 dB, whereas the return loss and isolation are greater than 20 dB. However, the size of this voltage controllable Wilkinson power divider occupies less than 3% area of original Wilkinson power divider structure.

5.1 INTRODUCTION

Power dividers are essential elements in RF and microwave systems. The Wilkinson power divider [86] is widely used because of its useful property of being perfectly matched at all ports and good isolation between the outputs [87]. However, because it requires a very large size, especially in low frequency, and its bandwidth is quite limited, circuit designers have tried to solve these problems. Thus, numerous articles have been published in this field of research [18-22]. Simply, to minimize size, they have used

synthetic lumped element transmission lines to replace λ/4 sections in a conventional Wilkinson power divider [18]. In this case, although the size is very small, it suffers from large insertion loss and narrowband performance. To increase bandwidth, multi λ/4 sections should be used at the expense of large area [19]. Recently, several dual-band and broadband power dividers are reported [20, 21, 23], but they still require microstrip transmission lines that make the size of the power divider large.

Periodically, loaded varactors on a transmission line form a nonlinear transmission line that can be used as a broadband phase shifter [47, 88]. By replacing a long transmission line with a lumped element inductor and varactor, a compact NLTL could be constructed [24, 25]. The main idea of this article is to replace the λ/4 sections of the conventional Wilkinson power divider with the lumped element NLTLs to minimize size and have frequency tunability. We have achieved a smaller size and more tunability compared to previous work [89] and presented theories to construct a compact Wilkinson power divider with NLTLs. Because of its compactness and wide range tunability, it is useful in modern multi-mode and multi-band wireless communication systems.

5.2 DESCRIPTION OF THEORY

5.2.1 NLTL theory

As there are numerous articles regarding NLTL theory [24], we only briefly review the background regarding NLTL physics. Figure 5.1 shows a section of a NLTL, which is constructed with a series inductor and a shunt varactor.

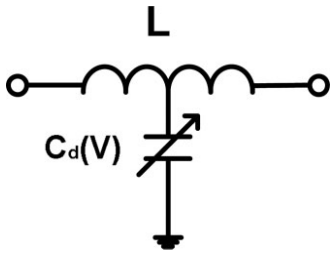

Figure 5.1 A section of a NLTL

As this is a low-pass filter structure, a periodic cutoff frequency (Bragg cutoff frequency) exists when we cascade several identical sections. This cutoff frequency is defined as

$$f_{Bragg} = \frac{1}{\pi \cdot \sqrt{L \cdot C_d(V)}} \tag{5.1}$$

where L is a series inductor and $C_d(V)$ is a shunt varactor capacitance. In this synthetic transmission line, when the frequency is much lower than Bragg cutoff frequency, the characteristic impedance (Z_{NLTL}) is approximated with (5.2)

$$Z_{NLTL} = \sqrt{\frac{L}{C_d(V)}} \tag{5.2}$$

The phase propagation constant (β_{NLTL}) is given as (5.3),

$$\beta_{NLTL} = \omega\sqrt{L \cdot C_d(V)} \tag{5.3}$$

Note that the diode capacitance can be controlled with DC-bias voltage, and every parameter is a function of diode capacitance.

5.2.2 Compact, tunable Wilkinson power divider

Figure 5.2 shows the main idea of this article that λ/4 Sections in a conventional Wilkinson power divider can be replaced by synthetic NLTL whose phase propagation constant is λ/4. Because the frequency for NLTL to have λ/4 phase propagation changes as we change DC bias voltage, the frequency tunable Wilkinson power divider can be constructed.

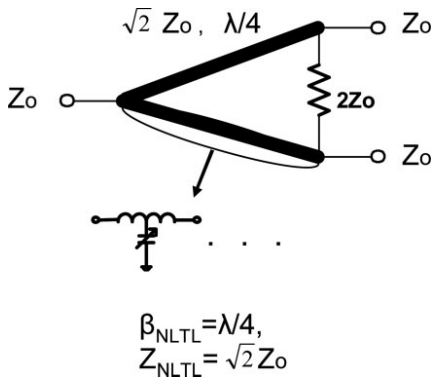

Figure 5.2 A compact, tunable Wilkinson power divider

5.2.3 Considerations for actual implementation

The frequency of interest should be much lower than Bragg cutoff frequency so that (5.2) and (5.3) are effective. Because several NLTL sections are cascaded in actual implementation, the total phase propagation (β_{NLTL_tot}) is

$$\beta_{NLTL\_tot} = n \cdot \omega \sqrt{L \cdot C_d(V)} \tag{5.4}$$

where n is the number of NLTL sections.

Because β_{NLTL_tot} should be $\pi/2$ for our novel Wilkinson power divider, the relationship between the frequency of the Wilkinson power divider and varactor capacitance is as follows:

$$f_{wilkinson} = \frac{1}{4n\sqrt{L \cdot C_d(V)}} \tag{5.5}$$

5.3 FABRICATION AND MEASUREMENT

For the size comparison, Figure 5.3 shows conventional Wilkinson power divider (left) whose frequency is 710 MHz and our novel Wilkinson power divider (right) side by side. Except input and output 50 Ω transmission lines, the size of ours is merely 4 mm by 8 mm which occupies around 3% of the space of conventional Wilkinson power divider shown in the left. For the fabrication of the suggested circuit, we used MACOM

MA46580 varactor whose capacitance varies from 2.1 to 1.0 pF for DC bias from 1 to 2 V. Three NLTL sections are cascaded. For the inductor, Taiyo Yuden 6.8 nH inductors are used. For 50 Ω input and output terminals, characteristic impedance of *λ/4* section should be 70.7 Ω. To minimize reflection, we set characteristic impedance to be around 70 Ω when the diode capacitance is 1.4 pF. Table 3 reveals maximum, median, and minimum diode capacitances and corresponding theoretical characteristic impedance (Z_{NLTL}) and frequency of Wilkinson power divider ($f_{Wilkinson}$). The circuits are fabricated with FR4 board.

Figure 5.4 shows the performance of our Wilkinson power divider. In the graph, we did not show S_{31}, S_{33}, and S_{32} because those parameters are very similar to S_{21}, S_{22}, and S_{23}, respectively. For DC bias voltage between 1 and 2 V, the insertion loss (S_{21}) was maintained above -3.52 dB, whereas return loss (S_{11} and S_{22}) and isolation (S_{23}) are maintained below -20 dB. The best performance was obtained when the DC bias was 1.4 V. At that voltage, insertion loss (S_{21}) was -3.41 dB and return loss (S_{11} and S_{22}) and isolation (S_{23}) were below -33 dB. The characteristic impedance was set to 70 Ω of *λ/4* sections at 1.4 V, and minimum reflection occurred at the voltage and best performance was obtained. The frequencies for tunable Wilkinson power divider were 710, 830, and 990 MHz for 1, 1.4, and 2 V, respectively. They agree well with calculated results shown in Table3. The measured insertion loss of conventional Wilkinson power divider shown in Figure 5.3 was -3.21 dB. The insertion loss of our tunable one shows 0.3 dB lager than conventional one. This is from resistance inside inductors and varactors.

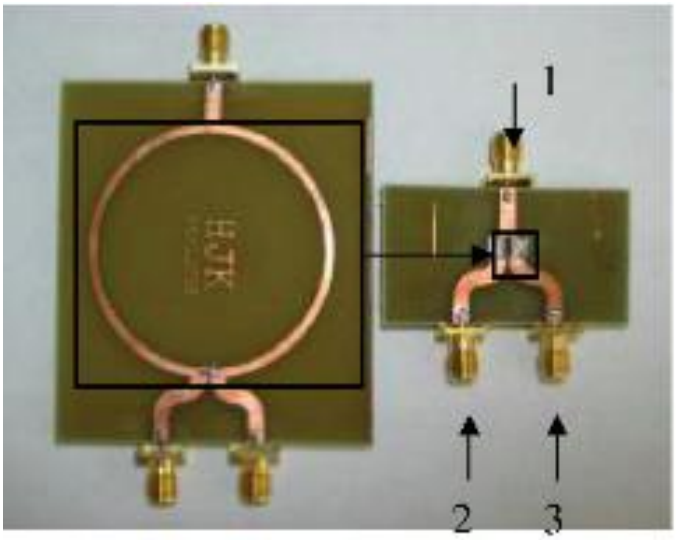

Figure 5.3 Our novel Wilkinson power divider (right) and conventional Wilkinson power divider (left), operating frequency of conventional one is 710 MHz, whereas our new one is frequency tunable between 680 and 990 MHz

Table 3. Maximum, Median and Minimum DC Biases and Corresponding Diode Capacitance, Characteristic Impedance, and Wilkinson Power Divider Frequency

DC (V)	1	1.4	2
Varactor Cap. (pF)	2.1	1.4	1.0
Z_{NLTL} (Ohm)	57	70	82.4
$F_{wilkinson}$ (MHz)	697	854	1010

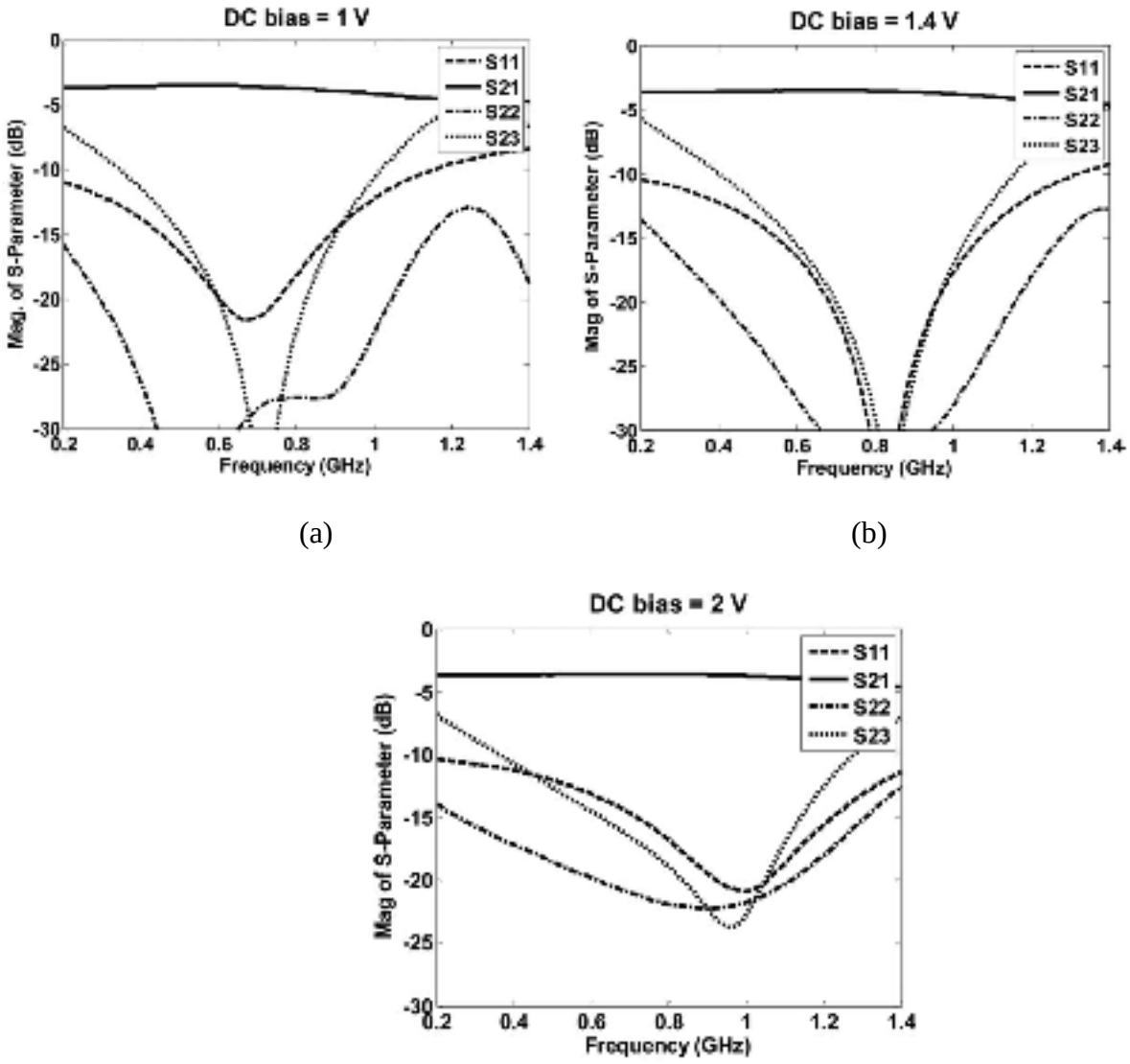

Figure 5.4 Performance of tunable Wilkinson power divider, (a) DC bias is 1 V, (b) DC bias is 1.4 V, and (c) DC bias is 2 V. Frequencies for Wilkinson power divider is 710, 830, and 990 MHz for 1, 1.4, and 2 V DC bias, respectively

5.4 SUMMARY

We demonstrated a very compact, broadband tunable Wilkinson power divider for the first time. By replacing λ/4 sections in conventional Wilkinson power divider structure

with series inductors and shunt varactors, both compactness and tunability have been achieved. We presented theories and equations regarding this novel Wilkinson power divider. The performance of this new prototype circuit matches well with theoretical prediction we have suggested. This structure is especially useful for low frequencies (less than 1 GHz) where λ/4 transmission lines occupy a large area in a conventional Wilkinson power divider design. Because of its compactness and wide range tunability, it is very useful in multi-mode, multi-band wireless or RADAR system, where compact and tunable power divider is needed.

6.0 SUBSTRATE INTEGRATED WAVEGUIDE ANTENNA ARRAY

Conformal array antennas have a wide range of application in the military and civilian application due to their benefits of aerodynamic superiority, wide angle coverage and volume reduced [26]. A typical application of the conformal antenna is the aircraft radar, which needs low profile, light weight and excellent performance for navigation and communication [90]. Because the conformal antennas are integrated with the non-planar surfaces of the object, supplementary air-resistance could be avoided, thus the fuel consumption could be significantly reduced.

Another important application of this conformal array antenna is for mobile robots. In [2, 3] a directional antenna is mounted on the robot for localization in unknown radio sources. This directional antenna has some limitation in beam coverage. In [4] Graefenstein J. et al rotated the directional antenna to achieve high accuracy of localization. However, the rotated antenna is driven by motor, which is slow and energy inefficiency. Therefore, the proposed multi-beam antenna provides a new option for robots mentioned above.

One approach to design cylinder conformal array antenna is to use a number of discrete antennas arrayed along the circumference of the cylinder [26]. Considerable works were done in the past 30 years [91]. The first conformal dipole arrays mounted on the cylinder was proposed in 1980 [92]. Six years later conformal cylindrical microstirp

array was invented [93]. Among all kinds of conformal antennas, slots antenna is a popular candidate because it adds advantage of fabrication simplicity, high efficiency and low cross-polarization level [27].

However, rectangular waveguide components are bulky and costly because high precision mechanical tuning is required in manufacture. To overcome these drawbacks, researchers developed the substrate integrated waveguide (SIW), which provides a wide application for microwave circuits [94]. Meanwhile, it shows excellent integration performance with microstrip and coplanar circuits. Furthermore, because of the tolerance control advantage, SIW technique is appropriate for mass production.

In this chapter, a SIW cylinder conformal multi-beam antenna, which is fed by a SIW conformal Butler matrix, is presented for the first time. Since the slots antennas and Butler matrix can be fabricated on a single substrate, not only the size, weight and cost are reduced, but also the reliability of the manufacture is enhanced.

Because the physical dimensions along the E-plane is much shorter than that along the H-plane, the radiation pattern tends to have a very wide beamwidth in the E-plane and a relatively small beamwidth in the H-plane. This problem can be solved by arranging slotted waveguides in parallel. By stacking waveguides, the E-plane beamwidth can be greatly reduced. In addition, by adding a phase delay to each waveguide, the array of the waveguides can be steered in the E-plane.

The achievements of this research are listed as follows:

1. Design of the conformal SIW slots antenna.
2. Design of the conformal SIW Butler Matrix.

3. Realization of the SIW multi-beam conformal array by combining the conformal SIW slots antenna and the conformal SIW Butler Matrix.

4. The characterization of the conformal far-field pattern calculation method is presented for the first time and the calculation result agrees with the experimental results well.

6.1 INTRODUCTION

SIW also named as post-wall waveguide or laminated waveguide, is a promising candidate for millimeter-wave application. This periodic waveguide, as shown in Figure 6.1, is composed of two rows of conducting cylinders embedded in a dielectric substrate that connect two parallel metal plates. In this system, a synthetic rectangular metallic waveguide filled with dielectric material is constructed in a planar form, thus allowing a complete integration with other planar transmission line circuits, such as microstrip and coplanar waveguide, on the same substrate. The main propagation mode is TE_{10}, and the character is dominated by *a, d, h, p.* '*a*' is the width of the SIW. '*d*' is the diameter of the conducting cylinder. '*h*' is the thickness of the substrate. '*p*' is the periodical distance of two cylinders. Now PCB and LTCC technology can achieve multi-layer SIW, which are similar to traditional waveguides [54, 64, 95, 96].

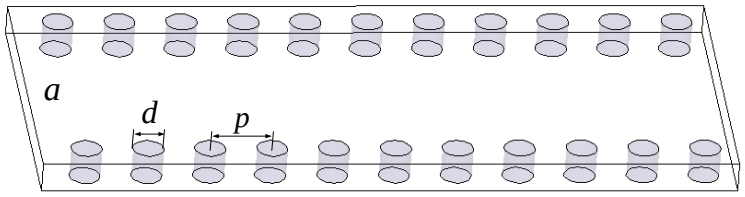

Figure 6.1 SIW structure

There are two analysis methods for SIW. One is full wave analysis; another is equivalent model method [95]. The former is the most accurate way for complicated electromagnetic structure. However, it takes a lot of computing time so the latter equivalent model method is used in this work.

Among all the structure character parameters, attention constant α and phase constant β are the most important ones. α represents the effect of energy leakage from gaps of the periodical cylinders, substrate insertion loss, and mental insertion loss. β dominates the wavelength and the electrical character. Based on the similar propagation character with traditional waveguide, the equivalent waveguide width can be expressed as follows:

$$\bar{a} = \xi_1 + \frac{\xi_2}{\frac{p}{d} + \frac{\xi_1 + \xi_2 - \xi_3}{\xi_3 - \xi_1}} \tag{6.1 a}$$

$$\xi_1 = 1.0198 + \frac{0.3465}{\frac{a}{p} - 1.0684}, \quad \xi_2 = -0.1183 - \frac{1.2729}{\frac{a}{p} - 1.2010}, \quad \xi_3 = 1.0082 - \frac{0.9163}{\frac{a}{p} + 0.2152}$$

(6.1 b)

The equivalent permittivity can be calculated by (6.2) and (6.3)

$$\varepsilon_{r_{eff}} = 1 + q(\varepsilon_r - 1) \tag{6.2}$$

$$q = \frac{1}{2}\left[1 + \left(1 + \frac{12h}{W}\right)^{-1/2}\right] \tag{6.3}$$

6.2 FUNDEMENTALS OF SLOTS ANTENNA

An antenna is typically defined as a structure that can transmit and receive a wave in free space. Theoretically, antenna can transfer all energy generated by the source to the receiver. However, in reality total transfer is impossible due to conduction-dielectric losses and mismatch. In wireless communication systems the antenna is on the front-end of RF chain, therefore, antenna electrical performance dominates the whole systems output power and sensitivity.

Large numbers of antenna have been invented for radio, television, cellular phone and satellite. In this section, various types of antenna are briefly introduced. The most popular antenna is wire antenna, which is used in everyday life on cars, buildings, ships, and aircrafts with the shapes of straight wire [97], loop [98] and helix [99]. These antennas are featured by low cost with acceptable performance.

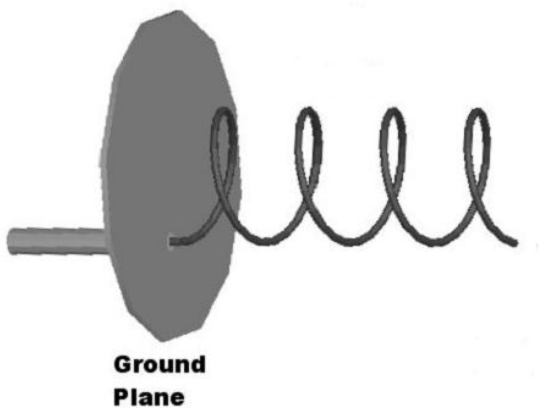

Figure 6.2 Helix antenna

Aperture antenna [99] is another popular one, which is widely used for aircraft and spacecraft since they can be easily flush-mounted on the skin of the aircraft (Figure 6.3). Furthermore, they can be covered with suitable dielectric materials to protect them from hazardous conditions of the environment.

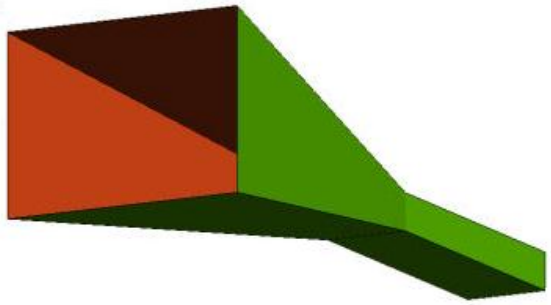

Figure 6.3 Aperture antenna

Microstrip antennas [99] have been widely used since 1970s for space borne applications. They are usually a metallic patch on a ground substrate as in Figure 6.4. Microstrip antennas are low-profile, conformable to planar surfaces and low-cost.

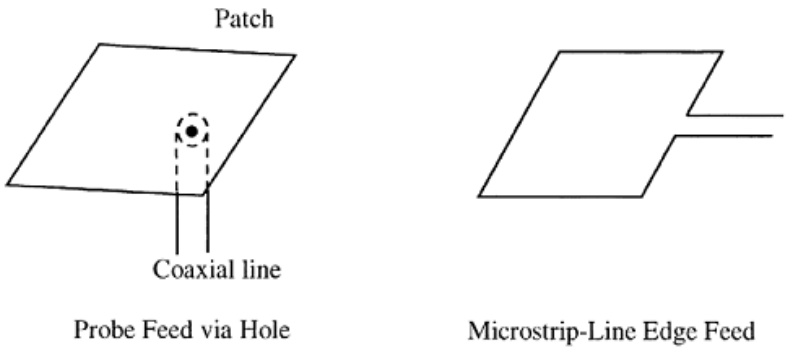

Figure 6.4 Rectangular microstrip patch antenna [99]

Slots antennas are used typically at frequencies between 300 MHz and 24 GHz. The slots antenna is popular because they can be cut out of whatever surface they are to be mounted on, and have radiation patterns that are roughly omnidirectional (similar to a linear wire antenna). The polarization of the slots antenna is linear. The slot size, the slot shape and what is behind the cavity, offer design variables that can be used to tune performance. The traditional slots antenna has problems such as large size, heavy weight, difficulty of integration and high cost. In comparison, SIW antenna can easily be integrated to passive and active circuit to minimize the system size and reduce the cost. The fabrication of SIW antenna does not need tuning and is suitable for mass production of millimeter wave circuits.

SIW slots antenna is designed based on waveguide slots antenna. This is the standard microwave antenna with numerous applications, such as radar and communication systems, which require narrow-beam or shaped-beam radiation patterns [99-102]. Resonant arrays of longitudinal slots in the broad wall of rectangular waveguides have an additional advantage of very low cross-polarization levels. Design procedures for these arrays are mainly based on the work published by Elliott [103] and Coetzee [101]. The

slot spacing of such an array should be one-half guide wavelength at the design frequency, in order to locate the slots at the standing wave peaks. All radiators have the same phase and their amplitude distribution must be arranged carefully to achieve the given gain and side-lobe levels. However, rectangular waveguide components are voluminous and expensive for industrial manufacture. High precision mechanical adjustment or a subtle tuning mechanism is needed to obtain the resonant slots at the standing wave peaks. According to theory in [104], the electromagnetic field in the traditional waveguide can be expressed as following,

For TE_{mn} mode:

$$\begin{aligned} H_z &= jH_{az}e^{\mp\gamma_\alpha z} \\ E_t &= E_{at}e^{\mp\gamma_\alpha z} \\ H_t &= \pm H_{at}e^{\mp\gamma_\alpha z} \end{aligned} \tag{6.4}$$

For TM_{mn} mode:

$$\begin{aligned} E_z &= jE_{az}e^{\mp\gamma_\alpha z} \\ E_t &= E_{at}e^{\mp\gamma_\alpha z} \\ H_t &= \pm H_{at}e^{\mp\gamma_\alpha z} \end{aligned} \tag{6.5}$$

where

$$
\begin{aligned}
H_{az} &= \cos\frac{m\pi x}{a}\cos\frac{n\pi y}{b} \\
E_{az} &= \sin\frac{m\pi x}{a}\sin\frac{n\pi y}{b} \\
\gamma_{\alpha} &= +\sqrt{(\frac{m\pi}{a})^2+(\frac{n\pi}{b})^2-k^2}
\end{aligned}
\tag{6.6}
$$

The transverse vector electromagnetic field can be expressed as follows:

For TE_{mn} mode:

$$
\begin{aligned}
E_{at} &= \frac{\omega\mu_0}{\gamma_{\alpha}{}^2+k^2}(l_x\frac{\partial H_{az}}{\partial y}-l_y\frac{\partial H_{az}}{\partial x}) \\
H_{at} &= -\frac{j\gamma_{\alpha}}{\gamma_{\alpha}{}^2+k^2}(l_x\frac{\partial H_{az}}{\partial x}+l_y\frac{\partial H_{az}}{\partial y})
\end{aligned}
\tag{6.7}
$$

For TM_{mn} mode:

$$
\begin{aligned}
E_{at} &= -\frac{j\gamma_{\alpha}}{\gamma_{\alpha}{}^2+k^2}(l_x\frac{\partial E_{az}}{\partial x}+l_y\frac{\partial E_{az}}{\partial y}) \\
H_{at} &= -\frac{\omega\varepsilon_0}{\gamma_{\alpha}{}^2+k^2}(l_x\frac{\partial E_{az}}{\partial y}-l_y\frac{\partial E_{az}}{\partial x})
\end{aligned}
\tag{6.8}
$$

When a slot is made on the waveguide, the incident wave generates all kinds of TE and TM mode. The energy can be radiated through the slot. The backward and forward scattering coefficients can be expressed as (6.9) and (6.10)

$$B_b = \frac{\int_{slot} (E_1 \times H_2) \cdot dS}{2\int_{s_1} (E_{bt} \times H_{bt}) \cdot l_z dS_1} \tag{6.9}$$

$$C_b = \frac{\int_{slot} (E_1 \times H_2) \cdot dS}{2\int_{s_2} (E_{bt} \times H_{bt}) \cdot l_z dS_2} \tag{6.10}$$

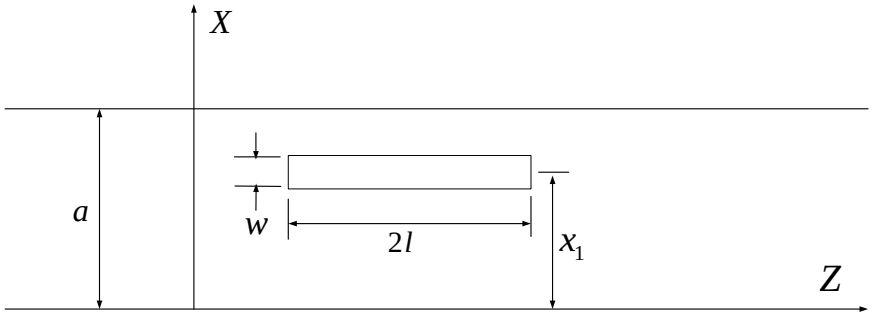

Figure 6.5 Configuration of slot on waveguide

Figure 6.5 shows a slot on the ideal waveguide. Figure 6.6 is the equivalent model for slot on waveguide. From (6.9) and (6.10) we can get following equation:

$$\int_{S_1} (E_{10,t} \times H_{10,t}) \cdot l_z dS_1 = \frac{\omega \mu_0 \beta_{10}}{(\pi / a)^2} \int_0^b d\eta \int_0^a \sin^2 \frac{\pi \xi}{a} d\xi = \frac{\omega \mu_0 \beta_{10} ab}{2(\pi / a)^2} \tag{6.11}$$

Thus

$$B_{10} = \frac{-j\int_{x_1-w/2}^{x_1+w/2} \cos\frac{\pi\xi}{a}\, d\xi \int_{-l}^{l} E_{1x}(\zeta) e^{-j\beta_{10}\zeta} d\zeta}{\omega\mu_0\beta_{10}ab/(\pi/a)^2}$$

$$B_{10} = \frac{(\pi/a)^2 \cos(\pi x_1/a)}{j\omega\mu_0\beta_{10}ab} \int_{-l}^{l} V(\zeta) e^{-j\beta_{10}\zeta} d\zeta \tag{6.12}$$

where $V(\zeta) = wE_{1x}(\zeta)$ is the voltage distribution over the slot.

$$C_{10} = \frac{(\pi/a)^2 \cos(\pi x_1/a)}{j\omega\mu_0\beta_{10}ab} \int_{-l}^{l} V(\zeta) e^{j\beta_{10}\zeta} d\zeta \tag{6.13}$$

Slot voltage $V(\zeta)$ is dominated by slot position and can be equivalent to a loaded transmission line. The characteristic impedance is G_0.

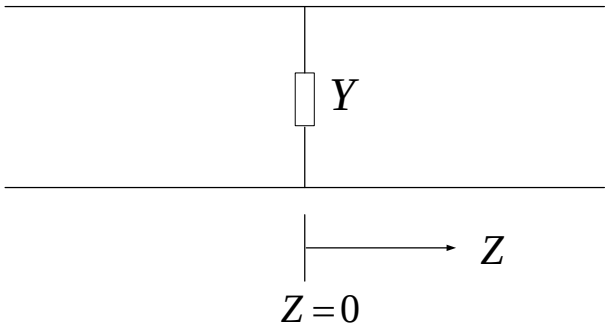

Figure 6.6 Equivalent model for slot on waveguide

A resistor with Y admittance is shunted at position Z=0. The current and voltage on the transmission line can be expressed as (6.14):

$$\begin{aligned} V(z) &= Ae^{-j\beta z} + Be^{j\beta z} \\ I(z) &= AG_0 e^{-j\beta z} - BG_0 e^{j\beta z} \end{aligned} \qquad z < 0$$

$$\begin{aligned} V(z) &= (A+C)e^{-j\beta z} \\ I(z) &= (A+C)G_0 e^{j\beta z} \end{aligned} \qquad z > 0 \tag{6.14}$$

From the boundary condition and symmetry scatting, we can get the incident power, reflection power and transmission power as follows:

$$P_{inc} = \frac{1}{2}\mathrm{Re}\int_{s_1}(A_{10}E_{10,t} \times A_{10}^{*}H_{10,t}^{*}) \cdot l_z dS_1 = \frac{\omega\mu_0\beta_{10}ab}{4(\pi/a)^2} A_{10}A_{10}^{*} \tag{6.15}$$

$$\begin{aligned} P_{refl} &= \frac{\omega\mu_0\beta_{10}ab}{4(\pi/a)^2} B_{10}B_{10}^{*} \\ P_{tr} &= \frac{\omega\mu_0\beta_{10}ab}{4(\pi/a)^2}(A_{10}+C_{10})(A_{10}+C_{10})^{*} \end{aligned} \tag{6.16}$$

The radiation power can be extracted from (6.16), therefore we can obtain (6.17),

$$\frac{\omega\mu_0\beta_{10}ab}{4(\pi/a)^2}[A_{10}^2 - B_{10}^2 - (A_{10}+B_{10})^2] = \text{Radiation power} \tag{6.17}$$

when $2l \cong \lambda_0/2$, the radiation power is simplified as (6.18)

$$-\frac{\omega\mu_0\beta_{10}ab}{2(\pi/a)^2} B_{10}(A_{10}+B_{10}) = 0.609\frac{V_m V_m^{*}}{\pi\eta} \tag{6.18}$$

Thus, we can extract characteristic impedance *G* of the slot as equation (6.19).

$$kl \cong \pi / 2$$

$$\frac{G}{G_0} = [2.09 \frac{(a/b)}{(\beta_{10}/k)} \cos^2(\frac{\beta_{10}}{k} \frac{\pi}{2})] \sin^2 \frac{\pi x}{a} \tag{6.19}$$

where $x = x_1 - (a/2)$, which is the offset of slot position. Using (6.19), we are able to calculate the admittance of a single slot.

6.3 SLOTS ANTENNA DESIGN METHOD

The method mentioned in Section 6.2 is not accurate for the SIW since slot resonate length changes due to the permittivity of the substrate. Elliott has presented a new method [103], which considers both self-admittance and mutual coupling. The method is quite suitable for SIW slots antenna design.

When the incident wave is TE_{10}, Elliott gave the first formula for slots antenna (6.20), which can be used to design the slot length and offset according to the voltage distribution.

$$\frac{Y_n^a}{G_0} = \{ j[\frac{8(a/b)}{\pi^2 \eta G_0 (\beta/k)}]^{1/2} (\cos \beta l_n - \cos k l_n) \sin \frac{\pi x_n}{a} \} \frac{V_n^s}{V_n} \tag{6.20}$$

Because there is mutual coupling existed between slots, the total slot voltage is composed of three parts.

$$V_n^s = V_{n,1}^s + V_{n,2}^s + V_{n,3}^s \tag{6.21}$$

where $V_{n,1}^s$ is slot voltage caused by the TE_{10} mode wave which propagating toward Z direction with magnitude A_{10}^n; $V_{n,2}^s$ is slot voltage caused by the TE_{10} mode wave which propagating toward -Z direction; $V_{n,3}^s$ is the slot voltage caused by the other slots.

From the reciprocity theorem, we can get equation (6.22)

$$\begin{aligned} V_{n,1}^s &= \frac{1}{Kf_n} \frac{\frac{Y}{G_0}(x_n, l_n)}{2 + \frac{Y}{G_0}(x_n, l_n)} A_{10}^n \\ V_{n,2}^s &= \frac{1}{Kf_n} \frac{\frac{Y}{G_0}(x_n, l_n)}{2 + \frac{Y}{G_0}(x_n, l_n)} D_{10}^n \end{aligned} \tag{6.22}$$

Figure 6.7 is the schematic diagram of the two slots on the waveguide. l_n is the nth slot length, x_n is the offset. z_n is the position of the center of the slot.

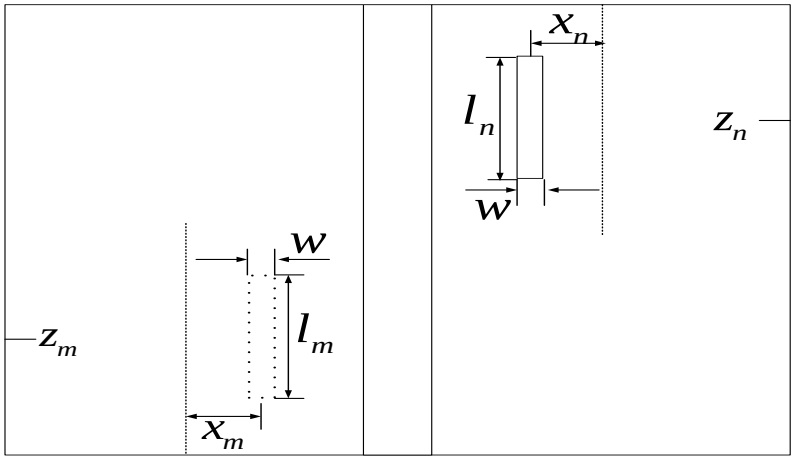

Figure 6.7 Schematic diagram of the two slots on the waveguide

From Elliott's theory, the $V_{n,3}^s$ can be expressed as following:

$$V_{n,3}^s = -j(\beta_{10}/k)(k_0 b)(a/\lambda)^3 \frac{1}{f_n^2} \frac{\frac{Y}{G_0}(x_n, l_n)}{2+\frac{Y}{G_0}(x_n, l_n)} \cdot \sum_{m=1}^{N} {}'V_m^s g_{mn}(x_m, l_m, x_n, l_n) \quad (6.23)$$

$$\begin{aligned} g_{mn} = \int_{-k_0 l_m/2}^{k_0 l_m/2} \Bigg\{ & \cos\left(\frac{z_m^{'}}{2l_m/\lambda_0}\right) \frac{1}{2l_m/\lambda_0} \cdot \left[\frac{e^{-jk_0 R_1}}{k_0 R_1} + \frac{e^{-jk_0 R_2}}{k_0 R_2} \right] \\ & + \left[1 - \frac{1}{(2l_n/\lambda_0)^2} \right] \cdot \int_{-k_0 l_n/2}^{k_0 l_n/2} \cos\left(\frac{z_n^{'}}{2l_n/\lambda_0}\right) \frac{e^{-jk_0 R}}{k_0 R} dz_n^{'} \Bigg\} dz_m^{'} \end{aligned} \quad (6.24)$$

where R is the distance between $P_n(0,0,\zeta_n^{'})$ and $P_m(0,0,\zeta_m^{'})$. R_1 and R_2 express the distances from P_m to $P_{n,1}(0,0,l_n)$ and P_m to $P_{n,2}(0,0,-l_n)$, respectively. From the total slot voltage, we get the second design formula (6.25).

$$\frac{Y_n^a}{G_0} = \frac{2 f_n^2(x_n, l_n)}{\frac{2 f_n^2(x_n, l_n)}{\frac{Y}{G_0}(x_n, l_n)} + j(\beta_{10} / k)(k_0 b)(a/\lambda)^3 \sum_{m=1}^{N}{}' \frac{V_m^s}{V_n^s} g_{mn}(x_m, l_m, x_n, l_n)} \tag{6.25}$$

With (6.21) and (6.25), we get the following design procedure. The initial value of the slot length l_n is set to half wavelength, and offset X_n equals zero. The initial value of (6.25) is calculated.

$$\sum_{m=1}^{N}{}' \frac{V_m^s}{V_n^s} g_{mn}(x_m, l_m, x_n, l_n) \tag{6.26}$$

where $\frac{V_m^s}{V_n^s}$ is the slot voltage distribution. We get a set of (x_n, l_n), which makes the denominator of right part of (6.25) real number. Another set of (x_m, l_m) is also found to meet the same requirement to make the denominator of right part of (6.25) real number. Both slots must comply the following equation (6.27) :

$$\frac{Y_n^a / G_0(x_n^{'}, y_n^{'})}{Y_m^a / G_0(x_m^{'}, y_m^{'})} = \frac{f_n(x_n^{'}, y_n^{'})}{f_m(x_m^{'}, y_m^{'})} \frac{\sin k l_n}{\sin k l_m} \frac{V_n^s / V_n}{V_m^s / V_m} \tag{6.27}$$

Once the n[th] slot (x_n, l_n) has been found, other slots parameters can be calculated and the values are unique. This procedure is iterated until the stable values are found.

6.4 CONFORMAL ANTENNA

A conformal antenna is an antenna that conforms to some object, which is a cylinder in our case. The purpose is to build the antenna so that it is integrated with the structure and does not cause extra drag. The purpose can also be that the antenna integration makes the antenna less disturbing and less visible to the human eyes.

A typical application of the conformal antenna is on the aircraft (Figure 6.8) [26], which has many antennas protruding from its structure, for navigation, communication, radar, and so on. Typically, twenty or more antennas are installed in the aircraft, causing considerable drag and increased fuel consumption. Thus, integrating antenna into the aircraft skin is important. Array antennas with radiation units on the surface of a cylinder, sphere, or cone, are usually called conformal arrays. These antennas may have their shape determined by a specific electromagnetic requirement such as beam width and angular coverage.

A cylindrical or circular array has a potential of 360-degree coverage by using an omnidirectional beam or multiple beams. Today lots of base stations in a mobile communication system are using this technology.

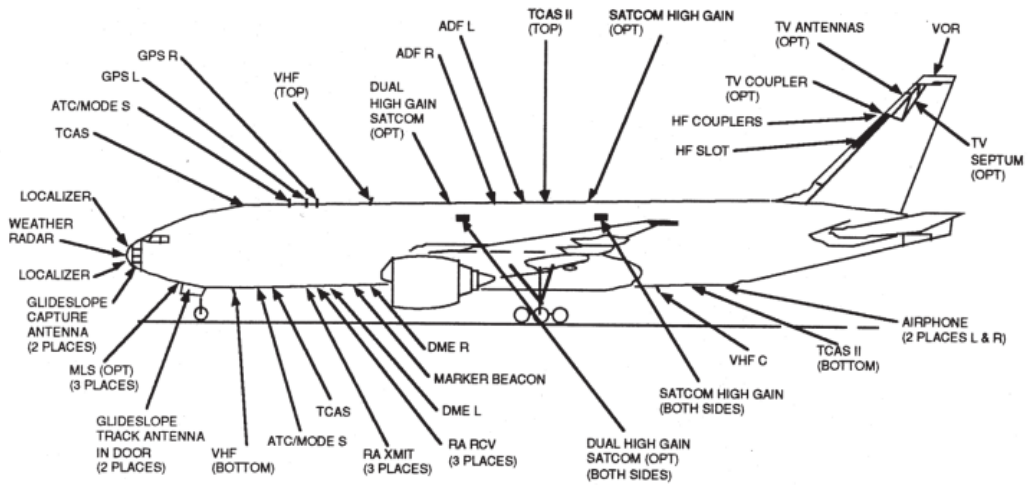

Figure 6.8 Antennas protrude from the skin of a modern aircraft [26]

For the past three decades, phased array has been always a popular research field. Many studies have been done for conformal arrays. With the solution for feeding and steering problems, electronically scanned and phased array antennas were used widely. Meanwhile, booming development of integrated circuit technology, including monolithic microwave integrated circuits (MMIC), provides perfect solution to reduce high cost [105]. Another technology, high rate digital processor, contributed enormously to the development of phased array system [106] because of its cost advantage.

On the other hand, electromagnetic models and design need to be developed. During the last two decades, electromagnetic analysis methods and the understanding of antennas on curved surfaces have improved tremendously. Important progress has been made in high-frequency techniques, including analysis of surface wave diffraction [107] and modeling of radiating sources on curved surfaces [108].

The conformal arrays first appeared in the nineteen thirties. Two decades later the circular array was attractive in electronic industry because of its rotational symmetry. Proper phasing of this array can create a directional beam, which can be scanned 360 ° in azimuth. Its applications were in broadcasting, communication, and later also navigation. During World War II, circular arrays were developed for radio signal intelligence gathering and direction finding in Germany. After the war, an experimental Wullenweber array [109] was developed at the University of Illinois. This array had 120 radiating elements in front of a reflecting screen. Many similar systems were built in other countries during the Cold War. Today 'smart skin' conformal antenna [110] is required for modern communications, which constitutes a complete RF system, including not only the radiating elements but also feed networks, amplifiers, control electronics, power distribution, cooling, filters, and so on, all in a multilayer design that can be tailored to various structural shapes [26].

6.5 DESIGN OF SIW CONFORMAL ANTENNA

In this section, we use SIW technology to design a cylinder conformal slots antenna. This SIW antenna is less expensive than conventional waveguide slots antenna, easier for fabrication in PCB, and more compactable with large power transmission. The achieved SIW conformal antenna is suitable for mass production without any mechanical tuning. The top view and the side view of the proposed antenna schematic diagrams are shown in Figure 6.9 and 6.10.

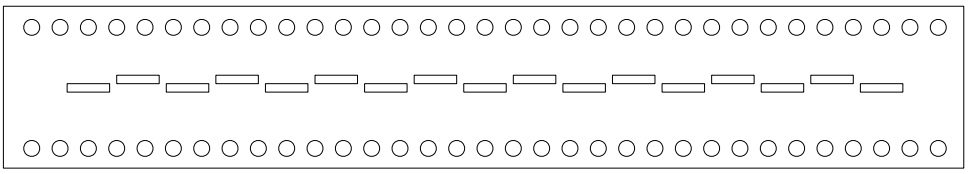

Figure 6.9 Top view of conformal slots antenna

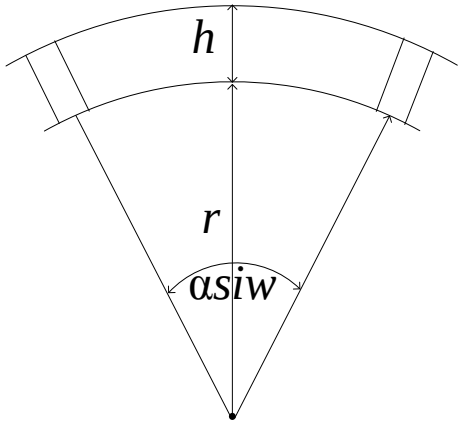

Figure 6.10 Side view of conformal slots antenna

Firstly, the initial values of slots size in the conventional waveguide are calculated by Elliott's method. Then the equivalent formulas were applied to convert the conventional design to SIW flat structure. Finally, with Computer Simulation Technology (CST) microwave studio optimization, we can get the SIW conformal slots antenna. The detail structures of the SIW conformal slots are shown in Figure 6.11.

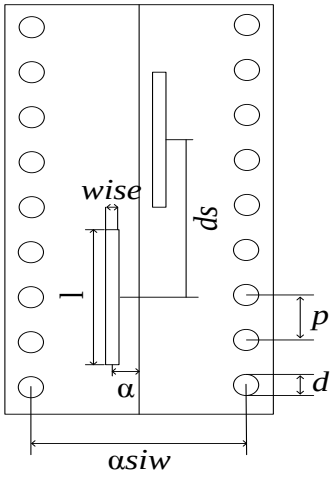

Figure 6.11 Two slots on the SIW structure

According to the optimization results, we can calculate the dimension of the antenna. The via diameter *d*=0.6 mm, distance between the via *p*=1.2 mm. The thickness of substrate *h*=0.5 mm, *r*=71.1 mm, α*siw*=8.78 degree, slot width *wise*=0.2 degree, *ds*=13.5 mm. The total length of the antenna is 385 mm. The dimensions of each slot are shown as in Table 4.

Table 4 17 Slots dimensions

N	*l/mm*	*α/degree*	N	*l/mm*	*α/degree*
1	11.5	-0.2	10	11.7	0.18
2	11.6	0.15	11	11.6	-0.2
3	11.5	-0.2	12	11.5	0.18
4	11.5	0.18	13	11.6	-0.2
5	11.6	-0.17	14	11.8	0.23
6	11.7	0.17	15	11.8	-0.2
7	11.5	-0.2	16	11.6	0.2
8	11.6	0.2	17	11.6	-0.2
9	11.5	-0.19			

6.6 MULITI-BEAM ANTENNA

In recent years, the growing demand of high-performance, low cost, compact scanning antennas for telecommunication and surveillance applications has boosted the development of planar electronic scanning antennas. The operation of a generic electronically-scanned multi-beam antenna can be presented schematically as in Figure 6.12. N radiators are fed by M input ports by means of a beam-forming network (BFN) that should provide the required phase and amplitude to each radiator in order to obtain the desired far-field pattern and pointing direction. Besides, to steer the antenna's main beam, the BFN should be able to control the phase gradient provided to each radiator. In the case of phased array, a dedicated transmitter/receiver module is used for each radiator for a continuous 2D scanning of the antenna's main beam at the expense of losses and increasing cost. These BFNs are usually realized by baseband processing. In this section, we introduce a new multi-beam antenna array, which includes SIW Butler Matrix [111] and SIW slots antenna.

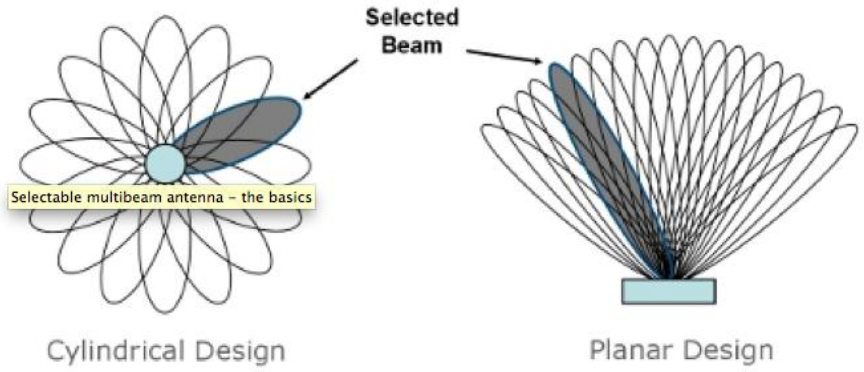

Figure 6.12 Cylindrical and planar multi-beam antennas [112]

6.6.1 Principle of the multi-beam antenna

The theory of multi-beam antenna has been discussed in [112]. In section 6.6.1 and section 6.6.2, we briefly introduce the fundamentals of the multi-beam antenna. Usually multi-beam antenna has M input ports and each port has a corresponding beam. Therefore, the incident wave and reflected wave at all ports can be expressed as matrixes [X], [Y].

$$[X]=\begin{bmatrix} x_1 \\ x_2 \\ \vdots \\ x_M \end{bmatrix} \quad , \quad [Y]=\begin{bmatrix} y_1 \\ y_2 \\ \vdots \\ y_M \end{bmatrix} \tag{6.28}$$

$$[Y]=[S][X]$$

where [S] is a reflection matrix for each port. When $x_k = 1, x_i = 0 \;\; i \neq k$ and input ports match with load, the antenna's far-field pattern can be described as follows.

$$E_k(\theta,\varphi) = q_k R_k(\theta,\varphi)\frac{e^{-jkr}}{r} \tag{6.29}$$

where q_k is constant. $R_k(\theta, \varphi)$ is normalized radiation power. Thus, the radiation power can be expressed as following equation (6.30).

$$(P_{rad})_k = |q_k|^2 \leq 1 \tag{6.30}$$

Since the input power P_{in}=1 and the reflected power $P_{ref} = \sum_{i=1}^{M} |S_{ik}|^2$, we can get equation (6.31).

$$|q_k|^2 \le 1 - \sum_{i=1}^{M} |S_{ik}|^2 \tag{6.31}$$

Due to the insertion loss of the antenna, the left part is always smaller than right part in (6.31). Furthermore, $|q_k|^2$ dominates the gain of an antenna. And the cross coupling between adjacent radiation units is the main reason to reduce the total radiation power. Additionally, when the multi-beam antenna works at the receiver side, its receiving cross section is $|q_k|^2$ times of omnidirectional antenna, which has the same far-field pattern $R_k(\theta, \varphi)$. Thus $|q_k|^2$ can be used to express the effect of cross coupling between adjacent radiation units.

The coupling coefficient of far-field patterns is shown in the following equation (6.32).

$$\beta_{kj} = 60\pi \int_0^{2\pi} \int_{-\frac{\pi}{2}}^{\frac{\pi}{2}} R_k^*(\theta, \varphi) \cdot R_j(\theta, \varphi) \cos\theta \, d\theta \, d\varphi \tag{6.32}$$

$$\beta_{jj} = 1, \quad |\beta_{kj}|^2 \le 1$$

If input power is provided at each port, we can get following equations.

$$P_{in} = [X]^{+}[X], \quad P_{ref} = [Y]^{+}[Y] = [X]^{+}[S]^{+}[S][X]$$

$$E(\theta,\varphi) = \sum_{k=1}^{M} x_k E_k(\theta,\varphi) \tag{6.33}$$

$$P_{rad} = \sum_{j\cdot k=1}^{M} x_k^{*} q_k^{*} \beta_{kj} q_j x_j = [X]^{+}[\Gamma][X]$$

Thus (6.34) can be deduced from above equations.

$$[X]^{+}[X] > [X]^{+}[S]^{+}[S][X] + [X]^{+}[\Gamma][X] \tag{6.34}$$

where "+" means conjugate transpose. $\Gamma_{kj} = q_k^{*}\beta_{kj}q_j$. Both $[\Gamma]$ and $[S]^{+}[S]$ are non-negative definite matrixes. A new vector is set as excitation matrix $[X']$.

$$[X] = [U][X'] \tag{6.35}$$

where $[U]$ is a unitary matrix, which diagonalizes $[\Gamma]$. Thus (6.34) becomes (6.36).

$$[X']^{+}([I]-[\gamma])[X'] > [X']^{+}([U]^{+}[S]^{+}[S][U])[X'] \tag{6.36}$$

Because $[U]^{+}[S]^{+}[S][U]$ is a hermitian and non-negative definite matrix, $([I]-[\gamma])$ is diagonal matrix. Thus, we can deduce (6.37) from (6.36).

$$(1-\gamma)_{kj} = \lambda_k^2 \delta_{kj}, \quad \lambda_k^2 = 1-\gamma_k \geq 0$$

$$\gamma_k \leq 1, \quad (\gamma_k)_{\max} \leq 1 \tag{6.37}$$

Therefore, when each branch has the same effective coefficient $(q_k = q)$, $\Gamma_{kj} = |q|^2 \beta_{kj}$ and $\gamma_{kj} = |q|^2 \beta_k$, we can get (6.38) from (6.37).

$$|q|^2 \leq 1/(\beta_k)_{\max} \leq 1 \tag{6.38}$$

According to (6.38), the effective coefficient has up and down limitations, which depends on the far-field pattern. When $\beta_{kj} = 0 (k \neq j)$, each far-field pattern is orthogonal. $[\beta]$ is diagonal matrix, $\beta_{jj} = 1 \quad (\beta_k)_{\max} = 1$, $|q|^2 \leq 1$. When $|q|^2 = 1$, all branches are completely orthogonal. On the other hand, if each far-field pattern is not orthogonal $\beta_{kj} \neq 0$, it is very difficult to get $(\gamma_k)_{\max}$ and $(\beta_k)_{\max}$.

6.6.2 Features of the multi-beam antenna

Multi-beam antenna is composed of radiation units and feeding network, which provides certain magnitude and phase distributions. Usually this feeding network is a multi-port network and can be described as a scattering matrix [S].

$$[b] = [S][a], \quad [S] = \begin{bmatrix} [S_{11}] & [S_{12}] \\ [S_{21}] & [S_{22}] \end{bmatrix} \tag{6.39}$$

where [a] and [b] are incident wave and reflected wave respectively. $[S_{11}]$ and $[S_{22}]$ are reflection matrixes at input and output ports. $[S_{12}]$ and $[S_{21}]$ are the transmission matrixes shown as (6.40). If two-way components are used in the network, we can get equation $[S_{12}]=[S_{21}]$.

$$[S_{12}]=\begin{bmatrix} S_{1,M+1}, & \cdots, & S_{1,M+N} \\ \vdots & & \\ S_{M,M+1}, & \cdots, & S_{M,M+N} \end{bmatrix} \tag{6.40}$$

where M is the number of input ports, N is the number of the output ports. $S_{k,M+1},\cdots,S_{k,M+N}$ are the signal magnitude at each output port if applying nominal power only at the K_{th} input port. If ignoring the cross coupling, we can get the following array factor (6.41).

$$\Psi_k(u)=a_k\sum_{n=1}^{N}S_{k,M+N}e^{jnu}\ ,\quad u=\frac{2\pi d}{\lambda}\sin\theta \tag{6.41}$$

where a_k is the signal magnitude of k_{th} input port, d is the space of radiation units. $\Psi_k(u)$ is 2π periodic function. Based on (6.41) we can get equation (6.42).

$$\frac{1}{2\pi}\int_{-\pi}^{\pi}\Psi_l(u)\Psi_k^*(u)du=a_l a_k^*\sum_{n=1}^{N}S_{l,M+n}S_{k,M+n}^* \tag{6.42}$$

Furthermore, the lossless condition of the beam-forming network is shown as (6.43),

$$\sum_{i=1}^{M+N} S_{l,i} S_{k,i}^{*} = \delta_{l,k} \tag{6.43}$$

where $\delta_{l,k} = \begin{cases} 1, & l = k \\ 0, & l \neq k \end{cases}$. The non-reflection and coupling conditions are listed as (6.44).

$$[S_{11}] = [S_{22}] = 0 \tag{6.44}$$

Based on above formulas, (6.45) can be deduced.

$$\int_{-\pi}^{\pi} \Psi_l(u) \Psi_k^{*}(u) du = 2\pi \left| a_l \right|^2 \delta_{l,k} \tag{6.45}$$

As a result, if every array factor of beam is orthogonal in a period, each radiation unit is uncorrelated. Thus, we can get following system described as (6.46).

$$[S_{12}] = \begin{bmatrix} \alpha_1\beta_1 & \alpha_2\beta_1\lambda_1 \cdots & \alpha_N\beta_1\lambda_1^{N-1} \\ \vdots & & \\ \alpha_1\beta_N & \alpha_2\beta_N\lambda_N \cdots & \alpha_N\beta_N\lambda_N^{N-1} \end{bmatrix} \cdot \frac{1}{\sqrt{N}} \tag{6.46}$$

where β_i is the complex magnitude of the i_{th} input port. $\alpha_k \lambda_i^{k-1} (k = 1, \cdots, N)$ is the excitation magnitude at each radiation unit with normalized power at the i_{th} input port. From (6.45) and (6.46), we can get equations shown as (6.47).

$$\begin{aligned} \alpha_i^2 \sum_{k=1}^{N} |\beta_k|^2 &= 1, \quad i = 1, \cdots, N \\ |\beta_k|^2 \sum_{i=1}^{N} \alpha_i^2 &= 1, \quad \mathrm{k} = 1, \cdots, N \end{aligned} \tag{6.47}$$

From the first formula of (6.47) we can find that each radiation unit has the same excitation magnitude $\alpha_i^2 = \left[\sum_{k=1}^{N} |\beta_k|^2 \right]^{-1}$. Thus, the far-field pattern has a uniform distribution on magnitude. The second formula of (6.47) shows that the absolute value of β_i should be the same. Provided $\beta_i = e^{j\theta_i}$, $[S_{12}]$ can be described as (6.48).

$$[S_{12}] = [D_1] \left[S_{12}{}' \right] [D_2] \tag{6.48}$$

where

$$[D_1] = \begin{bmatrix} 1 & 0 & \cdots & 0 \\ 0 & \lambda_1 & \cdots & 0 \\ \vdots & & & \vdots \\ 0 & 0 & \cdots & \lambda_1^{N-1} \end{bmatrix}, \quad [D_2] = \begin{bmatrix} e^{j\theta_1} & 0 & \cdots & 0 \\ 0 & e^{j\theta_2} & \cdots & 0 \\ \vdots & & & \vdots \\ 0 & 0 & \cdots & e^{j\theta_N} \end{bmatrix}$$

$$\left[S_{12}{}'\right]=\begin{bmatrix}1 & 1 & \cdots & 1\\ 1 & P_2 & \cdots & P_2^{N-1}\\ \vdots & \vdots & & \vdots\\ 1 & P_N & \cdots & P_N^{N-1}\end{bmatrix},\quad P_i=\frac{\lambda_i}{\lambda_1}$$

Therefore, we can get (6.49).

$$e^{jN(\varphi_i-\varphi_k)}=1,\quad N(\varphi_i-\varphi_k)=2n\pi,\quad \varphi_i-\varphi_k=\frac{2n\pi}{N},\quad n=0,\cdots,(N-1) \tag{6.49}$$

As a conclusion, the total number of the beams is the same as the number of radiation units (output ports). Each beam is equally distributed with distance $2\pi/N$. The array factor is described as (6.50).

$$\Psi_k(u)=\frac{\sin\frac{N}{2}(u-\frac{2k\pi}{N})}{N\sin\frac{1}{2}(u-\frac{2k\pi}{N})},\quad u=\frac{2\pi d}{\lambda}\sin\theta \tag{6.50}$$

where *k* is the beam sequence number.

6.6.3 Beam forming network

Figure 6.13 shows a cascaded beam forming network [112], which is composed by two systems. One is the antenna feeding system, while the other one is coupling system, which connects to the radiation units and feeding system.

In order to generate different beams, phase distribution needs to be carefully designed and the phase shifters are applied in the feeding system. The magnitude distribution is usually achieved by couplers but most couplers are two-way devices to cause unwanted energy from adjacent feeding line by cross coupling, which increases the side lobe and degrades the antenna system.

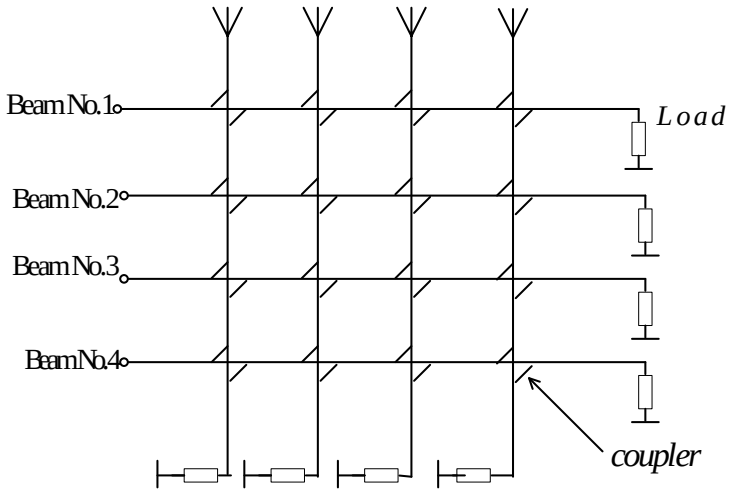

Figure 6.13 Cascade beam-forming network

Compared with the cascaded beam-forming network, the Butler Matrix network is more efficient. Depending on which of N inputs is accessed, the antenna beam is steered

in a specific direction in one plane. Butler Matrix can be combined in two ‘layers’ to facilitate 3D scanning. It performs a similar function to a phased array antenna system. The Butler matrix was first described by Jesse Butler and Ralph Lowe in a paper titled “Beam-Forming Matrix Simplifies Design of Electronically Scanned Antennas” [111].The primary characteristics of the Butler matrix are:

1. N inputs and N outputs, with N usually 4, 8 or 16;
2. Inputs are isolated from each other;
3. Phases of N outputs are linear with respect to their position and beam is tilted off main axis;
4. None of the inputs provides a broadside beam;
5. The phase increment between the adjacent outputs depends on the used input.

6.6.4 Butler matrix theory

It is obvious that Butler Matrix is the key device to form the multi-beam system. We also know that the most important components in Butler Matrix are 3 dB couplers and phase shifters [113-115]. Figure 6.14 shows a two-unit Butler Matrix multi-beam array, which uses the simplest Butler Matrix. The voltage and phase distributions are identified in the Figure 6.14. Antenna 1 and 2 are fed by the 3 dB coupler to form two beams.

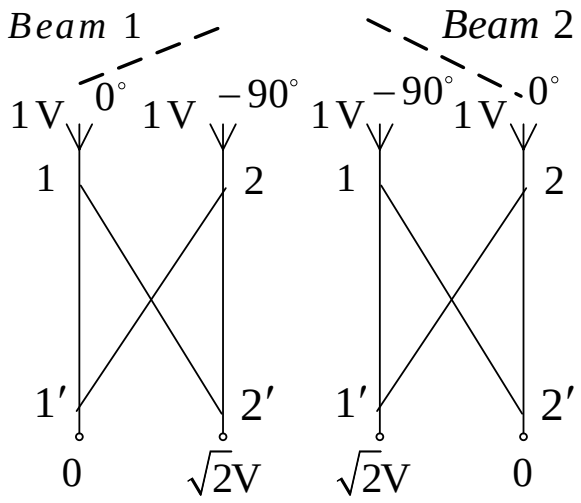

Figure 6.14 Two units Butler Matrix multi-beam array

Figure 6.15 is a four-beam forming network, which achieves four radiation beams. The phase difference and magnitude between adjacent output ports are described in Figure 6.15. Each beam direction is shown as in Figure 6.16. This Butler Matrix has following features:

1. The number of radiation units $N = 2^K$, where K is a positive integer;
2. The number of 3 dB coupler $N_c = \frac{N}{2}\log_2 N = \frac{N}{2}K$
3. The number of phase shifter $N_\varphi = \frac{N}{2}(\log_2 N - 1) = \frac{N}{2}(K-1)$
4. The bandwidth is determined by the couplers and phase shifters;
5. The insertion loss is dominated by the coupler.

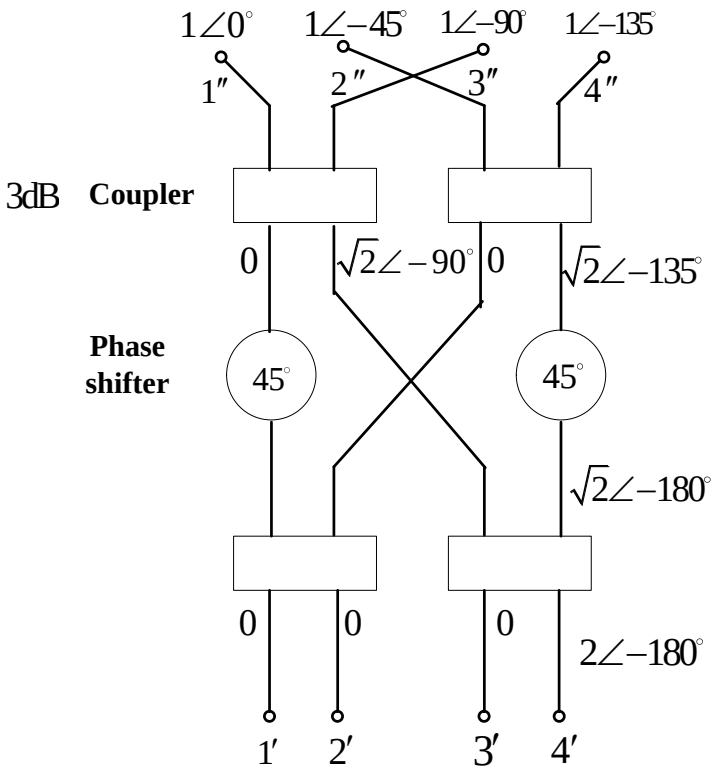

Figure 6.15 4 by 4 Butler Matrix

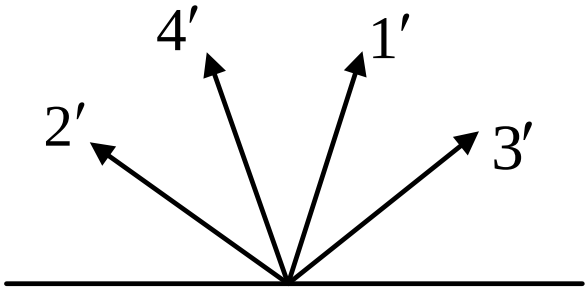

Figure 6.16 Four beams direction

6.6.5 Butler matrix far-field pattern

In this section, we discusses the Butler Matrix far-field pattern calculation [100, 111]. As for an N units array, the radiation pattern is as (6.51).

$$\left|F(\theta)\right| = \frac{\sin\frac{N}{2}\left(\frac{2\pi}{\lambda} d\sin\theta - \delta\right)}{N\sin\frac{1}{2}\left(\frac{2\pi}{\lambda} d\sin\theta - \delta\right)} \tag{6.51}$$

where d is the space of the adjacent radiation units, θ is the underlie angle, δ is the array phase difference due to the spatial phase difference between adjacent units. In order to compensate the spatial phase difference, δ should be π / N. As for the k_{th} beam, δ of the adjacent units can be described as (6.52).

$$\delta = (2k-1)\frac{\pi}{2}\cdot\frac{1}{N/2} = \frac{(2k-1)}{N}\pi \tag{6.52}$$

From (6.51) and (6.52), we can get the Butler multi-beam far-field pattern shown as (6.53).

$$\left|F(\theta)\right| = \frac{\sin N\left(\frac{\pi d}{\lambda}\sin\theta - \frac{2k-1}{N}\cdot\frac{\pi}{2}\right)}{N\sin\left(\frac{\pi d}{\lambda}\sin\theta - \frac{2k-1}{N}\cdot\frac{\pi}{2}\right)} \tag{6.53}$$

Based on equation (6.53), we can find several features for the butler matrix.

1. The position of the maximum magnitude for the k_{th} beam

When N is a large number, $|F(\theta)|$ is approximate to $\sin x / x$. When x=0, $\sin x / x$=1, we can get the maximum magnitude direction θ_k for the k_{th} beam by (6.54).

$$N\left[\frac{\pi d}{\lambda}\sin\theta - \frac{2k-1}{N}\cdot\frac{\pi}{2}\right] = 0 \tag{6.54}$$

$$\sin\theta_k = \frac{\lambda}{Nd}(k-\frac{1}{2}) \tag{6.55}$$

The beam sweep range can be described as (6.56)

$$\theta_{coverage} = 2\arcsin\left[\frac{(N-1)\lambda}{2Nd}\right] \tag{6.56}$$

Based on (6.56) we know that with large N and $d = \lambda/2$, the beam sweep range can cover the whole visual area. When $d > \lambda/2$, the sweep range is smaller, while grating lobes appear. However, we can control the grating lobe at the cost of gain by carefully designing the radiation units.

2. The zero position of the k_{th} beam

When $N\left[\frac{\pi d}{\lambda}\sin\theta - \frac{2k-1}{N}\cdot\frac{\pi}{2}\right] = p\pi$, $p = 1,2,3\cdots$ we can get the p_{th} zero position of the k_{th} beam.

$$\sin\theta_{kp} = \frac{\lambda}{Nd}\left(p+k-\frac{1}{2}\right) \tag{6.57}$$

3. The orthogonality of multi-beams

Based on (6.53) we deduce the internal product of the k_{th} and the m_{th} beams.

$$\int_{-\frac{\pi}{2}}^{\frac{\pi}{2}} F_k(\theta) F_m^*(\theta) d\theta = \delta(k-m) \tag{6.58}$$

We find that two ambient beams are orthogonal.

4. The intersection position of the side lobe

The intersection position can be calculated by (6.53). Due to the same magnitude of the k_{th} and the $(k+1)_{th}$ beams, we get (6.59).

$$\frac{\sin N\left(\frac{\pi d}{\lambda}\sin\theta - \frac{2k-1}{N}\cdot\frac{\pi}{2}\right)}{\sin\left(\frac{\pi d}{\lambda}\sin\theta - \frac{2k-1}{N}\cdot\frac{\pi}{2}\right)} = \frac{\sin N\left(\frac{\pi d}{\lambda}\sin\theta - \frac{2k+1}{N}\cdot\frac{\pi}{2}\right)}{\sin\left(\frac{\pi d}{\lambda}\sin\theta - \frac{2k+1}{N}\cdot\frac{\pi}{2}\right)} \tag{6.59}$$

The intersection angle is set to be θ_c .

$$\sin\theta_c = \frac{k\lambda}{Nd}, \theta_c = \arcsin\left(\frac{k\lambda}{Nd}\right) \tag{6.60}$$

Based on (6.60) and (6.53) the intersection level of the two beams can be described as follows.

$$\left|F(\theta_c)\right| = \frac{\sin N\left(\frac{\pi d}{\lambda}\cdot\frac{k\lambda}{Nd} - \frac{2k-1}{N}\cdot\frac{\pi}{2}\right)}{\sin\left(\frac{\pi d}{\lambda}\cdot\frac{k\lambda}{Nd} - \frac{2k-1}{N}\cdot\frac{\pi}{2}\right)} = \frac{1}{\sin\frac{\pi}{2N}} \tag{6.61}$$

6.7 CONFORMAL SIW BUTLER MATRIX DESIGN

In this section, we discuss how to realize the Butler Matrix using SIW technology.

The SIW Butler Matrix design includes two parts:

1. SIW coupler design;

2. SIW phase shifter design.

With carefully designing of the above components, we can get a multi-beam feeding network.

6.7.1 Conformal SIW coupler design method

The SIW coupler design method [116, 117] is described as follows. The matrix for a reciprocal four-port network is described as (6.62).

$$[S] = \begin{bmatrix} 0 & S_{12} & S_{13} & S_{14} \\ S_{12} & 0 & S_{23} & S_{24} \\ S_{13} & S_{23} & 0 & S_{34} \\ S_{14} & S_{24} & S_{34} & 0 \end{bmatrix} \tag{6.62}$$

If the network is lossless, we can get following equations.

$$S_{13}^{*}S_{23} + S_{14}^{*}S_{24} = 0 \tag{6.63}$$

$$S_{14}^{*}S_{13} + S_{24}^{*}S_{23} = 0 \tag{6.64}$$

We deduce (6.65) and (6.66) based on (6.63), (6.64).

$$S_{14}^{*}(|S_{13}|^2 - |S_{24}|^2) = 0 \tag{6.65}$$

$$S_{23}^{*}(|S_{12}|^2 - |S_{34}|^2) = 0 \tag{6.66}$$

One solution for (6.65), (6.66) is $S_{14} = S_{23} = 0$, which presents a direction coupler. Then we can get following formulas by multiplying each column by itself from (6.62).

$$\begin{aligned} |S_{12}|^2 + |S_{13}|^2 = 1 \quad |S_{12}|^2 + |S_{24}|^2 = 1 \\ |S_{13}|^2 + |S_{34}|^2 = 1 \quad |S_{24}|^2 + |S_{34}|^2 = 1 \end{aligned} \tag{6.67}$$

In order to simplify the above formulas, we set $S_{12} = S_{34} = \alpha$, $S_{13} = \beta e^{j\theta}$, where α and β are real numbers. The phase difference between port 1 and 3 is θ. The phase difference between port 2 and 4 is φ. Based on above formulas we can deduce the following equation.

$$\theta + \varphi = \pi \pm 2n\pi \tag{6.68}$$

If we ignore *2nπ*, two kinds of couplers can be achieved.

1. Symmetrical coupler ($\theta = \varphi = \pi / 2$)

The scattering matrix is described as equation (6.69).

$$[S] = \begin{bmatrix} 0 & \alpha & j\beta & 0 \\ \alpha & 0 & 0 & j\beta \\ j\beta & 0 & 0 & \alpha \\ 0 & j\beta & \alpha & 0 \end{bmatrix} \tag{6.69}$$

2. Directional coupler ($\theta = 0, \varphi = \pi$)

The phase difference is 180 degree. Thus the scattering matrix is described as (6.70).

$$[S] = \begin{bmatrix} 0 & \alpha & \beta & 0 \\ \alpha & 0 & 0 & -\beta \\ \beta & 0 & 0 & \alpha \\ 0 & -\beta & \alpha & 0 \end{bmatrix} \tag{6.70}$$

$$\alpha^2 + \beta^2 = 1.$$

Figure 6.17 shows a coupler schematic diagram. In this figure, the energy at the port 1 is coupled to the port 3 and this can be presented by the couple factor $|S_{13}|^2 = \beta^2$. The rest of the power is transferred to the port 2. Thus the transfer factor is $|S_{12}|^2 = \alpha^2 = 1 - \beta^2$. In an ideal coupler, no power is transferred to the port 4. The coupler factor *C*, direct transmission factor *D* and isolation *I* can be calculated by (6.71).

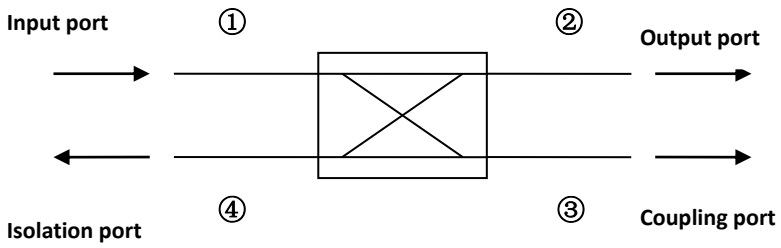

Figure 6.17 Coupler schematic

$$
\begin{aligned}
C &= 10\lg\frac{P_1}{P_3} = -20\lg\beta \ \text{ dB} \\
D &= 10\lg\frac{P_3}{P_4} = 20\lg\frac{\beta}{|S_{14}|} \ \text{ dB} \\
I &= 10\lg\frac{P_1}{P_4} = -20\lg|S_{14}| \ \text{ dB}
\end{aligned}
\tag{6.71}
$$

The relationship of these factors is expressed as following equation.

$$
I = D + C \tag{6.72}
$$

The ideal coupler has infinite transmission factor and isolation.

As we know the fundamental TE_{10} mode in SIW is similar as the fundamental mode in conventional rectangular waveguide. Thus, we can design the rectangular waveguide coupler first and then transfer it to SIW structure using equation (6.1). The following section introduces the procedure for designing a conformal SIW coupler.

Figure 6.18 shows a single slot coupler, which is dominated by the phase design of TE_{10} and TE_{20}. Generally the power at port 2 and 4 is proportional to $\cos(\beta_1 - \beta_2)l/2$ and $\sin(\beta_1 - \beta_2)l/2$ respectively. β_1 and β_2 are the propagation constants of TE_{10} and TE_{20} respectively. The length of slot l is proportional to (β_1-β_2). The coupler performance is also affected by the dielectric constant. When the dielectric constant is a small value, the β_2 is more sensitive than β_1 since the TE_{20} is the main mode in the coupling area. Therefore, the propagation constants of cross coupler and 3 dB coupler should meet the following relations.

$$\begin{cases} (\beta_1 - \beta_2)l/2 = \pi/4 & \text{(3dB coupler)} \\ (\beta_1 - \beta_2)l/2 = \pi/2 & \text{(cross coupler)} \end{cases} \tag{6.73}$$

We can deduce (6.75) from (6.74).

$$\begin{cases} \beta_2 = \dfrac{2n}{2n+1}\beta_1 = \dfrac{2}{3}\beta_1, \dfrac{4}{5}\beta_1, \cdots & \text{(3dB coupler)} \\ \beta_2 = \dfrac{2n-1}{2n+1}\beta_1 = \dfrac{1}{3}\beta_1, \dfrac{3}{5}\beta_1, \cdots & \text{(cross coupler)} \end{cases} \qquad n = 1, 2, 3, \cdots \tag{6.75}$$

where β_1 and β_2 can be calculated by following equations,

$$\beta = \sqrt{k^2 - (k_c)_{mn}^2} \tag{6.76}$$

$$(k_c)_{mn} = \sqrt{(\frac{m\pi}{a})^2 + (\frac{n\pi}{b})^2} \tag{6.77}$$

$$k = \omega\sqrt{\varepsilon\mu} \tag{6.78}$$

where *a* and *b* are length and width of the rectangular waveguide respectively. Using above formulas we can get the initial values of *w* and *l*. Then the waveguide structure can be transferred to a SIW one by (6.1). Finally based on the flat SIW coupler, conformal structure can be achieved by full-wave optimization using 3D EM field simulation software CST.

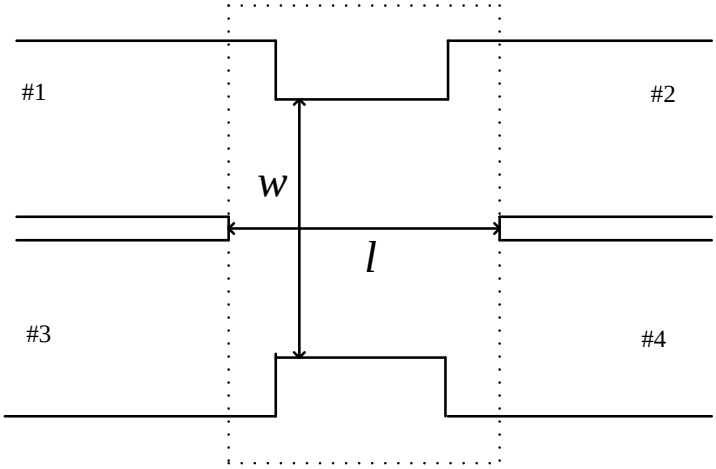

(a)

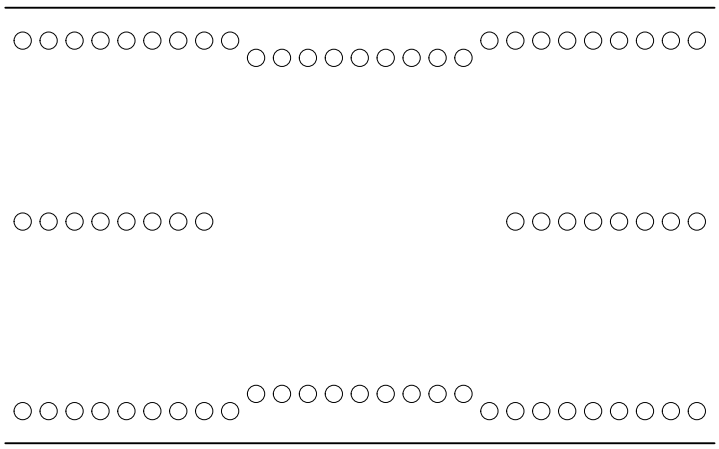

(b)

Figure 6.18 (a) Waveguide single slot coupler, (b) SIW single slot coupler

6.7.2 Conformal SIW phase shifter design method

Phase shifters are common components in phased array antennas and other microwave communication systems. Many researchers focus on the size, broad bandwidth and amplitude balance of a phase shifter. It is well known that ferrite toroidal phase shifter has excellent electrical performance such as high Q value and high power handing capability. This phase shifter is widely used in the phased array system [118]. However, its drawbacks are obvious including the bulky size, the high cost and the heavy weight. Recently, SIW has been proposed to replace the waveguide technology [119]. Compared with other technologies such as MMIC GaAs phase shifter [120], reflective-type phase shifter [121] and MEMS phase shifter [122], SIW phase shifter has following features such as high Q-factor, low insertion loss, possibility for mass-production and easiness of integration with planar circuits [52].

Figure 6.19 shows the schematic diagram of SIW phase shifter. The width of waveguide is in proportion to the propagation constant. Therefore, we can control the width of the waveguide to realize different phase transmission. The initial values of a_1 and a_2 can be calculated by (6.79).

$$\sqrt{\left(\frac{2\pi}{\lambda}\right)^2-\left(\frac{1}{a_1}\right)^2}-\sqrt{\left(\frac{2\pi}{\lambda}\right)^2-\left(\frac{1}{a_2}\right)^2}=\frac{\text{phase difference}}{l} \tag{6.79}$$

The Substrate Integrated Waveguide is equivalent to a conventional metallic rectangular waveguide filled with dielectric. Therefore, we can use (6.1) to transfer the traditional phase shifter to SIW structure. The conformal SIW phase shifter is optimized based on the flat structure.

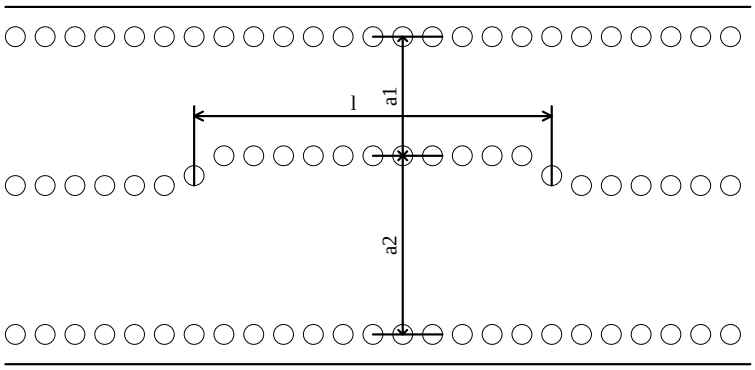

Figure 6.19 SIW phase shifter

6.7.3 Conformal SIW Butler matrix design results

We design a conformal SIW Butler Matrix, which has four input ports shown in Figure 6.20. Each port has a corresponding radiation beam. The relationship between port and phase difference is listed in Table 5. The 3 dB couplers and cross couplers are applied in this Butler Matrix. Both couplers have 90 degree phase shifting.

Table 5 Phase difference between adjacent output ports according to each input port

Input port	1	2	3	4
Phase difference	-45	135	-135	45

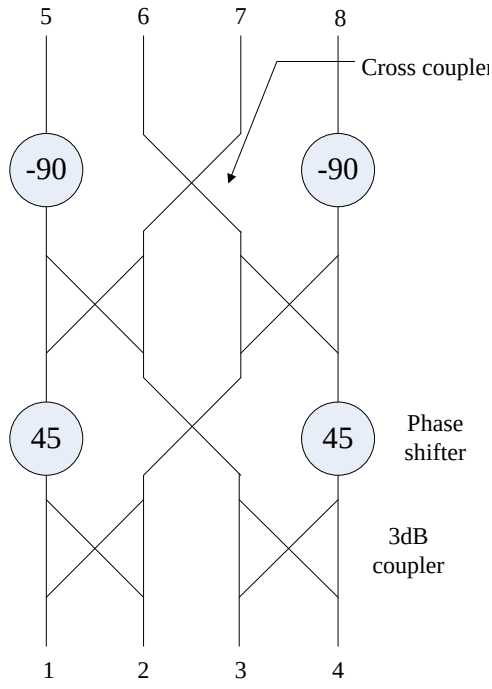

Figure 6.20 Butler Matrix with four input ports

Figure 6.21 shows the SIW Butler Matrix schematic diagram. The vias are put on a single layer PCB. The top and bottom layers of the PCB are copper. The substrate relative dielectric constant is 2.2. The thickness of substrate is 0.5 mm. The structure parameters are listed as follows.

Table 6 SIW Butler Matrix parameters

w/mm	*w1*/mm	*l1*/mm	*w2*/mm	*l2*/mm	*w3*/mm	*l3*/mm	*w4*/mm	*l4*/mm
10.97	20.74	13.19	12.4	40.8	10.52	19.95	20.94	25.2

where *w* is the SIW width, *w1* and *l1* are the width and the slot length of the 3 dB coupler, respectively. *w2* and *l2* are the width and the length of the 45 degree phase shifter, respectively. *w3* and *l3* are the width and the length of the -90 degree phase shifter, respectively. *w4* and *l4* are the width and the slot length of the cross coupler, respectively. The commercial software Microwave Studio Office CST 3D simulation has been used in this design.

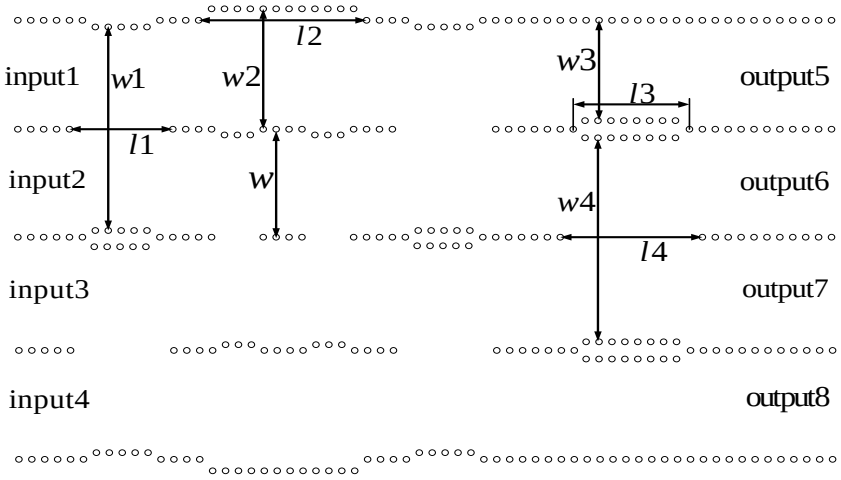

Figure 6.21 SIW Butler Matrix

Figure 6.22 shows the simulated return loss and isolation at the input port 1 in the bandwidth of 11-12 GHz. The isolations are close to 20 dB from 11.2-11.6 GHz, while the return loss is better than 20 dB. Figure 6.23 presents simulated transmission coefficients when the matrix is fed at port 1. They are close to the theoretical value of 6 dB over the operating frequency band.

The theoretical relative phase between adjacent output ports is shown in Table 5. Figure 6.24 shows the simulated phase difference for port 1. The phase difference between different output ports when the signal is fed at port 1 is -45°±5° over the frequency range.

Figure 6.25 shows the simulated return loss and isolation at the input port 2 in the bandwidth of 11-12 GHz. The isolations are close to 20 dB from 11.2-11.6 GHz, while the return loss is better than 15 dB. Figure 6.26 presents simulated transmission coefficients when the matrix is fed at port 2. They are close to the theoretical value of 6 dB over the operating frequency band. Figure 6.27 shows the simulated phase difference

for port 2. The phase difference between different output ports when the signal is fed at port 2 is 136° ±5° over the frequency range.

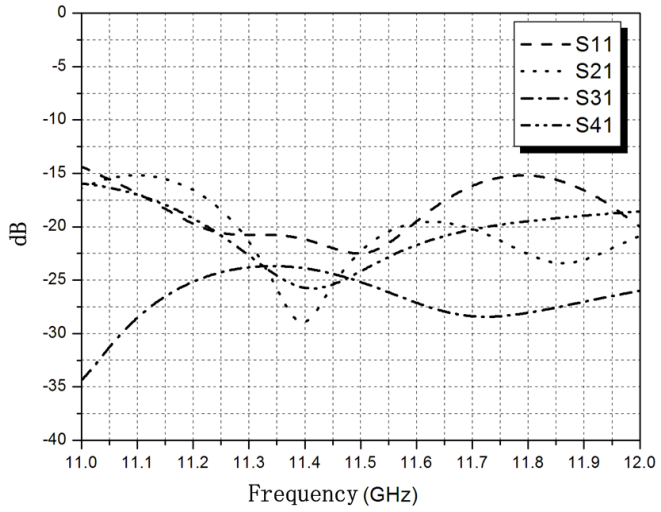

Figure 6.22 S11, S21, S31, S41 when input signal at port1

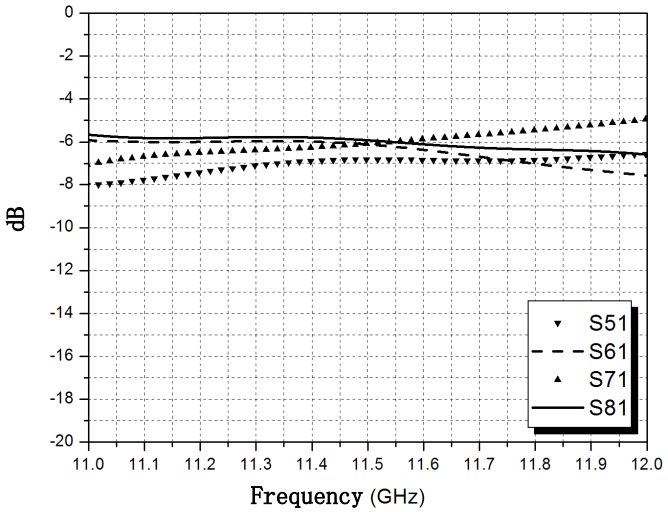

Figure 6.23 S51, S61, S71, S81 when input signal at port1

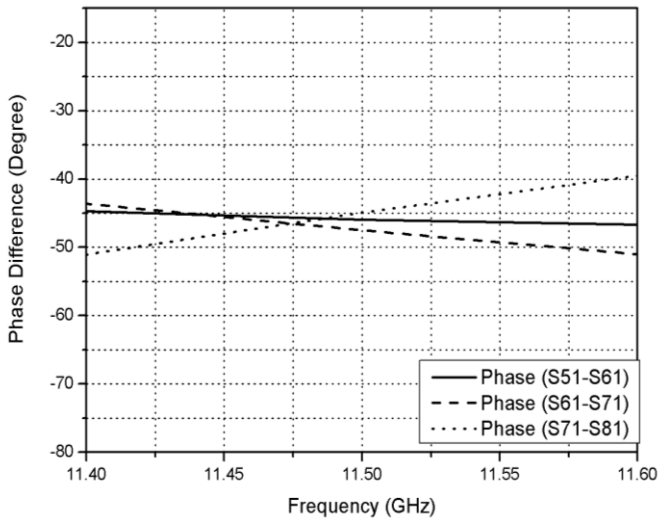

Figure 6.24 Phase difference between adjacent output ports when input signal at port1

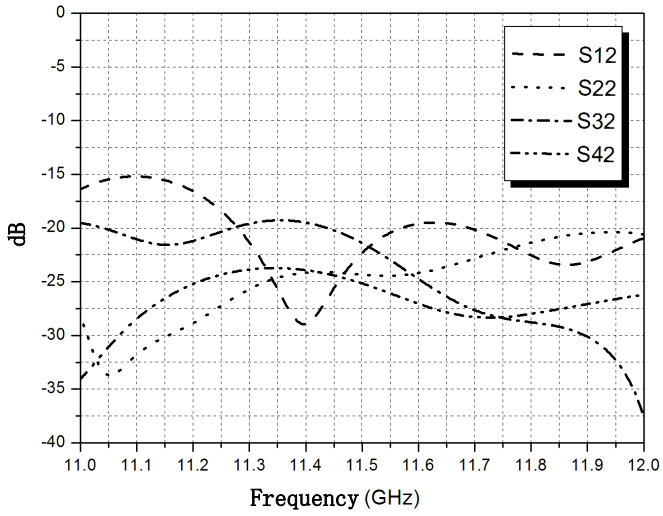

Figure 6.25 S12, S22, S32, S42 when input signal at port2

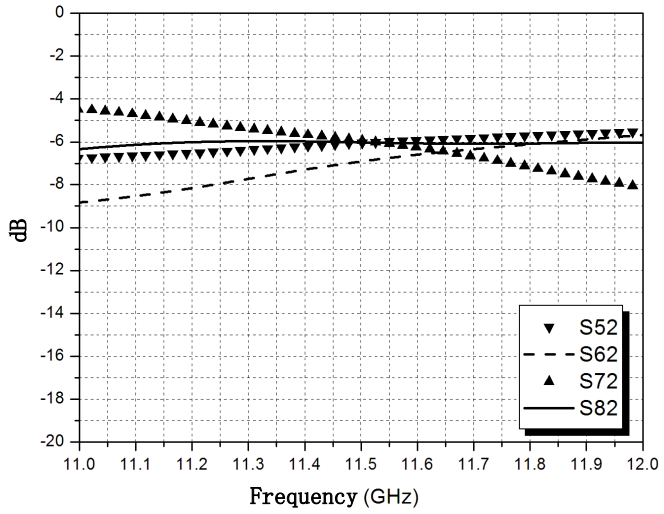

Figure 6.26 S52, S62, S72, S82 when input signal at port2

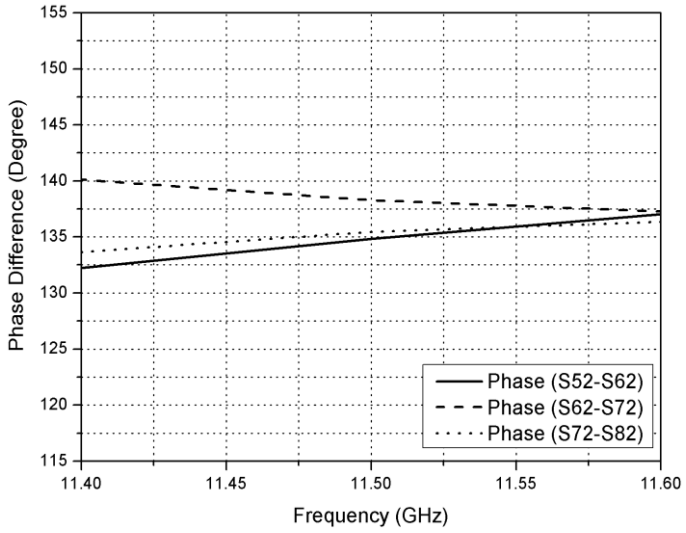

Figure 6.27 Phase difference between adjacent output ports when input signal at port2

Due to the symmetrical structure, the frequency responses of the port 3 and 4 are similar to port 2 and 1. From Figure 6.24 and 6.27, we can get the conclusion that the phase difference between adjacent output ports is the key factor to limit the bandwidth.

6.8 CYLINDER CONFORMAL ARRAY FAR-FIELD PATTERN CALCULATION METHOD

The far-field pattern of single slots antenna can be calculated by Coetzee formulation (6.80) [101],

$$E_{\phi}(\theta,\phi)=\sum_{i=1}^{N}\frac{V_i^s}{j\pi}F(k_0 l_i/2,\theta)\frac{\sin[k_0\sin\theta\cos\phi w/2]}{k_0\sin\theta\cos\phi w/2}\times\exp[\,jk_0(x_i\sin\theta\cos\phi+z_i\cos\theta)] \tag{6.80}$$

$$F(c,\theta)=\frac{\cos[c\cos(\theta)]-\cos c}{\sin\theta} \tag{6.81}$$

Thus, we get the antenna gain at (θ_0,ϕ_0) direction.

$$G(\theta_0,\phi_0)=\frac{4\pi(1-|\Gamma|^2)|E_{\phi}(\theta_0,\phi_0)|^2}{\int_0^{\pi}\int_0^{\pi}|E_{\phi}(\theta,\phi)|^2\sin\theta d\theta d\phi} \tag{6.82}$$

The cylinder conformal array far-field pattern can be synthesized by following formula.

$$E_{\phi}(\theta,\phi)=E(\theta,\phi_1)+E(\theta,\phi_2)\angle\varphi_2+....+E(\theta,\phi_i)\angle\varphi_i+E(\theta,\phi_N)\angle\varphi_N \tag{6.83}$$

where i=3, 4… N-1. φ_i is the phase difference between the first antenna and the i_{th} one. $E(\theta,\phi_i)$ is the electric field of the i_{th} antenna at ϕ_i direction. Figure 6.28 shows the

schematic diagram of two antennas far-field pattern relationship. The calculation method for multiple antennas is similar to this two antennas system.

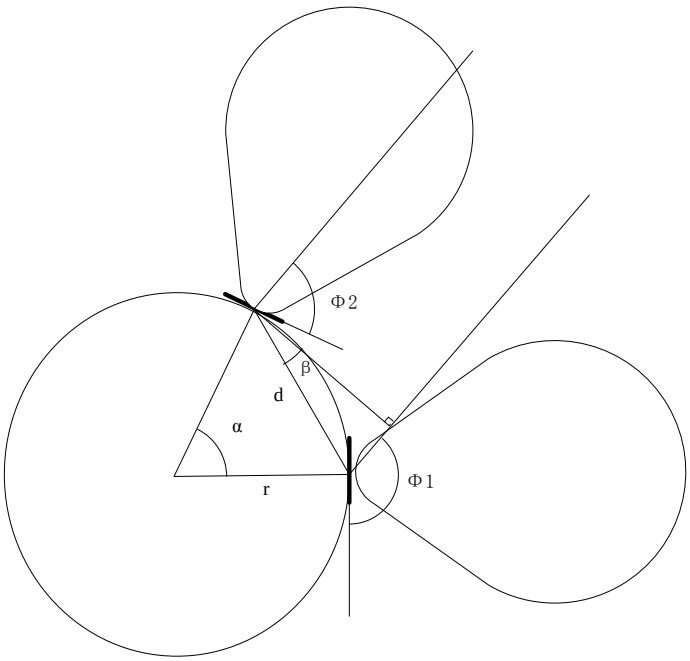

Figure 6.28 The schematic diagram of two antennas far-field pattern

The relationship between the angles in Figure 6.28 is listed as follows.

$$\phi_2 = -\alpha + \phi_1 \tag{6.84}$$

$$\beta = -\alpha / 2 - 90 + \phi_1 \tag{6.85}$$

The distance between two antenna is described as (6.86)：

$$d = 2 \times r \times \sin(\alpha / 2) \tag{6.86}$$

Thus, we can get the phase difference (6.87).

$$\varphi_2 = 2 \times \pi \times d / \lambda \tag{6.87}$$

With above formulas we can calculate the far-field pattern $E(\theta, \phi)$.

6.9 SIW BUTLER MATRIX CONFROMAL ARRAY TEST RESULT

The SIW conformal slots antennas and Butler matrix on the same substrate is fabricated as shown in Figure 6.29. The radius of the cylinder is 80 mm. A vector network analyzer is utilized to measure the return loss. Unused ports are terminated by 50 ohm resistors. The measured return loss is shown in Figure 6.30. Similarly, the port 2 return loss is shown in Figure 6.31. Due to the symmetrical structure, the S parameters of the port 3 and 4 are the same as the S parameters of port 2 and 1. The return losses of all the input ports are better than 10 dB from the 11 GHz to 12.7GHz.

The radiation patterns of the antenna are tested with a microwave antenna test system in an anechoic chamber. The measured E-plane radiation pattern (normalized at 11.5 GHz) is shown in Figure 6.32. It can be observed that the main beam directions are 30°, 72°, 112° and 156° corresponding to input port 3, 1, 4 and 2, respectively. The side lobe levels (SLLs) of the beams corresponding to input port 1 and 4 are less than -16 dB, and the SLLs of the beams corresponding to input port 2 and 3 are less than -12 dB. With -10 dB SLL restriction, usable bandwidth of the antenna is about 400 MHz, which is 3.5% with

respect to the designed frequency 11.5 GHz. The measured gain of each beam is shown in Table 7. Mismatching of SMA coaxial connector to SIW, PCB fabrication tolerance and measurement error contribute almost ±1 dB gain uncertainty at each beam corresponding to input port. Thus, the measured gain at each port has a maximum difference of 1.9 dB. The measured results agree with the calculated beams. Because of the insertion loss of the substrate, the fabrication and the measurement error, the measured frequency shifts around 2%.

Table 7 Gain of four beams

Port 1	Port 2	Port 3	Port 4
15.14 dB	16 dB	16.53 dB	14.6 dB

.

Figure 6.29 Multi-beam SIW conformal array

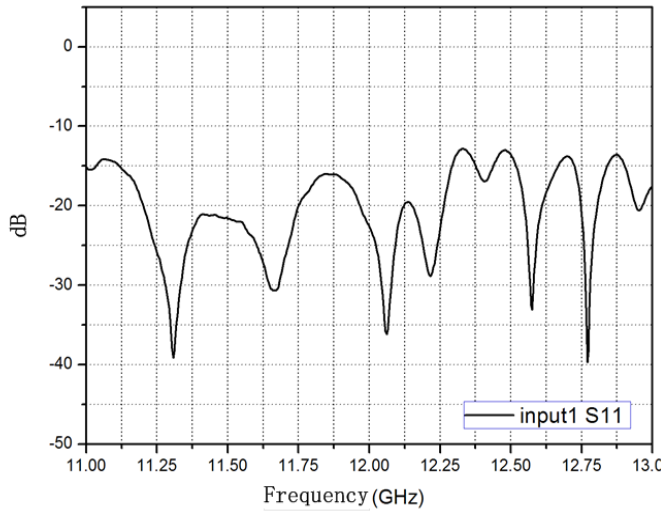

Figure 6.30 Measured return loss of port 1

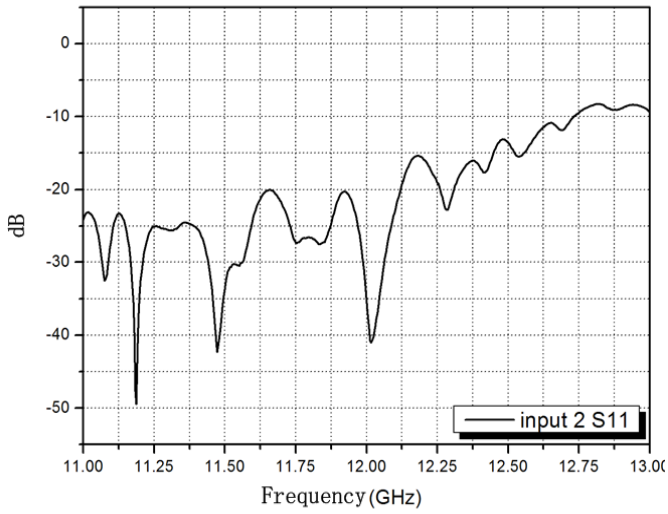

Figure 6.31 Measured return loss of port 2

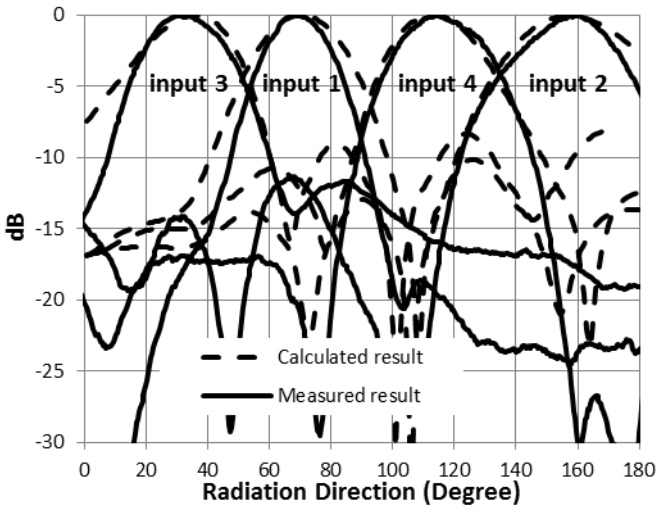

Figure 6.32 Calculated and measured far-field patterns (normalized) at 11.5 GHz

6.10 SUMMARY

In this chapter, a conformal multi-beam antenna based on SIW has been presented for the first time. Applying the SIW technology, the antenna can be mounted on the surface of a cylinder easily. The experiment results demonstrate good electrical performance. During the designing process, we find that the Butler Matrix has limitation in bandwidth, which caused the limitation of slot coupler and the phase shifter. Therefore, this antenna array is featured with narrow band. Due to its compact size and low cost compared to waveguide array, this multi-beam antenna has the potential to be an ideal candidate for airplane radar system and mobile robot antenna.

7.0 CONCLUSION AND FUTURE WORK

This chapter summarizes our work, achievements, and outlines future works regarding the NLTL and multi-beam antenna.

1. We present a method to make a perfectly linear phase shifter for broadband frequency and the simulation results agree with the theoretical analysis. With a specially doped hyper-abrupt varactor in the LH NLTL, a novel phase shifter can be made, which has several additional advantages such as compactness, high resolution, low power consumption and wide bandwidth. Thus, it is an ideal candidate for modern phased array radar or smart antenna systems, which require accurate phase modulation and compactness.

2. We make a compact large delay line based on LH NLTL. Through experiments in the laboratory, we verify that this compact delay line offers a tunable large group delay ranges from 1.2 nS to 2 nS at 1.42 GHz, which is near the Bragg cut-off frequency. Because this circuit can achieve large group delay and delay adjustment with very small length, it is a promising candidate for modern microwave systems, which requires large group delay with small form factor such as a feed-forward amplifier.

3. We fabricate a frequency translator based on the LH NLTL for the first time. Due to its linearity feature of the phase shifter versus DC bias voltage, the frequency-modulated signal has 30 dB carrier and spurious signal suppression without the adjustment of

modulation signal. Furthermore, it can be easily made in a monolithic form, as it requires only varactors and inductors. Therefore, it has a wide application for microwave instruments and velocity deception ECM systems.

4. We demonstrate a compact, broadband tunable Wilkinson power divider for the first time by replacing λ/4 sections in conventional Wilkinson power divider structure with series inductors and shunt varactors. Therefore, both compactness and tunability have been achieved. This structure is especially useful for low frequencies (less than 1 GHz) where λ/4 transmission lines occupy a large area in a conventional Wilkinson power divider. Because of the above features, it has potential applications in multi-mode, multi-band wireless or RADAR system.

5. We design and fabricate a conformal multi-beam antenna based on SIW, which is presented for the first time. During the designing process, we find that the Butler Matrix has limitation in the bandwidth. And the single slot coupler and the phase shifter are limited by the bandwidth. Therefore, this antenna array is featured with narrow band. Due to its compact size and low cost compared to waveguide array, this multi-beam antenna is an ideal candidate for airplane radar system and mobile robot antenna.

Based on the good performance of LH NLTL and SIW as mentioned before, the future work extends this technology to the chip level. So far, every circuit is fabricated on the PCB board. Compared with the chip level design, the PCB circuit has larger size and is affected by parasitic capacitance and inductance, which introduce big error in the design and the fabrication. By using the integrated circuit processing skill, the electrical performance is well controlled. Meanwhile the circuit size can be reduced to micrometer level. Furthermore, the LH NLTL phase shifter can be used as a feed network for phase

array antenna. Due to its linear phase feature, the size and the performance of phase array are greatly improved. In the SIW multi-beam antenna part, future design may apply other voltage distributions on the slots, which could reduce the lower side lobe level. Another issue in the current multi-beam antenna is the limited bandwidth, which is caused by phase balance of the Butler Matrix. In the future work, this drawback could be overcome by using thicker substrate with lower dielectric constant.

PUBLICATION LIST

1. Wenjia Tang, Hongjoon Kim, “Compact, Tunable Large Group Delay Line,” Microwave and Optical Technology Letters, Vol. 51, No. 12, pp 2893-2895, December 2009

2. Wenjia Tang, Hongjoon Kim, “Low Spurious, Broadband Frequency Translator Using Left-handed Nonlinear Transmission Line,” IEEE MWCL, vol 19, no. 4, pp 221-223, April, 2009

3. Wenjia Tang, Jiho Ryu and Hongjoon Kim, “Compact, Tunable Wilkinson Power Divider Using Tunable Synthetic Transmission Line,” Microwave and Optical Technology Letters, vol 52, issue 6, pages 1434-1436, June 2010

4. Wenjia Tang, Jizhong Xiao, “Compact, Cylinder Conformal Multi-beam Antenna,” International Journal on Communications Antenna and Propagation, accepted.

5. Wenjia Tang, Hongjoon Kim, “Compact tunable large group delay line,” IEEE Wireless and Microwave Technology Conference, WAMICON ‘09, IEEE 10th Annual, pp 1-3, 2009.

6. Hongjoon Kim, Wenjia Tang, Jiho Ryu, “Perfectly linear phase shifter for broadband frequency using a metamaterial”, US Patent, pending.

BIBLIOGRAPHY

[1] C. M. Johnson, "Ferrite Phase Shifter for the UHF Region," *IRE Trans. Microwave Theory and Techniques,* vol. 7, pp. 27-31, 1959.

[2] D. Song, Yi, J., Coodwin, Z., "Localization of Unknown Networked Radio Sources Using a Mobile Robot with a Directional Antenna," in *the 2007 American Control Conference*, Marriott Marquis Hotel at Times Square, 2007, pp. 5952-5957.

[3] D. Song, Kim, C., Yi, J., "Monte Carlo Simultaneous Localization of Multiple Unknown Transient Radio Sources Using a Mobile Robot with a Directional Antenna," presented at the IEEE International Conference on Robotics and Automation, Kobe, Japan, 2009.

[4] J. Graefenstein, Albert, A., Biber, P., Schilling, A., "Wireless Node Localization based on RSSI using a Rotating Antenna on a Mobile Robot," in *THE 6th WORKSHOP ON POSITIONING, NAVIGATION AND COMMUNICATION*, 2009, pp. 253-259.

[5] M. P. Gaynor, *System-in-package RF design and applications*: Artech House, 2007.

[6] U. Hiroshi, Takeshi, T., Fujii, M., "Development of a laminated waveguide," *IEEE Trans Microwave Theory Tech.,* vol. 46, pp. 2438-2443, 1998.

[7] D. Deslands, Wu, K., "Single substrate integration technique of planar circuits and waveguide filters," *IEEE Trans Microwave Theory Tech.,* vol. 51, pp. 593-596, 2003.

[8] K. Wu, "Towards system-on-substrate approach for future millimeter-wave and photonic wirelss applications," presented at the Asia-Pacific Microwave Conf., 2006.

[9] D. Deslandes, Wu, K., "Single-substrate integration technique of planar circuits and waveguide filters," *IEEE Trans Microwave Theory Tech.,* vol. 51, pp. 593-596, 2003.

[10] J. Chen, Hong, W., Hao, Z., Li, H., Wu, K., "Development of a low cost microwave mixer using a broad-band substrate integrated waveguide (SIW) coupler," *Ieee Microw. Wirel. Compon. Lett,* vol. 16, pp. 84-86, 2006.

[11] G. Diemer, Knol, K. S., "Frequency conversion by phase variation," *Philips Res. Rep,* vol. 4, pp. 161-167, 1949.

[12] H. Jin, Wen, G., "A novel four-way Ka-band spatial power combiner based on HMSIW," *Ieee Microw. Wirel. Compon. Lett,* vol. 18, pp. 515-517, 2008.

[13] W. D'Orazio, Wu, K., "Substrate-integrated-waveguide circulators suitable for millimeter-wave integration," *IEEE Trans Microwave Theory Tech.*, vol. 54, pp. 3675-3680, 2006.
[14] P. Akkaraekthalin, Kee, S., van der Weide, D. W., "Distributed Broad-Band Frequency Translator and its Use in a 1-3GHz Coherent Reflectometer," *IEEE Trans. Microwave Theory Tech.*, vol. 46, pp. 2244-2250, Dec 1998.
[15] S. R. Mazumder, Isham, C. M., "Performance of a 6 to 18GHz frequency translator utilizing GaAs MMIC 5-bit Digital Phase Shifter," presented at the IEEE Microwave and Millimeter-Wave Monolithic Circuit Symp. Dig., 1995.
[16] J. S. Jaffe, Mackey, R. C., "Microwave Frequency Translator," *IEEE Trans. Microwave Theory Tech.*, vol. 13, pp. 371-378, May 1965.
[17] S. Lucyszyn, Robertson, I. D., Aghvami, A. H., "24 GHz Serrodyne Frequency Translator Using a 360o Analog CPW MMIC Phase Shifter," *IEEE Trans. Microwave and Guided Wave Lett.*, vol. 4, pp. 71-73, Mar. 1994.
[18] J. Kim, Rebeiz, G. M., "Miniture four-way and two-way 24 GHz Wilkinson power dividers in 0.13 lm CMOS," *IEEE Microwave Wireless Comp. Lett.*, vol. 17, pp. 658-670, May 2008.
[19] C. Q. Li, Li, S. H., Bosisio, R. G., "CAD/CAE design of an improved, wideband Wilkinson power divider," *Microwave Journal*, pp. 125-130, Nov. 1984.
[20] L. Wu, Sun, Z., Yilmaz, H., Berroth,M., "A dual-frequency wilkinson power divider," *IEEE Trans Microwave Theory Tech.*, vol. 54, pp. 278-284, Jan 2006.
[21] Y. Sun, Freundorfer, A. P., "Broadband folded Wilkinson power combiner/splitter," *IEEE Microwave Wireless Comp. Lett.*, vol. 14, pp. 295-297, June 2004.
[22] M. C. Scardelletti, Ponchak, G. E., Weller, T. M., "Miniaturized Wilkinson power dividers utilizing capacitive loading," *IEEE Microwave Wireless Comp. Lett.*, vol. 12, pp. 6-8, Jan. 2002.
[23] M. Park, Lee, B., "A dual-band Wilkinson power divider," *IEEE Microwave Wireless Comp. Lett.*, vol. 18, pp. 85-87, Feb. 2008.
[24] H. Kim, et al, "Combined left and right-handed tunable transmission lines with tunable passband and 0 phase shift," *IEEE Trans Microwave Theory Tech.*, vol. 54, pp. 4178-4184, Dec. 2006.
[25] F. Ellinger, et al, "Varactor-Loaded Transmission-Line Phase Shifter at C-Band Using Lumped Elements," *IEEE Trans. Microwave Theory Tech.*, vol. 51, pp. 1135-1140, April 2003.
[26] L. Josefsson, Persson, P., *Conformal Array Antenna Theory and Design*: Wiley-IEEE Press, 2006.
[27] P. N. Richardson, Lee, H. Y., "Design and analysis of slotted waveguide arrays," *Microwave J.*, pp. 109-125, June 1988.
[28] D. Stancil, *Theory of Magneto Static Waves*: Springer Verlag, 1993.
[29] V. Veselago, "The electrodynamics of substances with simultaneously negative values of ε and μ," *Soviet Physics Uspekhi*, vol. 10, pp. 509-514, Feb. 1968.
[30] D. R. Smith, Padilla, W. J., Vier, D. C., Nemat-Nassser, S. C., "Composite medium with simultaneously negative permeability and permittivity," *Phys. Rev. Lett.*, vol. 84, pp. 4184-4187, May 2000.

[31] R. A. Shelby, Smith, D. R., Schultz, S. , "Experimental verification of a negative index refraction," *Science*, vol. 292, pp. 77-79, Apr 2001.
[32] R. A. Shelby, Smith, D. R. , Nemat-Nassser, S. C., Schultz, S. , "Microwave transmission through a two-dimensional, isotropic, left-handed material," *App. Phys. Lett.*, vol. 78, pp. 489-491, Jan 2001.
[33] S. E. B. Gralak, and G. Tayeb, "Anomalous refractive properties of photonic crystals," *J. Opt. Soc. Amer.*, vol. 17, pp. 1012-1020, June 2000.
[34] C. Caloz, Chang,C.-C.,Itoh, T. , "Full-wave verification of the fundamental properties of left-handed materials inwaveguide configurations," *J. App. Phys.*, vol. 1, pp. 5483-5486, Dec. 2001.
[35] R. W. Ziolkowski, Heyman, E., "Wave propagation in media having negative permittivity and permeability," *Phys. Rev. E*, vol. 64, pp. 1-15, Nov. 2001.
[36] J. B. Pendry, "Negative refraction makes a perfect lens," *Phys. Rev. Lett.*, vol. 85, pp. 3966-3969, Oct. 2000.
[37] C. Caloz, Sanada, A., Liu, L., Itoh, T., "A broadband left-handed (LH) coupled-line backward coupler with arbitrary coupling levels," in *IEEE MTT-S Int. Symp.* , Philadelphia, PA, 2003, pp. 317-320.
[38] I. Lin, Caloz, C., and T. Itoh, "A branch line coupler with two arbitrary operating frequencies using left-handed transmission lines," in *IEEE MTT-S Int. Symp.*, Philadelphia, PA, 2003, pp. 325-327.
[39] H. Okabe, Caloz, C., Itoh, T., "A compact enhanced hybrid ring using a left-handed transmission line section," in *IEEE MTT-S Int. Symp.*, Philadelphia, PA, 2003, pp. 329-332.
[40] A. Grbic, Eleftheriades, G. , "A backward-wave antenna based on negative refractive index," in *IEEE AP-S Int. Symp.*, San Antonio, TX, 2002, pp. 340-343.
[41] R. E. Collin, *Foundations for Microwave Engineering*: McGraw-Hill, 1992.
[42] A. K. Iyer, Eleftheriades, G. V., "Negative refractive index metamaterials support-ing 2-D waves," presented at the IEEE-MTT Int'l Symp, Settle, WA, 2002.
[43] A. A. Oliner, "A periodic-structure negative-refractive-index medium without resonant elements," presented at the URSI Digest, IEEE-AP-S USNC/URSI National Radio Science Meeting, San Antonio, TX, 2002.
[44] C. Caloz, Itoh, T., "Application of the transmission line theory of left-handed (LH) materials to the realization of a microstrip LH transmission line," presented at the Proc. IEEE-AP-S USNC/URSI National Radio Science Meeting, San Antonio, 2002.
[45] C. Caloz, Okabe, H., Iwai, T., Itoh, T., "Anisotropic PBG surface and its transmis-sion line model," presented at the IEEE-AP-S USNC/URSI National Radio Science Meeting, San Antonio, TX, 2002.
[46] S. Ramo, Whinnery, J. R., Duzer, T. Van, *Fields and Waves in Communication Electronics*: John Wiley & Sons, 1994.
[47] M. Rodwell, et al, "GaAs nonlinear transmission lines for picosecond pulse generation and millimeter-wave sampling," *IEEE Trans. Microwave Theory Tech.*, vol. 39, pp. 1194-1204, July 1991.

[48] A. Kozyrev, van der Weide, D., "Nonlinear Wave Propagation Phenomena in Left-Handed Transmission Line Media," *IEEE Trans. Microwave Theory and Tech.*, vol. 53, pp. 238-245, Jan 2005.

[49] H. Kim, et al, "Band pass Filter with Tunable Pass band and 0 ° Phase Shift Near Center Frequency," *IEEE Trans. Microwave Theory Tech.*, vol. 54, pp. 4178-4184 Dec. 2006.

[50] H. Kim, et al, "Linear Tunable Phase Shifter Using a Left-Handed Transmission Line," *IEEE Microwave Wireless Comp. Lett.*, vol. 15, pp. 366-368, May 2005.

[51] W. M. Zhang, Hsia, R. P., Liang, C., Song, G., Domier, C. W., Luhmann, N. C., "Novel low-loss delay line for broadband phase antenna array applications," *IEEE Microwave Guided Wave Lett.*, vol. 6, pp. 395-397, Nov. 1996.

[52] Y. Chen, Hong, W., Wu, K., "Novel Substrate Integrated Waveguide fixed phase shifter for 180-degree Directional Coupler," *IEEE/MTT-S International, Microwave Symposium*, pp. 189-192, June 2007.

[53] Y. Cassivi, Wu, K., "Low cost microwave oscillator using substrate integrated waveguide cavity," *IEEE Microw. Wirel. Compon. Lett*, vol. 13, pp. 48-50, 2003.

[54] L. Yan, et al, "Simulation and experiment on SIW slot array antennas," *IEEE Microwave Wireless Comp. Lett.*, vol. 14, pp. 446-448, Sep. 2004.

[55] Y. Cassivi, Perregrini, L., Arcioni, P., Bressan, M., Wu, K., "Dispersion characteristics of substrate integrated rectangular waveguide," *IEEE Microw. Wirel. Compon. Lett*, vol. 12, pp. 333-335, 2002.

[56] M. Bozzi, Perregrini, L., Wu, K., "Modeling of conductor, dielectric and radiation losses in substrate integrated waveguide by the boundary integral-resonant mode expansion method," *IEEE Trans Microwave Theory Tech.*, vol. 56, pp. 3153-3161, 2008.

[57] M. Bozzi, Perregrini, L., Wu, K., "Modeling of losses in substrate integrated waveguide by boundary integral-resonant mode expansion method," presented at the IEEE Int. Microwave Symp. (IMS 2008) Digest, Atlanta, GA, 2008.

[58] N. Grigoropoulos, Izquierdo, B.S., Young, P. R., "Substrate integrated folded waveguides (SIFW) and filters," *Ieee Microw. Wirel. Compon. Lett*, vol. 15, pp. 829-831, 2005.

[59] Q. Lai, Fumeaux, Ch., Hong, W., Vahldieck, R., "Characterization of the propagation properties of the half-mode substrate integrated waveguide," *IEEE Trans Microwave Theory Tech.*, vol. 57, pp. 1996-2004, 2009.

[60] G. H. Zhai, Hong, W., Wu, K., "Folded half mode substrate integrated waveguide 3 dB coupler," *IEEE Microw. Wirel. Compon. Lett*, vol. 18, pp. 512-514, 2008.

[61] M. Bozzi, Deslandes, D., Arcioni, P., Perregrini, L., Wu, K., Conciauro,Gaynor, M. P., "Efficient analysis and experimental verification of substrate integrated slab waveguides for wideband microwave applications," *Int. J. RF Microw. Comput. Aided Eng.*, vol. 15, pp. 296-306, 2005.

[62] W. Che, Li, C., Russer, P., Chow, Y.L, "Propagation and band broadening effect of planar integrated ridged waveguide in multilayer dielectric substrates," presented at the IEEE MTT-S Int. Microwave Symp. Digest,, Atlanta, GA, 2008.

[63] M. Bozzi, Winkler, S.A., Wu, K., "Broadband and compact ridge substrate integrated waveguides," *IET Microw. Antennas Propag.*, vol. 4, pp. 1965-1973, 2010.

[64] F. Xu, et al, "Finite-difference frequency-domain algorithm for modeling guided-wave properties of substrate integrated waveguide," *IEEE Trans Microwave Theory Tech.*, vol. 51, pp. 2221-2227, Nov. 2003.
[65] X. H. Wu, Kishk, A.A., "Analysis and design of substrate integrated waveguide using hybrid method," in *Synthesis Lectures on Antennas*, ed: Morgan & Claypool Publishers, 2010.
[66] A. W. Houghton, Brennan, P.V. , "Phased array control using phase-locked-loop phase shifters," in *Microwaves, Antennas and Propagation, IEE Proceedings H*, 1992, pp. 31-37.
[67] S. Han, Kim, Y., "A Compact Broadband Phased Array Antenna for IMT-2000," presented at the Antennas and Propagation Society International Symposium, IEEE, , 2003.
[68] J. Wallace, Redd, H., Furlow, R. , "Low cost MMIC DBS chip sets for phased array applications," presented at the IEEE MTT-S Int. Microwave Symp, Anaheim, 1999.
[69] S. K. Koul, Bhat, B., , *Microwave and Millimeter Waver Phase Shifters*. Norwood: Artect House, 1991.
[70] H. Hayashi, Muraguchi, M., "An MMIC active phase shifter using a variable resonant circuit," *IEEE Trans. Microwave Theory Tech.*, vol. 47, pp. 2021-2026, Oct. 1999.
[71] F. Ellinger, Vogt, R., et al, "Compact reflective type phase shifter MMIC for C-band using a lumped element coupler," *IEEE Trans. Microwave Theory Tech.*, vol. 49, pp. 913–917, May 2001.
[72] H. Mosallaei, Sarabandi, K., "Periodic meta-material structures in electromagnetics: concept, analysis, and applications," presented at the Antennas and Propagation Society International Symposium, IEEE, 2002.
[73] C. Caloz, Lin, I. H., Itoh, T., "Characteristics and potential applications of nonlinear left-handed transmission lines," *Microwave and Opt. Tech. Lett.*, vol. 40, pp. 471-473, Feb 2004.
[74] H. Kim, et al, "Compact Left-Handed Transmission Line as a Linear Phase–Voltage Modulator and Efficient Harmonic Generator," *IEEE Trans. Microwave Theory and Tech.*, vol. 55, pp. 571-578, Mar. 2007.
[75] R. F. Pierret, *Semiconductor Device Fundamentals*: Addison-Wesley, 1996.
[76] H. T. Su, Wang, Y., Huang, F., Lancaser, M. J., "Wide-band superconducting microstrip delay line," *IEEE Trans. Microwave Theory Tech.*, vol. 52, pp. 2482-2487, Nov 2004.
[77] S. G. Gopani, Thompson, J. H., Dean R., "GHz SAW delay line for direct sequence spread spectrum, CDMA in-door communication system," in *IEEE Ultrason. Symp.*, 1993, pp. 89-93.
[78] W. S. Ishak, "Magnetostatic wave technology: A review," in *Proc. IEEE*, 1998, pp. 171-187.
[79] M. M. Tumer, Branch, G., Smith, P. W., "Methods of theoretical analysis and computer modeling of the shaping of electrical pulses by nonlinear transmission lines and lumped-element delay lines," *IEEE Trans. Electron Devices*, vol. 38, pp. 810-816, 1991.

[80] J. D. Lanzinger, "Group delay caused by impedance mismatch," presented at the 29th ARFTG Conf., 1987.
[81] S. Abielmona, Gupta, S., Caloz, C., "Experimental demonstration and characterization of a tunable CRLH delay line system for impulse/continuous wave," *IEEE Microwave Wireless Comp. Lett.*, vol. 17, pp. 864-866, Dec. 2007.
[82] G. V. Eleftheriades, Iyer, A. K., Kremer, P. C., "Planar negative refractive index media using periodically L–C loaded transmission lines," *IEEE Trans. Microwave Theory Tech.*, vol. 50, pp. 2702-2712, Dec 2002.
[83] S. Lucyszyn, Robertson, I. D., Aghvami, A. H., "Novel applications in microwave communication systems for small-shift frequency translators," presented at the IEEE Int. Telecommunications, Dubai, 1994.
[84] A. W. Rudge, Miline, K., Olver, A. D., Knight, P., *The handbook of antenna design*. London: Peter Peregrinues Ltd., 1982.
[85] Peter A. Rizzi, *Microwave Engineering-Passive Circuits*, Pearson Education, 2010
[86] E. J. Wilkion, "An N-way hybrid power divider," *IEEE Trans Microwave Theory Tech.*, vol. 8, pp. 116-118, 1960.
[87] D. M. Pozar, *Microwave engineering*, , 3rd ed. New York: Wiley, 2005.
[88] H. Kim, et al, "Balanced distributed element phase shifter," *IEEE Microwave Wireless Comp. Lett.*, vol. 15, pp. 147-149, 2005.
[89] E. Lourandakis, et al, "Reduced size and tunable microwave circuits using BST thin-film varactors," *IEEE Trans Microwave Theory Tech.*, vol. 56, pp. 3093-3099, Dec 2008.
[90] T. Morton, Pasals, K., "Perormance analysis of conformal conical arrays for airborne vehicles," *IEEE Trans. Aerospace and Electronic Systems*, vol. 42, pp. 876-890, July 2006.
[91] R. J. Mailoux, "Conformal array Antenna Theory and Design [Reviews and Abstracts]," *IEEE Trans. Antennas Propag.*,, vol. 49, pp. 126-127, October 2007.
[92] K. Lee, Eichmann, G., "Elementary pattern for conformal dipole arrays mounted on dielectrically clad conduction cylinders," *IEEE Trans. Antennas Propag*,, vol. 28, pp. 811-818, November 1980.
[93] J. Jayakumar, Garg, R., Sarap, B., Lal, B., "A conformal cylindrical microstrip array for producing omnidirectional radiation pattern," *IEEE Trans. Antennas Propag*,, vol. 34, pp. 1258-1261, October 1986.
[94] D. Deslandes, Perregrini, L., Arcioni, P., et al, "Dispersion characteristics of substrate integrated rectangular waveguide," *IEEE Microwave Wireless Component Letter*, vol. 12, pp. 333-335, September 2002.
[95] F. Xu, et al, "Domain Decomposition FDTD Algorithm Combining with Numerical TL Calibration Technique and Its Application in Parameter Extraction of Substrate Integrated Circuits," *IEEE Trans Microwave Theory Tech.*, vol. 53, pp. 329-338, 2005.
[96] Z. C. Hao, et al, "Compact Super-Wide Bandpass Substrate Integrated Waveguide (SIW) Filters," *IEEE Trans Microwave Theory Tech.*, vol. 53, pp. 2968-2977, 2005.

[97] N. Kalyanasundaram, "On the distribution of current on a straight wire antenna " in *Microwaves, Antennas and Propagation, IEE Proceedings H*, 2008, pp. 407-410.
[98] R. Li, et al, "Development of a Cavity-Backed Broadband Circularly Polarized Slot/Strip Loop Antenna With a Simple Feeding Structure " *IEEE Trans. on Antennas and Propagation,* vol. 56, pp. 312-318, Feb. 2008.
[99] J. D. Kraus, Marhefka, R. J., *Antennas for all applications*. Boston: McGraw-Hill, 2002.
[100] S. Yamamoto, Hirokawa, J., Ando, M., "A Beam Switching Slot Array with a 4-Way Butler Matrix Installed in Single Layer Post-Wall Waveguides," *IEICE Trans. Commun.,* vol. 85, pp. 1653-1659, 2003.
[101] J. C. Coetzee, "Off-center-frequency analysis of a complete planar slotted-waveguide array consisting of sub-arrays " *IEEE Trans. on Antennas and Propagation,* vol. 48, pp. 1746-1755, 2000.
[102] A. Piloto, Leahy, K., Flanick, B., Zaki, K. A., "Waveguide filters having a layered dielectric structures," 1995.
[103] R. S. Eillott, *Antenna Theory and Design*. Englewood Cliffs: Prentice-Hall, Inc., 1981.
[104] Cockrell, "The Input Admittance of the Rectangular Cavity-Backed Slot Antenna," *IEEE Trans. on Antennas and Propagation,* vol. 24, pp. 288-294, May 1976.
[105] Y. Mancuso, "Components and technologies for T/R modules " *Aerospace and Electronic Systems Magazine, IEEE,* vol. 25, pp. 39-43, Oct. 2010.
[106] J. Mong, Wang, S., Huang, Y., "A new digital processor for phased-array ultrasound system," presented at the Engineering in Medicine and Biology Society, 1988. Proceedings of the Annual International Conference of the IEEE 1988.
[107] C. Chuang, "Surface wave diffraction by a truncated inhomogeneous dielectric slab recessed in a conducting surface " *IEEE Trans. on Antennas and Propagation,* vol. 34, pp. 496-502, Apr. 1986.
[108] P. Li, Lau, K.L., Luk, K.M., "A study of the wide-band L-probe fed planar patch antenna mounted on a cylindrical or conical surface " *IEEE Trans. on Antennas and Propagation,* vol. 53, pp. 3385-3389 Oct. 2005.
[109] M. T. Ma, Walters, L. C., "Theoretical methods for computing characteristics of Wullenweber antennas " *Electrical Engineers, Proceedings of the Institution of* vol. 117, pp. 2095-2101, Nov. 1970.
[110] A. K. Poddar, Pandey, K. N., "Circularly polarized active circulator smart skin antenna " presented at the High Performance Electron Devices for Microwave and Optoelectronic Applications, 2000 8th IEEE International Symposium 2000.
[111] J. Butler, Lowe, R, "Beam-forming matrix simplifies design of electronically scanned antennas," *Electron Design,* vol. 9, pp. 170-173, April 1961.
[112] M. Wang, Lv, S., Liu, R., *Phased array antenna analysis and synthesize*: University of Electronic Science and Technology Press, 1989.
[113] J. L. Allen, "A theoretical limitation of the formation of lossless beams in linear arrays," *IRE Trans. Antennas and Propagation,* vol. 9, pp. 350-352, July 1961.

[114] W. K. Cahn, Kuress, H., "The uniqueness of the lossless feed network for a multi-beam array," *IRE Trans. Antennas and Propagation,* vol. 10, pp. 100-101, Jan. 1962.
[115] R. C. Hansen, *Phased Array Antennas*: A Wiley-interscience Publication, John Wiley&Sons, Inc., 1997.
[116] W. Hong, "Development of microwave antennas, components and subsystems based on SIW technology," presented at the Microwave, Antenna, Propagation and EMC Technologies for Wireless Communications, 2005. MAPE 2005. IEEE International Symposium 2005.
[117] B. Liu, et al, "Substrate integrated waveguide 180-degree narrow-wall directional coupler," presented at the Microwave Conference Proceedings, APMC 2005, 2005.
[118] W. J. Ince, Stern, E., "Nonreciprocal remanence phase shifters in rectangular waveguide," *IEEE Trans. Microwave Theory Tech. ,* vol. MTT-15, pp. 87-95, Feb. 1967.
[119] K. Wu, Deslandes, D., Cassivi, Y., "The substrate integrated circuits - a new concept for high-frequency electronics and optoelectronics," presented at the 6th Int. Conf. on TMSCBS, 2003.
[120] P. Chen, Huang, T., Wang, H., Wang, Y., Chen, C., Chao, P., "K-band HBT and HEMT monolithic active phase shifters using vector sum method " *IEEE Trans., Microwave Theory and Tech.,* vol. 52, pp. 1414-1424, May 2004.
[121] H. Zarei, Charles, C., Allstot, D., "Reflective-Type Phase Shifters for Multiple-Antenna Transceivers " *IEEE Trans. Circuits and System I: Regular Papers,* vol. 54, pp. 1647-1656, Aug. 2007.
[122] N. Somjit, Stemme, G., Oberhammer, J., "Deep-Reactive-Ion-Etched Wafer-Scale-Transferred All-Silicon Dielectric-Block Millimeter-Wave MEMS Phase Shifters " *Microelectromechanical Systems,* vol. 19, pp. 120-128, Feb. 2010.